Diploma Thesis

Performance of Air-Entrained Concrete with Recycled Concrete Aggregates under Severe Exposure Conditions

submitted in satisfaction of the requirements for the degree of
Diplom-Ingenieur / Diplom-Ingenieurin
of the TU Wien, Faculty of Civil and Environmental Engineering

---

Diplomarbeit

Leistungsfähigkeit von luftporenhaltigem Beton mit rezykliertem Betongranulat unter anspruchsvollen Umgebungsbedingungen

ausgeführt zum Zwecke der Erlangung des akademischen Grads
Diplom-Ingenieur / Diplom-Ingenieurin
eingereicht an der TU Wien, Fakultät für Bau- und Umweltingenieurwesen

von

Tareq Lemcherreq
Matr.Nr.: 01227969

Betreuung: Prof. doc. Dr.techn. Dipl.-Ing. **Ildiko Merta**
Projektass. BSc MSc **Bayram Tutkun**
Institut für Werkstofftechnologie, Bauphysik und Bauökologie
Forschungsbereich Bauphysik
Fakultät für Bau- und Umweltingenieurwesen
Technische Universität Wien,
Karlsplatz 13/E207-02, 1040 Wien, Österreich

Wien, im Januar 2026

Die approbierte gedruckte Originalversion dieser Diplomarbeit ist an der TU Wien Bibliothek verfügbar
The approved original version of this thesis is available in print at TU Wien Bibliothek.

Die approbierte gedruckte Originalversion dieser Diplomarbeit ist an der TU Wien Bibliothek verfügbar
The approved original version of this thesis is available in print at TU Wien Bibliothek.

Danksagung

Der Weg zu meinem Studienabschluss war geprägt von zahlreichen lehrreichen Erfahrungen und Begegnungen, die mich sowohl in meinem privaten als auch in meinem fachlichen Werdegang noch lange begleiten werden. Gleichzeitig war dieser Weg herausfordernd und verlangte von mir, meine eigenen Grenzen zu überschreiten. Durch die Unterstützung meiner Kolleginnen und Kollegen, meiner Freundinnen und Freunde und meiner Familie stehe ich nun am Ende dieses Weges und kann zufrieden darauf zurückblicken. Dafür möchte ich Ihnen an dieser Stelle ganz herzlich danken.

Zum Abschluss meines Studiums ist es mir eine besondere Freude, diese Arbeit meinen Eltern und meinen Schwestern zu widmen, die mich während des gesamten Studiums mit Vertrauen, Geduld und stetiger Unterstützung begleitet haben.

Ein besonderer Dank gilt dem Team des Forschungsbereichs Bauphysik am Institut für Werkstofftechnologie, Bauphysik und Bauökologie, insbesondere Professor Ildiko Merta und meinem Betreuer Bayram Tutkun, für das entgegengebrachte Vertrauen sowie die fachliche Unterstützung bei der Erstellung dieser Arbeit. Ebenso danke ich Farshad Ameri, Daniella Mehanni und Nico Scherzer für ihre Hilfe im Labor und bei der Auswertung der Ergebnisse.

Die approbierte gedruckte Originalversion dieser Diplomarbeit ist an der TU Wien Bibliothek verfügbar
The approved original version of this thesis is available in print at TU Wien Bibliothek.

Die approbierte gedruckte Originalversion dieser Diplomarbeit ist an der TU Wien Bibliothek verfügbar
The approved original version of this thesis is available in print at TU Wien Bibliothek.

Abstract

The increasing depletion of natural resources and the negative impact of raw material extraction on the environment drive the search for sustainable alternatives in the construction sector. Recycled concrete aggregate (RCA), obtained from demolished concrete structures, presents a promising substitute for natural aggregates (NA) in concrete production. However, concerns regarding its influence on concrete performance, particularly under severe exposure conditions, have limited its use to non-structural applications.

This thesis investigates the performance of B7 concrete (exposure classes XC4, XW2, XD3, XF4, XA1L) incorporating varying proportions of pre-saturated RCA of high purity. The study aims to evaluate the effects of RCA content on the physical properties of fresh concrete, as well as on the mechanical and the durability performance of hardened concrete. The two-stage mixing approach (TSMA) was employed to optimise the use of pre-saturated RCA and mitigate its adverse effects on workability and strength.

Experimental testing included measurements of workability, air content, density, compressive strength, and durability indicators such as chloride penetration resistance, freeze–thaw resistance with de-icing salts, water penetration depth, and carbonation resistance. Additionally, an air void investigation was conducted to assess the microstructural characteristics relevant to the freeze–thaw performance.

The inclusion of RCA slightly lowered fresh concrete workability, while the mechanical performance remained adequate for structural applications. In terms of durability, chloride ingress and carbonation depth increased with RCA content due to the higher porosity of recycled aggregates. The most critical limitation was observed in freeze–thaw resistance, linked to an insufficient micropore structure in the RCA.

Overall, properly pre-treated and quality-controlled RCA can be used to produce concrete with adequate mechanical performance; however, its durability under severe environmental conditions remains the main restriction.

Die approbierte gedruckte Originalversion dieser Diplomarbeit ist an der TU Wien Bibliothek verfügbar
The approved original version of this thesis is available in print at TU Wien Bibliothek.
TU Bibliothek Your knowledge hub WIEN

Die approbierte gedruckte Originalversion dieser Diplomarbeit ist an der TU Wien Bibliothek verfügbar
The approved original version of this thesis is available in print at TU Wien Bibliothek.

Kurzfassung

Die zunehmende Erschöpfung der natürlichen Ressourcen und die mit der Rohstoffgewinnung verbundene Umweltbelastung treiben die Suche nach nachhaltigen Alternativen im Bausektor voran. Rezykliertes Betongranulat (RCA), das aus Betonabbruch gewonnen wird, stellt eine vielversprechende Alternative zu natürliche Zuschlagstoffe (NA) in der Betonherstellung dar. Bedenken hinsichtlich seines Einflusses auf die Betoneigenschaften, insbesondere unter extremen Umgebungsbedingungen, haben jedoch seine Verwendung auf nachrangige Anwendungen beschränkt.

Diese Arbeit untersucht die Leistungsfähigkeit von B7-Beton (Expositionsklassen XC4, XW2, XD3, XF4, XA1L) unter Verwendung unterschiedlicher Anteile von vorgesättigtem RCA mit geringen Verunreinigungen. Ziel der Studie ist es, die Auswirkungen des RCA-Gehaltes auf die physikalischen Eigenschaften von Frischbeton sowie auf die mechanischen Eigenschaften und die Dauerhaftigkeit von ausgehärtetem Beton zu bewerten. Durch den Einsatz eines zweistufigen Mischverfahrens (TSMA) wurden eine Abschwächung der negativen Auswirkungen von RCA auf die Verarbeitbarkeit und Festigkeit erreicht.

Die experimentellen Untersuchungen umfassten Messungen der Verarbeitbarkeit, des Luftgehalts, der Dichte, der Druckfestigkeit und der Dauerhaftigkeitsmerkmale wie Chloridwiderstand, Frost-Tausalz-Beständigkeit, Wassereindringtiefe und Karbonatisierungsbeständigkeit. Zusätzlich wurde eine Luftporenanalyse durchgeführt, um die für die Frost-Tausalz-Beständigkeit relevanten mikrostrukturellen Poreneigenschaften zu charakterisieren.

Die Zugabe von RCA verringerte die Verarbeitbarkeit von Frischbeton geringfügig, während die mechanischen Eigenschaften befriedigend waren. In Bezug auf die Dauerhaftigkeit nahmen der Chloridgehalt und die Karbonatisierungstiefe mit dem RCA-Gehalt aufgrund der höheren Porosität der rezyklierten Zuschlagstoffe zu. Die kritischste Einschränkung wurde bei der Frost-Tausalz-Beständigkeit beobachtet, die mit einer unzureichenden Mikroporenstruktur im RCA zusammenhängt.

Insgesamt kann ordnungsgemäß vorbehandeltes und qualitätsgeprüftes RCA zur Herstellung von Beton mit hohen mechanischen Anforderungen verwendet werden; seine Dauerhaftigkeit unter anspruchsvollen Umgebungsbedingungen bleibt jedoch die wesentliche Herausforderung.

Die approbierte gedruckte Originalversion dieser Diplomarbeit ist an der TU Wien Bibliothek verfügbar
The approved original version of this thesis is available in print at TU Wien Bibliothek.
TU Bibliothek Your knowledge hub WIEN

Die approbierte gedruckte Originalversion dieser Diplomarbeit ist an der TU Wien Bibliothek verfügbar
The approved original version of this thesis is available in print at TU Wien Bibliothek.

Contents

1 Introduction 1
2 Literature Review 3
2.1 Introduction to Recycled Concrete Aggregate 3
2.1.1 Production of Recycled Concrete Aggregate 3
2.1.2 Properties of Recycled Concrete Aggregate 4
2.1.3 Interfacial Transition Zone 6
2.2 Challenges in the use of RCA in Concrete 7
3 Materials and Methods 9
3.1 B7 Concrete according to ÖNORM B 4710-1 9
3.2 Materials 10
3.2.1 Cement 10
3.2.2 Supplementary Cementitious Materials 11
3.2.3 Natural Aggregates 12
3.2.4 Recycled Concrete Aggregates 14
3.2.5 Water 19
3.2.6 Admixtures 19
3.3 Mixture Design 21
3.4 Mixing Approach – Two-stage Mixing Approach 23
3.5 Specimen Preparation 25
3.6 Experimental Methods 27
3.6.1 Fresh Concrete Properties 27
3.6.2 Density of hardened Concrete 30
3.6.3 Compressive Strength 31
3.6.4 Chloride Resistance 31
3.6.5 Freeze-Thaw Resistance - Scaling 33
3.6.6 Depth of Penetration 34
3.6.7 Carbonation Resistance 35
3.6.8 Air Void Analysis 36
4 Results and Interpretation 42
4.1 Fresh Concrete Properties 42
4.1.1 Temperature 42
4.1.2 Consistency 42
4.1.3 Fresh Density 44
4.1.4 Air Content 45
4.1.5 Water Content 46
4.2 Hardened Density 46
4.3 Compressive Strength 47

Die approbierte gedruckte Originalversion dieser Diplomarbeit ist an der TU Wien Bibliothek verfügbar
The approved original version of this thesis is available in print at TU Wien Bibliothek.
TU Bibliothek Your knowledge hub WIEN

4.4 Chloride Resistance 50
4.5 Freeze-thaw Resistance – Scaling 52
4.6 Depth of Penetration 54
4.7 Carbonation Resistance 55
4.8 Air Void Analysis 57
4.8.1 Image Editing and Processing in *ImageJ* 57
4.8.2 Image Analysis in *MATLAB* 65
4.8.3 Computed Sphere Distribution 68
5 Conclusion 72
5.1 Summary of Findings 72
5.2 Fresh Concrete Properties 72
5.3 Mechanical Properties 72
5.4 Durability Properties 73
5.5 Overall Assessment 74
Bibliography 75
List of Figures 80
List of Tables 82
Appendix A – MATLAB Code 83

Die approbierte gedruckte Originalversion dieser Diplomarbeit ist an der TU Wien Bibliothek verfügbar
The approved original version of this thesis is available in print at TU Wien Bibliothek.

1 Introduction

The contribution of the construction sector to the depletion of natural resources and the production of waste materials in industrial countries presents a major challenge. In the European Union, around 50% of all extracted raw materials can be attributed to the construction sector [1], and one third of all waste generated is construction and demolition waste (CDW). The increasing amount of CDW, coupled with the limited availability of land for quarries and their environmental impact, has led to a growing interest in sustainable alternatives such as recycled aggregate (RA).

The incorporation of RA into new concrete allows the replacement of a primary raw material by a secondary one, which can bring several benefits for the natural and built environment and for the construction sector:

- Resource conservation through the reduction of resource extraction activities and their ecological impacts (e.g. loss of vegetation and soil, habitat destruction, groundwater contamination, alteration of ecosystems)
- Landfill disposal reduction and moving towards a circular economy
- CO_2 emissions reduction in certain cases through reduced transport distances
- Material cost reduction

Despite these advantages, the use of RA in structural concrete remains limited. Difficulties in processing CDW, splitting composite materials and an end-product with varying properties and quality present challenges to a large-scale use. Even high-grade recycled concrete aggregate (RCA), produced by processing concrete from road-, bridge- and engineering constructions, is often subject to downcycling, and being primarily used for lower-quality purposes, such as backfilling, unbound upper and lower base course in road construction, drainage layer, etc. [2]

RCAs differ significantly from natural aggregates (NA) in terms of their physical and microstructural characteristics. The mortar attached to recycled concrete aggregate increases porosity and water absorption, while reducing density and strength. These features can negatively affect concrete workability, mechanical strength, and long-term durability. Nevertheless, recent studies have shown that pre-saturation of RCA and the application of modified mixing techniques, such as the two-stage mixing approach, can mitigate these drawbacks and improve the performance of recycled aggregate concrete (RAC).

Die approbierte gedruckte Originalversion dieser Diplomarbeit ist an der TU Wien Bibliothek verfügbar
The approved original version of this thesis is available in print at TU Wien Bibliothek.
TU Bibliothek Your knowledge hub WIEN

This master's thesis was conducted in the framework of the *UP!crete* research project [1] and serves as a foundation for further investigations into the upcycling potential of recycled concrete. The research aims to develop innovative methods that enhance the properties of recycled aggregates and enable their use at higher replacement levels, contributing to more sustainable concrete production.

In this context, the objective of the present thesis is to experimentally evaluate the mechanical and durability-related performance of concrete under severe exposure conditions (B7 Concrete) incorporating varying ratios of pre-saturated recycled concrete aggregate and produced using a two-stage mixing approach. The investigation focuses on the influence of RCA content on the properties of fresh and hardened concrete, including workability, strength development, and durability parameters such as chloride resistance, carbonation depth, and freeze–thaw resistance.

The structure of this thesis is as follows: The first chapter presents the research motivation and objectives. The second chapter provides a literature review on the production process, the properties and the influence of recycled concrete aggregate on concrete according to the current state of knowledge. Chapter 3 details the materials, mix designs and experimental methods, followed by a presentation and discussion of the test results in Chapter 4. Finally, Chapter 5 summarises the findings and conclusions derived from this research.

Die approbierte gedruckte Originalversion dieser Diplomarbeit ist an der TU Wien Bibliothek verfügbar
The approved original version of this thesis is available in print at TU Wien Bibliothek.
TU Bibliothek Your knowledge hub WIEN

2 Literature Review

2.1 Introduction to Recycled Concrete Aggregate

While natural aggregates remain predominant in concrete production due to their consistent quality and durability, recycled aggregates can offer environmental and economic advantages by reducing waste generation, conserving natural resources and reducing transportation costs. Nonetheless, the use of recycled concrete aggregates in concrete production presents many challenges and as a result, its usage is essentially limited to road base construction, high quality backfill material, drainage layers, and aggregate for concrete with low requirements [2].

2.1.1 Production of Recycled Concrete Aggregate

The production of RCA consists of transforming construction and demolition waste into usable aggregate fractions that comply with the guidelines for material composition and physical characteristics for concrete applications. The production process begins with the recovery of waste concrete from demolition sites or construction activities. The construction waste is then processed with various mechanical treatments such as crushing, screening, and sorting to produce aggregate fractions that are suitable for concrete production [3].

The objective of processing construction and demolition waste is to obtain recycled building materials with designated, reproducible properties. The quality of the resulting RCA will greatly depend on the homogeneity of the source material and the methods and technologies associated with the processing. Homogeneous source materials can be processed using relatively simple equipment, whereas heterogeneous waste material requires more complex, selective treatment in order to produce acceptable aggregate quality.

Crushing of the CDW involves the mechanical reduction of large pieces of waste concrete into smaller aggregates. The crushing process can also assist in separating composite materials, allowing for a subsequent sorting. Jaw crushers and impact crushers are commonly used during this stage, they break down the concrete by applying compressive and impact forces to it. The screening process is performed to classify the crushed material based on particle size. It separates the aggregate using vibrating screen decks with uniform openings. This process can be implemented either before or after crushing, depending on the specific processing strategy. Sorting is the separation of materials based on type and physical characteristics, such as bulk density, colour, shape, and grain size. This process is a very important step in eliminating contaminants such as wood, plastics, glass, or other undesired components. The degree of sorting depends on the variability of the demolition waste and the desired quality of the

Die approbierte gedruckte Originalversion dieser Diplomarbeit ist an der TU Wien Bibliothek verfügbar
The approved original version of this thesis is available in print at TU Wien Bibliothek.
TU Bibliothek Your knowledge hub WIEN

final recycled product. For the production of high-quality recycled materials intended for structural concrete applications, sensor-based colour sorting technologies are recommended as they allow the separation of concrete from brick and other materials [4].

The efficiency of every processing step, particularly sorting, has a large influence over the mechanical performance and durability of RAC. Clean and well-graded RCA with minimal impurities can produce concrete that will perform similarly to concrete produced with natural aggregates. However, if the source concrete includes heterogeneous or poorly sorted materials, the product is likely to show increased variability in strength, workability, and long-term performance.

2.1.2 Properties of Recycled Concrete Aggregate

2.1.2.1 Mortar Content

A defining characteristic of RCA is the adhesion of the old mortar from the source concrete to the aggregate. While most of the mortar detaches during crushing, a significant quantity remains bonded to the aggregate (**Fig. 1**). Studies have shown that adhered mortar can make up a substantial portion of RCA mass and volume. Verian [5] observed up to 28,9% adhered mortar content. Similarly, Etxeberria et al. [6] reported levels of approximately 20% for RCA fractions of 10 to 25 mm.

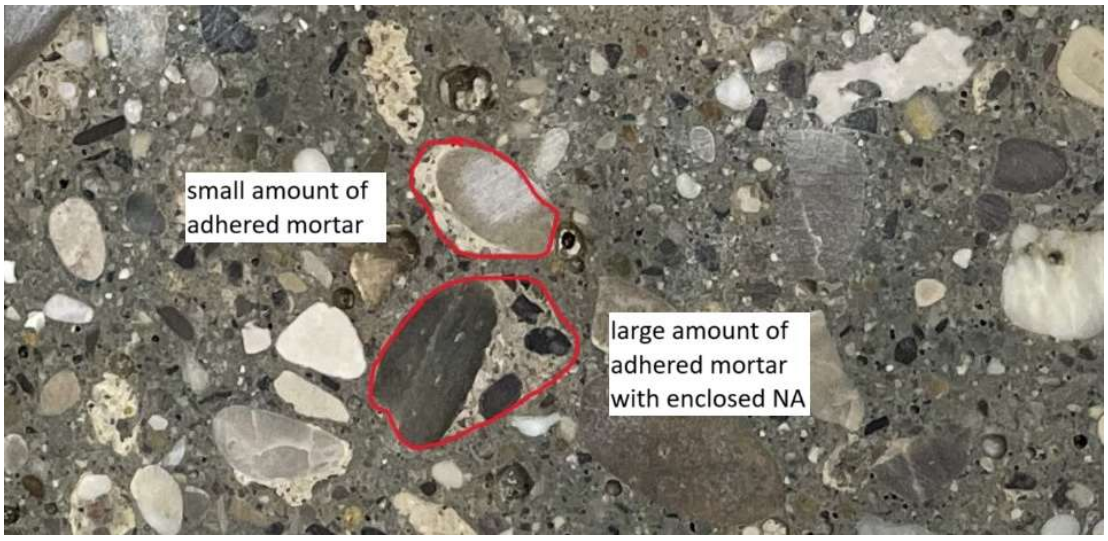

Fig. 1: Image of RCA in the concrete matrix taken from the produced samples [photo by author]

The high mortar content leads to an increase in porosity and water absorption of RCA, and decreases its specific gravity compared to natural aggregates [5], causing higher plastic shrinkage, reduced strength, and greater cracking potential in concrete. The presence of adhered mortar also entails the existence of additional interfacial transition zones (ITZs) in the concrete. These ITZs are weak points in the concrete microstructure and negatively affect

Die approbierte gedruckte Originalversion dieser Diplomarbeit ist an der TU Wien Bibliothek verfügbar
The approved original version of this thesis is available in print at TU Wien Bibliothek.

durability and mechanical performance [7]. The effect of the additional ITZ on recycled aggregate concrete will be discussed in detail in section 2.1.3.

2.1.2.2 Density

Recycled concrete aggregates usually have a lower density than natural aggregates, mainly due to the presence of adhered old mortar as stated above. The attached mortar has a significantly lower density compared to virgin aggregate, which reduces the overall bulk density of RCA.

Fig. 2 shows a microscopic image of concrete with NA and RA under UV light, the dense gravel (left) appears dark, whereas the hydrated cement surrounding it appears lighter. On the right image, the old, attached mortar within the recycled grain is clearly visible due to its very light colour. Its density is lower than that of the surrounding cement stone.

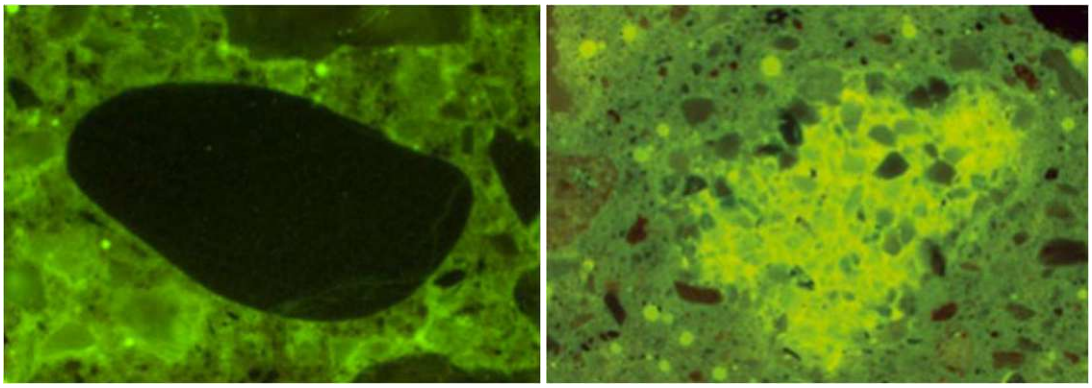

(a) (b)

Fig. 2: Microscopic image under UV light of NA (a) and RCA (b) [8]

Kurda et al. [9] states that the density of coarse gravel and fine sand typically is around 2600 kg/m³, while coarse and fine RCA usually have a density of 2400 and 2200 respectively. Gorjinia et al. [10] reported that RCA can be up to 20% lighter than NA due to the considerable volume of porous mortar. The density of RCA will also decrease with lower strength of the source concrete and with each recycling cycle, as the amount of attached mortar increases with each generation [11].

2.1.2.3 Water Absorption

Water absorption is a key parameter in evaluating aggregate quality, as it influences concrete workability, durability, strength, and water-cement ratio. High water absorption can result in inconsistent concrete mixes, increased water demand, and ultimately reduced mechanical performance.

Die approbierte gedruckte Originalversion dieser Diplomarbeit ist an der TU Wien Bibliothek verfügbar
The approved original version of this thesis is available in print at TU Wien Bibliothek.

Because of the porous structure of the adhering mortar and the microcracks induced during the crushing process, RCA has a much higher capacity to absorb water than natural aggregate. According to Verian [5], absorption values for natural aggregates ranged from 0,4% to 1,49%, while RCA values ranged from 3,3% to 9,25%. According to Luo et al. [12], smaller RCA particles are often capable of absorbing even more water because of their larger specific surface area.

Furthermore, Khoshkenari et al. [10] found that the water absorption of RCA derived from 30 MPa concrete can be higher by as much as 11,5 times for coarse aggregates and 3,5 times for fine aggregates than that of the corresponding natural aggregates. These findings highlight the influence of the source material properties on the resulting RCA characteristics.

Factors such as particle size, mortar content, and properties of the original concrete play a role in determining RCA's water absorption. It is important to understand and control these parameters in order to use RCA optimally and produce concrete that preforms similarly to conventional concrete mixes.

2.1.3 Interfacial Transition Zone

The interfacial transition zone between cement paste and aggregate is a critical section in the concrete matrix, and considered the weakest link in the structure of the material [13]. The ITZ designates the area around the aggregate particles that is disturbed by the presence of the aggregate, this area is characterised by an increased porosity and the concentration of smaller cement particles. This disturbance is primarily due to the compaction of cement grains relative to the larger aggregates, which prevents seamless contact between the two materials. As a result, voids form next to the surface of the aggregate and are consequently filled with small cement particles, air, and water (**Fig. 3**) [14], [15]. Despite its narrow thickness, typically around 20–50 µm, the ITZ occupies a significant proportion of the cement paste and has been estimated to represent 20% to 40% of the total volume of the cement binder [16], [17].

The macro-mechanical characteristics of concrete are significantly impacted by the ITZ. This zone tends to be the main site of failure under stress, determining the overall strength and durability of the concrete because it is usually weaker than the bulk cement paste due to its increased porosity. Reducing the amount of wood, plastic, glass, and asphalt in the RA, however, can lessen the severity of these impacts as these constituent elements form a weak link with the cement matrix [18].

Die approbierte gedruckte Originalversion dieser Diplomarbeit ist an der TU Wien Bibliothek verfügbar
The approved original version of this thesis is available in print at TU Wien Bibliothek.
TU Bibliothek Your knowledge hub WIEN

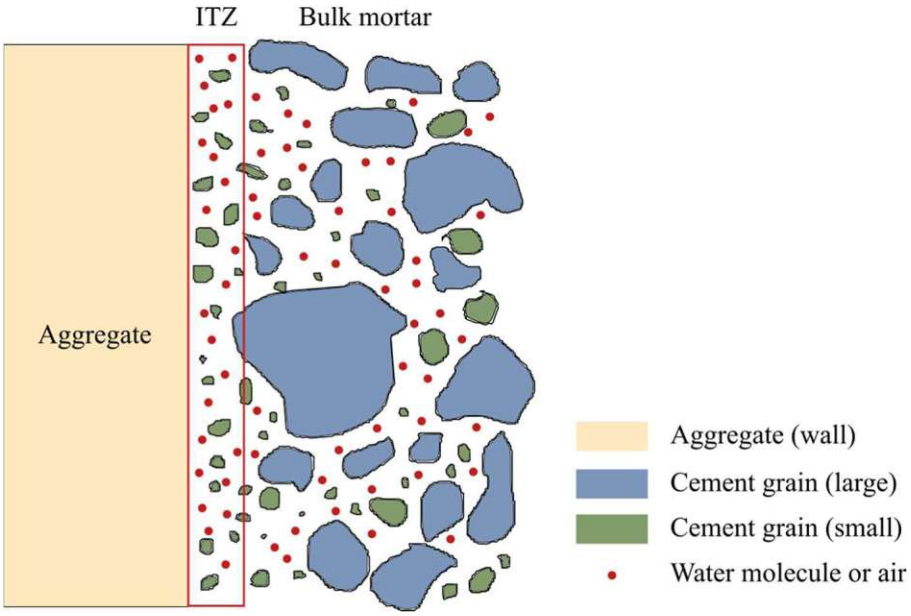

Fig. 3: Illustration of the formation of the ITZ along the aggregate surface from Wang et al. [15]

With the presence of two ITZs in RAC, its structure is more intricate than that of natural aggregate concrete. As shown in **Fig. 4**, there is one ITZ in RAC between the natural aggregate and the old mortar (old ITZ) and another between the recycled aggregate and the new cement paste (new ITZ). The high porosity of the old ITZ increases water absorption during mixing, leaving less water available for hydration alongside the RAs, and its voids and cracks impair the bonding between the cement paste and the RAs [13].

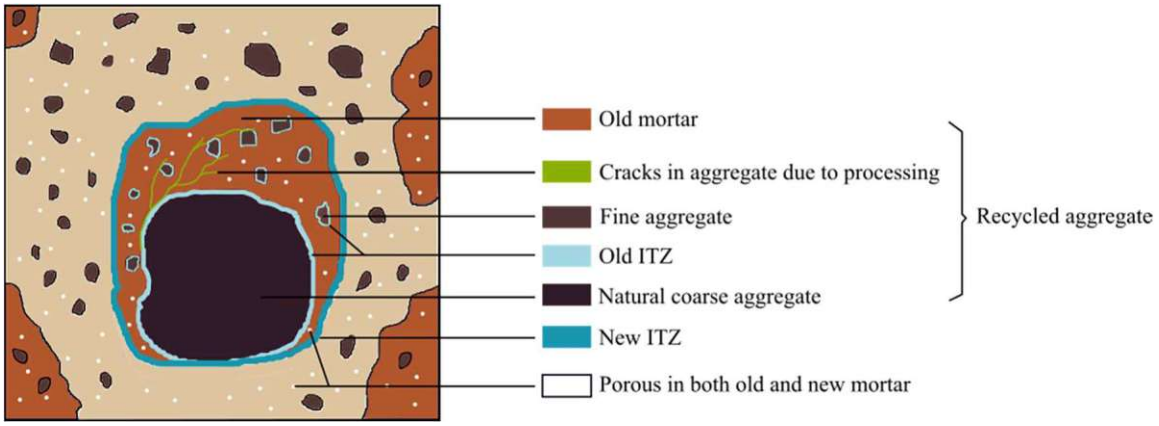

Fig. 4: Illustration of RA in RAC from Wang et al. [15]

2.2 Challenges in the use of RCA in Concrete

Due to the distinct characteristics of RCA in comparison to NA, and the variation of its characteristics based on the source material and the crushing and processing methods, concrete made with RCA can present very inconsistent properties. In general, RAC performance is inferior to that of NAC in terms of strength (compressive, flexural and tensile strength) and durability (permeability, chloride resistance, freeze-thaw-resistance) [15].

Die approbierte gedruckte Originalversion dieser Diplomarbeit ist an der TU Wien Bibliothek verfügbar
The approved original version of this thesis is available in print at TU Wien Bibliothek.
TU Bibliothek Your knowledge hub WIEN

In addition to the challenges regarding the quality of the recycled aggregate, a large-scale use of RCA is limited by the economic viability of high-quality RCA. Low costs for NA and for landfill disposal compared to high costs for the transport and production process of RCA restricts the demand for RCA [19].

Moreover, the use of RA in concrete is limited by restrictive standards, unclear regulations, and lack of trust in the quality of recycled building materials. These issues reduce demand and hinder the development of efficient infrastructure for the recycling and management of CDW. In the EU, only around 6% of recycled concrete is reused in concrete production, while Switzerland leads with 25%, driven by supportive legal framework and high natural aggregate costs resulting from resource scarcity [19].

Die approbierte gedruckte Originalversion dieser Diplomarbeit ist an der TU Wien Bibliothek verfügbar
The approved original version of this thesis is available in print at TU Wien Bibliothek.
TU Bibliothek Your knowledge hub WIEN

3 Materials and Methods

3.1 B7 Concrete according to ÖNORM B 4710-1

In the Austrian standard for concrete and reinforced concrete ÖNORM B 4710-1 [20], different types of concrete are classified using short designations. These designations are designed to simplify the selection of concrete mixtures for various environmental conditions based on the durability and resistance of the concrete to specific exposure classes. The short designations (e.g., B1, B2, B3, etc.) provide guidelines for properties such as water-binder ratio (W/B) and air content, ensuring the appropriate concrete mix for specific use cases.

This experimental study investigates the incorporation of recycled concrete aggregates in B7 concrete. B7 concrete is designed for usage in highly aggressive environments and must withstand severe stresses during its service life. To ensure its durability and longevity, the standard defines high requirements regarding exposure to environmental conditions.

B7 concrete as defined in ÖNORM B4710-1 covers the exposure classes XC4, XW2, XD3, XF4 and XA1L (A). They are detailed as follows:

- **XC exposure classes:** Exposure classes for corrosion risk caused by carbonation
  XC4: Corrosion induced by carbonation under alternating wet and dry cycles
- **XW exposure classes:** Exposure classes for water impermeability
  XW2: Water impermeability against pressing water for water heights over 10m
- **XD exposure classes:** Exposure classes for corrosion risk caused by chlorides, excluding seawater
  XD3: Corrosion induced by an increased chloride contamination from water, including de-icing salt but excluding seawater, in alternating wet and dry conditions
- **XF exposure classes:** Exposure classes for risk of frost attack with or without de-icing agents
  XF4: Freeze-thaw attack under high water saturation with de-icing agent
- **XA exposure classes**: Exposure classes for chemical attack
  XA1L (A): Dissolving chemical attack in mildly aggressive environments

In addition to the exposure classes, the standard stipulates the following limit values for:

- **Air Content**: 4,5 to 8,5 % for 16 mm maximum aggregate size
- **Water-Binder Ratio (W/B)**: ≤ 0,45

Die approbierte gedruckte Originalversion dieser Diplomarbeit ist an der TU Wien Bibliothek verfügbar
The approved original version of this thesis is available in print at TU Wien Bibliothek.
TU Bibliothek Your knowledge hub WIEN

B7 concrete is conceived for environments where concrete faces extreme freeze-thaw cycles, high chloride exposure, and strong chemical attack. The air content is increased to provide additional freeze-thaw protection, and the low water-binder ratio ensures reduced permeability, which prevents chloride ingress. B7 concrete is used in highly demanding conditions where both mechanical and chemical durability are important. The usual fields of application for B7 concrete are road pavements, bridge slabs, traffic barriers and parking decks.

3.2 Materials

The components listed in **Tab. 1** were used for the preparation of the concrete samples tested during the experimental campaign.

Tab. 1: Components of the B7 concrete mixtures

Material	Name	Manufacturer
Cement	Portland composite cement CEM II/B-M (S-LL) 42,5 N	Rohdorfer
Supplementary Cementitious Materials	AHWZ-Flumix	Baumit
Superplasticiser for NAs	Dynamon SF 14S	Mapei
Superplasticiser for RAs	Dynamon RC 910	Mapei
Air-Entraining Agent	Mapeair LP X9	Mapei
Natural aggregates 0-4 and 4-16	NA 0-4 NA 4-16	Lasselsberger
Recycled aggregates 0-4 and 4-16	RB 0-4 gew. RB 4-16 ungew.	Lasselsberger

3.2.1 Cement

Cement as a hydraulic binder, is one of the main components of concrete. The cement matrix formed after hydration defines the characteristics and performance of the concrete. Due to the high energy demand during the production of Portland clinker, and the large amount of carbon dioxide emitted in the process, there has been an ongoing shift towards the utilization of blended cements in which parts of the clinker are substituted with latent hydraulic or pozzolanic additives, often obtained as by-products of the industry. The addition of these supplementary cementitious materials (SCM) allows the production of a more sustainable binder and furthermore improves the workability, the strength development and the durability aspects of the concrete [21].

During this experimental campaign, we used a Portland composite cement CEM II (**Fig. 5**) according to ÖNORM EN 197-1 [22] provided by *Rohdorfer Baustoffe Austria GmbH*. Its properties are as described in the following:

- **Type**: Portland Composite Cement CEM II/B-M (S-LL) 42,5 N.

Die approbierte gedruckte Originalversion dieser Diplomarbeit ist an der TU Wien Bibliothek verfügbar
The approved original version of this thesis is available in print at TU Wien Bibliothek.

- **Composition**: According to ÖNORM EN 197-1, CEM II/B-M is a Portland composite cement that consists of 65 to 79% clinker by mass. The remaining portion consists of granulated blast furnace slag (S) and limestone (LL).

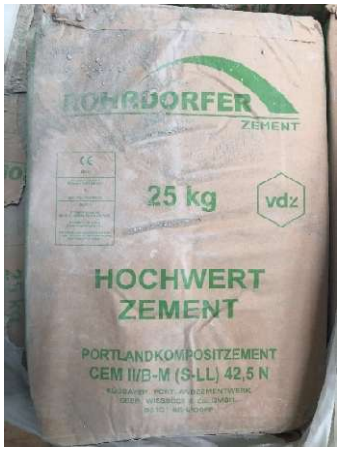

Fig. 5: Image of cement bag used for concrete production during the experimental campaign [photo by author]

3.2.2 Supplementary Cementitious Materials

The concrete mixture designs incorporate supplementary cementitious materials both as a cement component as a substitute for Portland clinker, and as a concrete ingredient replacing cement. As stated above, the Portland composite cement includes ground granulated blast furnace slag (GGBFS) and limestone powder. In addition to that, the processed hydraulic additive (AHWZ: *„aufbereitete, hydraulisch wirksame Zusatzstoffe"*) is added during the mixing process. The AHWZ is labelled GC/GC-HS and is a combination product of GGBFS, fly ash, and limestone powder in specific proportions provided in ÖNORM B 3309-1 [23].

3.2.2.1 Ground Granulated Blast Furnace Slag

Molten slag from the smelting of iron ore in a blast furnace is quickly cooled to create blast furnace slag. Its hydraulic properties improve the strength and durability of the concrete. To guarantee that its hydraulic activity is appropriate, GGBFS must be finely ground.

By partially replacing the fast-reacting ordinary Portland cement (OPC), which is hydraulically active and hydrates quickly, with the latent hydraulic and slower reacting suitably Ground GGBFS, the rate of heat generation and total hydration heat during the curing of concrete is reduced. This is particularly beneficial for mass concrete as it helps prevent cracks that could occur from thermal shrinkage. This replacement also enhances the workability of the concrete. As a result, there can be a decrease in the water/binder ratio, the amount of superplasticizer, or the paste content compared to a mix based solely on Portland cement [24], [25]. The slower Hydration rate of GGBFS leads to a delayed setting time and a lower com-

Die approbierte gedruckte Originalversion dieser Diplomarbeit ist an der TU Wien Bibliothek verfügbar
The approved original version of this thesis is available in print at TU Wien Bibliothek.
TU Bibliothek Your knowledge hub WIEN

pressive strength at an early age. However, the compressive strength development in slag concrete is superior, and its late strength usually surpasses that of Portland concrete [26].

3.2.2.2 Fly Ash

Fly ash is a by-product of coal-fired power plants resulting from the combustion of pulverised coal. It has become widely accepted as a substitute for cement in concrete for conventional structural applications. This utilization offers several significant advantages, both in terms of material properties and environmental impact. Concrete mixtures containing fly ash demonstrate better consistency during the fresh stage due to the ball-bearing effect of spherical fly ash particles. The incorporation of fly ash also leads to improved strength, reduced water requirements, and an extended service life of concrete structures. This is partly due to the pozzolanic reaction of fly ash, which helps reduce permeability and minimises the exposure of concrete to damaging agents like moisture, oxygen, chlorides, and carbon dioxide. Furthermore, fly ash-based concrete exhibits reduced corrosion of reinforcing steel due to the refined pore structure, making it more resistant to corrosion, freeze-thaw cycles, and aggressive chemicals [27], [28].

3.2.2.3 Limestone Powder

Limestone powder is used in concrete, both as a supplementary cementitious material and as a filler. It improves the particle size distribution of cement when interground with clinker, enhancing the overall performance of the composite cement. When added separately, limestone powder helps produce more stable and robust mixes, it can improve fresh concrete workability and flow without changing the water-binder ratio or adding chemical admixtures. In the hardened state, limestone-modified concrete exhibits better strength development and helps mitigate sulphate attack, improving durability in aggressive environments [29].

The limestone used in the cement has a calcium carbonate (CaCO3) content of at least 75% by mass, contributing to improved workability and long-term durability of the concrete. The clay content does not exceed 1.20 g/100 g, and the total organic carbon (TOC) content is below 0.20% by mass.

3.2.3 Natural Aggregates

In terms of quantity and volume, aggregates represent the main component of concrete, accounting for about 60 – 80% of the total concrete volume. Therefore, their properties also largely determine those of the concrete.

Die approbierte gedruckte Originalversion dieser Diplomarbeit ist an der TU Wien Bibliothek verfügbar
The approved original version of this thesis is available in print at TU Wien Bibliothek.
TU Bibliothek Your knowledge hub WIEN

Aggregates are the primary structural material, providing bulk and strength to the concrete and forming a solid matrix with the cement paste, but they influence both the fresh and hardened properties of the mix.

The particle size distribution of aggregates is particularly important as it affects the compaction and overall performance of concrete. Well-graded aggregates help achieve a stable mixture with a low amount of entrapped air voids, resulting in stronger and more durable concrete. The geometric, physical and chemical requirements for concrete aggregates are defined depending on the type of use and the origin of the aggregate.

In ÖNORM EN 12620 [30], general grading requirements are specified for concrete aggregates depending on their size designation d/D, as shown in **Fig. 6**.

Aggregate	Size	Percentage passing by mass					Category G_d
		2 D	1,4 D [a, b]	D [c]	d [b]	$d/2$ [a, b]	
Coarse	$D/d \leq 2$ or $D \leq 11{,}2$ mm	100 100	98 to 100 98 to 100	85 to 99 80 to 99	0 to 20 0 to 20	0 to 5 0 to 5	G_C85/20 G_C80/20
	$D/d > 2$ and $D > 11{,}2$ mm	100	98 to 100	90 to 99	0 to 15	0 to 5	G_C90/15
Fine	$D \leq 4$ mm and $d = 0$	100	95 to 100	85 to 99	–	–	G_F85
Natural graded 0/8	$D = 8$ mm and $d = 0$	100	98 to 100	90 to 99	–	–	G_{NG}90
All-in	$D \leq 45$ mm and $d = 0$	100 100	98 to 100 98 to 100	90 to 99 85 to 99	–	–	G_A90 G_A85

[a] Where the sieves calculated are not exact sieve numbers in the ISO 565:1990 R 20 series then the next nearest sieve size shall be adopted.

[b] For gap graded concrete or other special uses additional requirements may be specified.

[c] The percentage passing D may be greater than 99 % by mass but in such cases the producer shall document and declare the typical grading including the sieves D, d, $d/2$ and sieves in the basic set plus set 1 or basic set plus set 2 intermediate between d and D. Sieves with a ratio less than 1,4 times the next lower sieve may be excluded.

[d] Other aggregate product standards have different requirements for categories.

Fig. 6: General grading requirements for aggregates as specified in ÖNORM EN 12620 [30]

The natural aggregates used in the concrete mixtures during this experimental campaign are divided into two fractions (**Fig. 7**) depending on the particle size:

- Fraction 0/4: Fine natural aggregates, hereafter referred to as NA 0-4
- Fraction 4/16: Coarse natural aggregates, hereafter referred to as NA 4-16

Die approbierte gedruckte Originalversion dieser Diplomarbeit ist an der TU Wien Bibliothek verfügbar
The approved original version of this thesis is available in print at TU Wien Bibliothek.

(a) (b)

Fig. 7: Images of (a) fine natural aggregates NA 0-4, and (b) coarse natural aggregates NA 4-16 [photo by author]

The particle size distributions for the fine and coarse NAs were determined in the laboratory using the sieving machine *Beckel SM Basic 3000 ZN* and were found to comply with the normative requirements. The results are represented in **Fig. 9**.

Tab. 2 shows the grading requirements for NA 0-4 and NA 4-16 according to ÖNORM EN 12620 as specified in **Fig. 6**.

Tab. 2: Grading requirements for NA 0-4 and NA 4-16

Aggregate	Particle size	Percentage passing by mass					Category
		2 D	*1,4 D*	*D*	*d*	*d/2*	***G***
NA 4-16	$D/d > 2$ and $D > 11{,}2$ mm	100%	100%	94,40%	2,38%	2,16%	$G_c90/15$
NA 0-4	$D \leq 4$ and $d = 0$	100%	-	87,12%	-	-	G_f85

The requirements for natural aggregates as stated in the ÖNORM EN 12620, are not discussed in this section, as they are not the subject of the study.

3.2.4 Recycled Concrete Aggregates

The recycled concrete aggregates used for this experimental campaign were provided by *Lasselsberger GmbH*. The aggregate mixture is composed of two separately processed aggregate fractions (**Fig. 8**):

- Fraction 0/4: Fine recycled aggregates with the designation *"RB 0-4 gew.Lasselsberger"*, hereafter referred to as RB LSB 0-4
- Fraction 4/16: Coarse recycled aggregates with the designation *"RB 4-16 ungew. Lasselsberger"*, hereafter referred to as RB LSB 4-16

Die approbierte gedruckte Originalversion dieser Diplomarbeit ist an der TU Wien Bibliothek verfügbar
The approved original version of this thesis is available in print at TU Wien Bibliothek.

(a) (b)

Fig. 8: Images of (a) recycled fine concrete aggregates RB LSB 0-4 and (b) recycled coarse concrete aggregates RB LSB 4-16 [photo by author]

The particle size distributions of the RCA fractions were determined in the lab similar to the procedure with NAs. The grading curves of aggregate fractions from NAs and RCAs are shown in **Fig. 9**. The grading curves of natural and recycled aggregates differ from each other, with the difference being more pronounced for the coarse aggregate fractions. Herein, we determined that the amount of particles from 4 to 8 mm in the RCA is almost half of the amount in NA. The differences between the NA 0-4 and RB LSB 0-4 fractions are less pronounced.

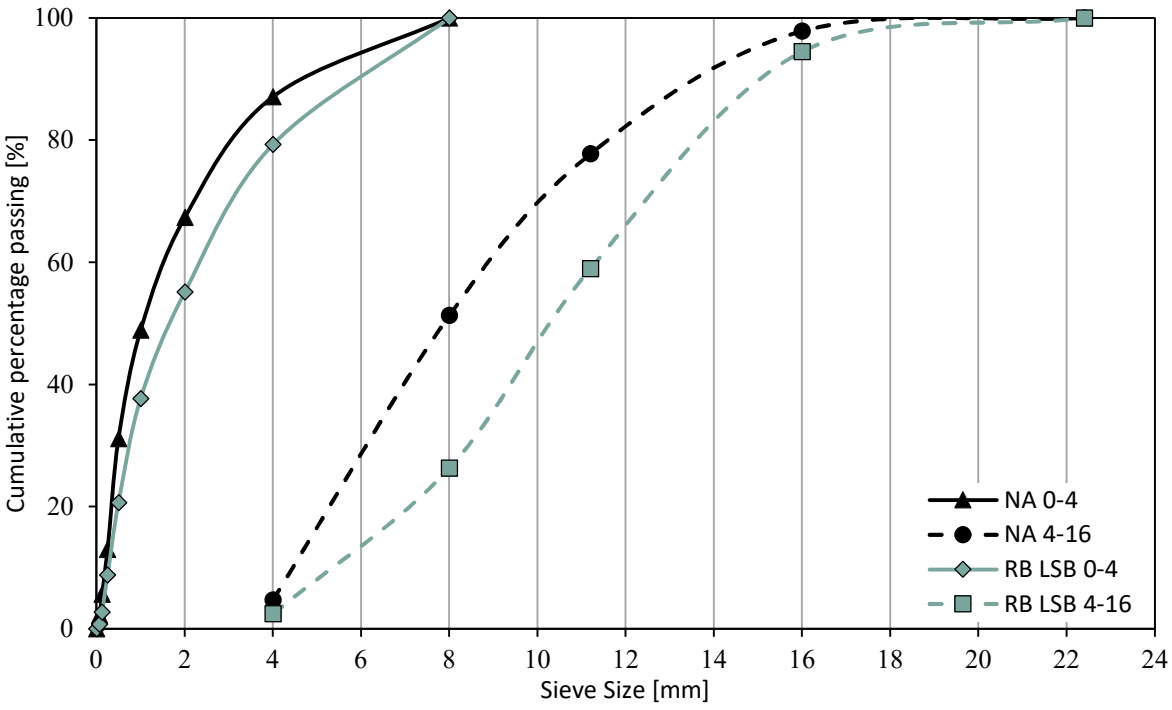

Fig. 9: Aggregate particle size distribution of NA 0-4, NA 4-16, RB LSB 0-4 and RB LSB 4-16

The recycled aggregates are assigned to the category RB-A1 as defined in ÖNORM B 3140 [31], indicating the highest quality for use in structural concrete as they are sourced from un-

Die approbierte gedruckte Originalversion dieser Diplomarbeit ist an der TU Wien Bibliothek verfügbar
The approved original version of this thesis is available in print at TU Wien Bibliothek.
TU Bibliothek Your knowledge hub WIEN

corrupted demolished concrete and have minimal amounts of impurities. The constituents of the aggregate fraction according to ÖNORM EN 12620 are presented in **Tab. 3**:

Tab. 3: Constituents of recycled aggregates RB LSB 0-4 and RB LSB 4-16

Constituents	**Content** [Mass-%]	**Limit value according to EN 12620** [Mass-%]
Rc	95,0	≥ 90
Ru	3,5	No requirement
Rc + Ru	98,5	≥ 95
Rb	0,8	No requirement
Ra	0,7	≤ 1
X+Rg	0,0	≤ 1

Where according to EN 12620 [30]:

Rc: *„Concrete, concrete products, mortar, concrete masonry units"*

Ru: *„Unbound aggregate, natural stone, hydraulically bound aggregate"*

Rb: *„Clay masonry units (i.e. bricks and tiles), calcium silicate masonry units, aerated non-floating concrete"*

Ra: *„Bituminous materials"*

X: *„Other:*

cohesive materials (i.e. clay and soil)

Miscellaneous: Metals (ferrous or non-ferrous), non-floating wood, plastic and rubber, gypsum plaster"

Rg: *„Glass"*

The RCAs meet the minimum requirements for recycled aggregates for B7 concrete designations dictated by the ÖNORM B 4710-1 Table E.2, as presented in **Tab. 4**.

Die approbierte gedruckte Originalversion dieser Diplomarbeit ist an der TU Wien Bibliothek verfügbar
The approved original version of this thesis is available in print at TU Wien Bibliothek.

Tab. 4: Requirements for recycled aggregates for B7 concrete according to ÖNORM B 4710-1 [20]

Requirements for aggregates	B7 concrete		
	ÖNORM B 4710-1	**RB LSB 0-4**	**RB LSB 4-16**
Particle density	≥ 2,00 Mg/m³	2,31 Mg/m³	2,47 Mg/m³
particle size distribution > 4 mm	$G_c90/15$	-	passed
particle size distribution ≤ 4 mm	G_f85	passed	-
Shape of coarse aggregate	FI_{NR}	-	-
	SI_{40}	-	NA
Shell content of coarse aggregate	SC_{10}	-	NA
Fines content of coarse aggregate	$f_{1,5}$	-	1,40 %
Fines content of fine aggregate	f_3	2,30 %	-
Fines quality	passed	passed	passed
freeze-thaw resistance > 4 mm	F_1	-	NA
freeze-thaw resistance ≤ 4 mm	FS_1	NA	-
Volume stability - drying shrinkage	passed (≤ 0,075 %)	NA	NA
Acid-soluble chloride ion content	≤ 0,01 %	< 0,01 %	< 0,01 %
Water-soluble sulphate content	$SS_{0,2}$	< 0,01 %	< 0,01 %
Acid-soluble sulphate content	$AS_{0,8}$	0,27 %	0,27 %
Influence of water-soluble materials from RA on the initial setting time of cement paste	A_{10}	10 min	NA

According to ÖNORM EN 1097-6 [32], the water absorption capacity of RA was determined to be 11,1% for fine aggregates and 6,2% for coarse aggregates. It is significantly higher than absorption capacity of natural fine and coarse aggregates (**Fig. 10**) and represents one of the main disadvantages of RCA. The higher absorption capacity can lead to challenges with the mix design and may have an impact on the concrete's strength and workability. It is particularly challenging to anticipate the behaviour of the concrete mix due to the fluctuation in water absorption, necessitating careful adjustments throughout production.

Die approbierte gedruckte Originalversion dieser Diplomarbeit ist an der TU Wien Bibliothek verfügbar
The approved original version of this thesis is available in print at TU Wien Bibliothek.

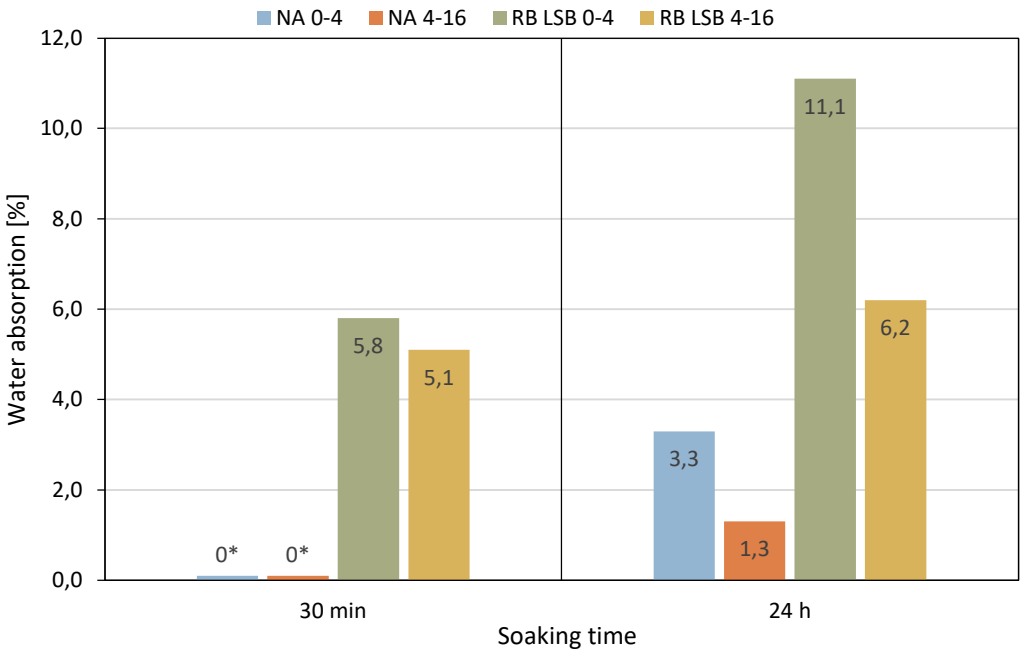

*The water absorption of NA 0-4 and NA 4-16 after 30 min soaking time was found to be < 1,5% which was assumed as 0% according to ONR 23303

Fig. 10: Water absorption capacity of NA 0-4, NA 4-16, RB LSB 0-4 and RB LSB 4-16

3.2.4.1 Pre-saturation of the RCAs

As previously established, the high porosity of the old mortar attached to the RCA, and the consequential high water-absorption of the aggregate cause some of the mixing water to be absorbed, thereby modifying the Water/Binder-ratio (w/b-ratio) and affecting the strength and durability properties of the concrete. Various studies have suggested that a pre-saturation of the RCA can have a positive impact, as it prevents the excessive water absorption around the surface of the aggregates and strengthens the new ITZ.

Through pre-saturating the aggregates to around 50% of their absorption capacity, García-González et al. [33] reported an improvement of the consistency of the fresh concrete, and a loss of compressive strength of only about 13% when using 100% RCA. Brand et al. [34] compared the strength performance of RAC using aggregates with different moisture conditions and found that the highest compressive strength is achieved with the partially saturated (80% saturated surface dry) RCA. A complete saturation of the aggregates can prove detrimental, as it can lead to lower compressive strength due to "bleeding" of excess water [35].

Based on these findings, we aimed for an 80% partial pre-saturation of the recycled aggregates used during these tests. To achieve that, first the water content of the RCA was determined, the amount of water necessary to reach an 80% saturation was calculated and added to the aggregates evenly. The aggregates were then stored in a sealed plastic box to achieve an equal distribution of the moisture content.

Die approbierte gedruckte Originalversion dieser Diplomarbeit ist an der TU Wien Bibliothek verfügbar
The approved original version of this thesis is available in print at TU Wien Bibliothek.

3.2.5 Water

Potable tap water was used throughout the experiment for mixing and curing, it is free from contaminants that could adversely affect the concrete's setting and curing process.

3.2.6 Admixtures

Chemical admixtures are crucial ingredients in contemporary concrete technology, as they enable precise control of both the fresh and hardened properties of concrete. They are used to improve construction-related properties such as workability, pumpability, setting behaviour and surface quality, while optimising long-term performance aspects such as mechanical strength, durability, frost-thaw resistance and shrinkage behaviour [36].

Air-entraining agents (AEAs) and superplasticisers (SPs) were used in the production of the concrete for this study. These are essential for the production of concrete with a high air content and low water-binder ratio. AEAs introduce microscopic, evenly distributed air voids into the concrete matrix, which significantly improve resistance to freeze–thaw cycles and scaling by allowing water to expand as it freezes.

Superplasticisers, on the other hand, improve the flowability of fresh concrete, and thus enable the production of concrete with high workability while maintaining a low water-binder ratio.

The admixtures used are presented in the following:

- **MAPEI Dynamon SF 14S**:

A universal superplasticiser based on polycarboxylate ether, used to enhance workability and reduce the w/b-ratio without compromising strength or durability (**Fig. 11**). *Dynamon SF 14S* superplasticiser was used exclusively for concrete mixtures containing NA.

According to the manufacturer, this product should provide excellent slump retention and low stickiness, allowing for high water reduction, leading to higher strength, lower permeability, and increased durability.

Die approbierte gedruckte Originalversion dieser Diplomarbeit ist an der TU Wien Bibliothek verfügbar
The approved original version of this thesis is available in print at TU Wien Bibliothek.

Fig. 11: Image of the superplasticiser *MAPEI Dynamon SF 14S* [photo by author]

- **MAPEI Dynamon RC 910**:

A universal superplasticiser based on polycarboxylate ether for ready-mixed concrete. It is designed for use with absorbent raw materials such as recycled aggregates (**Fig. 12**). *Dynamon RC 910* superplasticiser was used for concrete mixtures containing RA.

Fig. 12: Image of the Superplasticiser *MAPEI Dynamon RC 910* [photo by author]

According to the manufacturer, this product should improve strength, lower permeability, and enhance durability, making it ideal for mixes with RCA.

- **MAPEI Mapeair LP X9**:

An air-entraining agent used to improve frost resistance in concrete, especially in environments exposed to freeze-thaw cycles and de-icing agents.

According to the manufacturer, *Mapeair LP X9* (**Fig. 13**) enhances workability by creating small, closed air pockets, reducing capillary absorption, and providing space for freezing water, thus increasing durability.

Die approbierte gedruckte Originalversion dieser Diplomarbeit ist an der TU Wien Bibliothek verfügbar
The approved original version of this thesis is available in print at TU Wien Bibliothek.
TU Bibliothek Your knowledge hub WIEN

Fig. 13: Image of air-entraining-agent *MAPEI Mapeair LP X9* [photo by author]

3.3 Mixture Design

The mixture Design for the B7 concrete was developed in accordance with the requirements for the designated environmental conditions and the restrictions for the concrete composition according to the standard ÖNORM B 4710-1. The design was then optimised based on the input and expertise of the project partners involved in project *"UP!crete*".

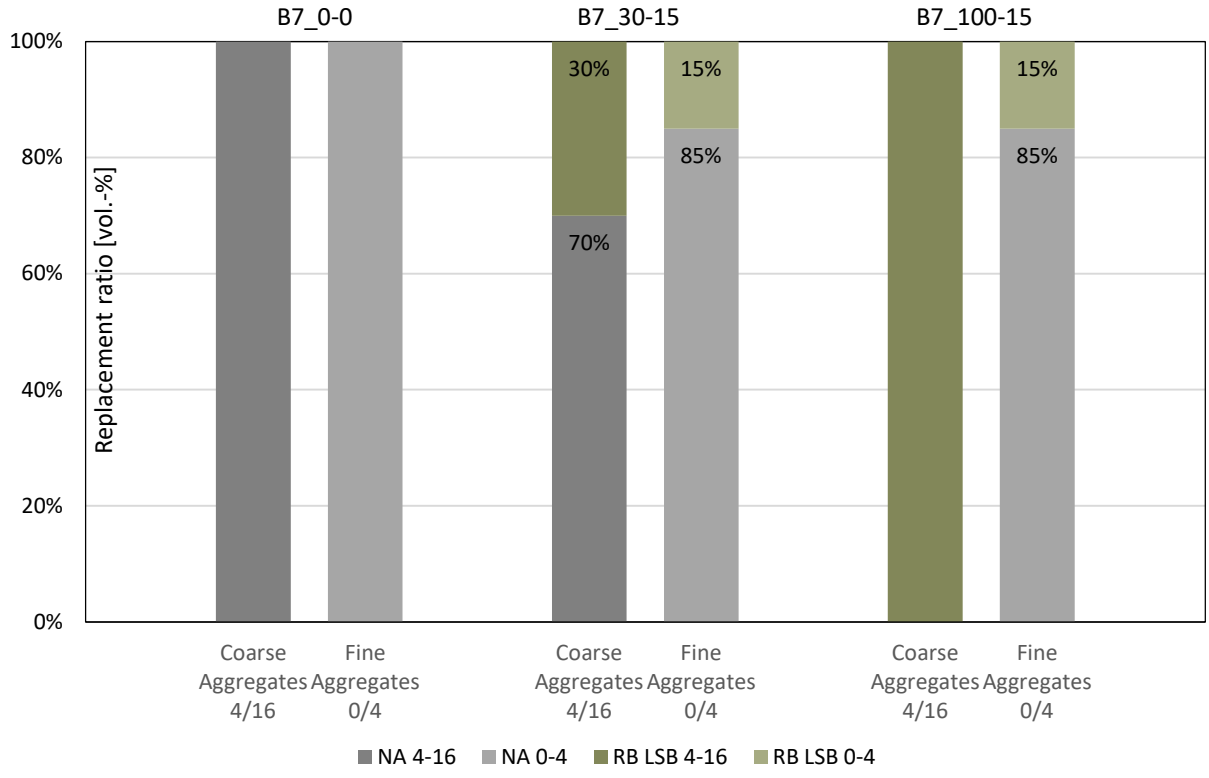

Fig. 14: Aggregate replacement ratios for the concrete mixtures

For the tests conducted within the scope of this thesis, three concrete mixtures with different aggregate replacement ratios were produced, with the first mix, including only natural

Die approbierte gedruckte Originalversion dieser Diplomarbeit ist an der TU Wien Bibliothek verfügbar
The approved original version of this thesis is available in print at TU Wien Bibliothek.
TU Bibliothek Your knowledge hub WIEN

aggregates and serving as a reference (hereafter referred to as B7_0-0). For the second mix, 30 vol.-% of the coarse natural aggregates NA 4-16 were replaced with the coarse recycled concrete aggregates RB LSB 4-16, along with 15 vol.-% of the fine natural aggregates NA 0-4 that were replaced with the fine recycle concrete aggregates RB LSB 0-4 (hereafter referred to as B7_30-15). In the third concrete mix, the coarse aggregates are entirely consisting of recycled aggregates RB LSB 4-16, with the replacement rate for the fine aggregates kept identical to the second mix at 15 vol.-% (hereafter referred to as B7_100-15). **Fig. 14** summarises the use of aggregates for the three concrete mixes.

The mixing ratio of fine and coarse aggregates for the produced concrete is 55% by mass of fine aggregates and 45% of coarse aggregates. The resulting combined aggregate gradation curves for B7_0-0, B7_30-15 and B7_100-15 concrete mixtures are illustrated in **Fig. 15**. The RAC curves mainly differ from the B7_0-0 sieve line in the proportions of sand and fine gravel, with the ratio of aggregates from 0,5 to 4,0 mm increasing and the ratio of aggregates from 4,0 to 8,0 mm decreasing equally.

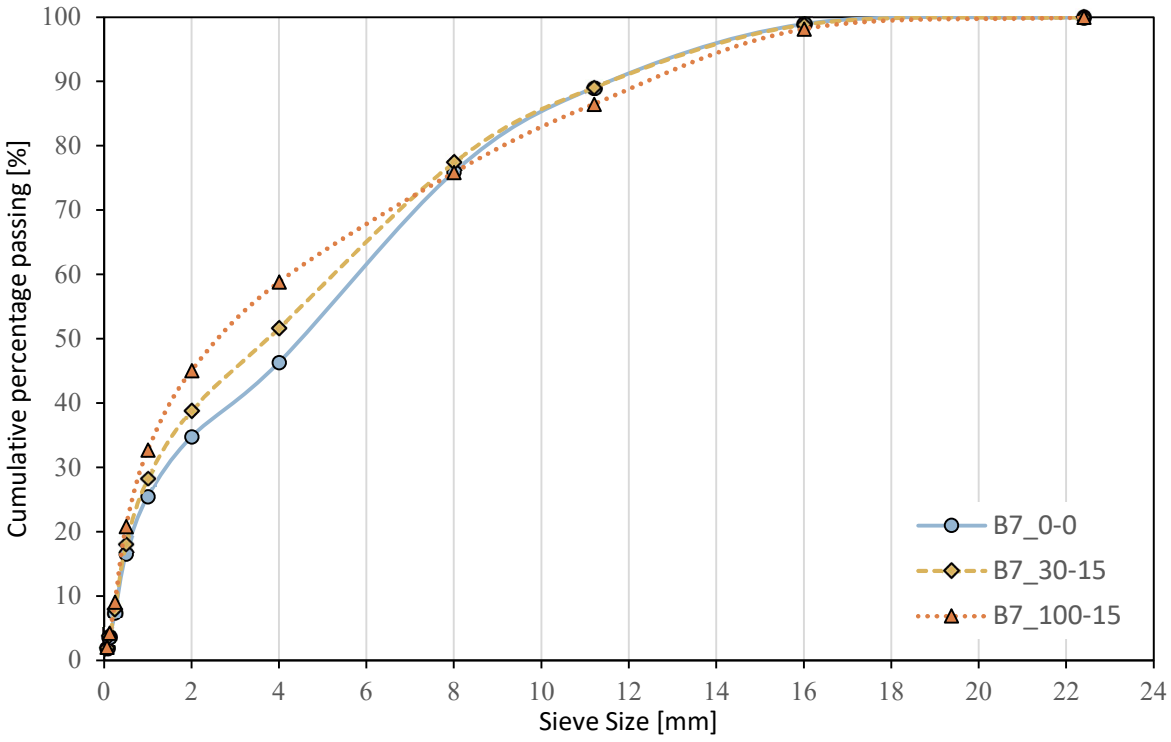

Fig. 15: Particle size distribution of aggregates used for B7_0-0, B7_30-15, and B7_100_15

To counter the alteration of the fresh and hardened concrete properties resulting from the inclusion of RCA and to reach our targeted concrete properties, the amounts of superplasticiser and air-entraining agent added in the concrete recipe were adapted.

Die approbierte gedruckte Originalversion dieser Diplomarbeit ist an der TU Wien Bibliothek verfügbar
The approved original version of this thesis is available in print at TU Wien Bibliothek.
TU Bibliothek Your knowledge hub WIEN

Tab. 5 presents the recipes for all three concrete mixtures, B7_0-0, B7_30-15, and B7_100-15, tested during this campaign. The values shown in the table are for the production of 1 m³ of concrete.

Tab. 5: Concrete recipe to produce 1 m^3 of concrete

Components		Mass [Kg]		
		B7_0-0	B7_30-15	B7_100-15
Water		180	180	180
Cement		378	378	378
Supplementary cementitious materials		42	42	42
Superplasticiser		2,82	3,15	3,69
Air-Entraining Agent		1,13	1,31	1,33
Aggregate	NA 0-4	871	741	739
	NA 4-16	761	534	0
	RB LSB 0-4	0	109	104
	RB LSB 4-16	0	199	636
	Aggregate total	1632	1583	1479
Total		**2236**	**2187**	**2084**

3.4 Mixing Approach – Two-stage Mixing Approach

In addition to the partial pre-saturation of the RCA as a measure to improve the properties of the produced concrete, a two-stage mixing approach (TSMA) was implemented during the mixing process for the three concrete mixtures.

Studies suggest that the TSMA offers advantages in terms of consistency, workability, and overall strength, especially for concrete with large ratios of recycled aggregates.

Based on the two-stage mixing approach proposed by Tam et al. (2005) [13], an adapted two-stage mixing approach (hereinafter referred to as $TSMA_{Ad}$) was used to produce the concrete and minimise the negative effects of the incorporation of RCA on the fresh and hardened concrete properties, mainly the high water-absorption. In contrast to the normal mixing approach (NMA), the TSMA splits the mixing process into two phases, adding water in two separate stages at different moments of the mixing process. **Fig. 16** illustrates the main steps of the three mentioned mixing approaches.

Die approbierte gedruckte Originalversion dieser Diplomarbeit ist an der TU Wien Bibliothek verfügbar
The approved original version of this thesis is available in print at TU Wien Bibliothek.

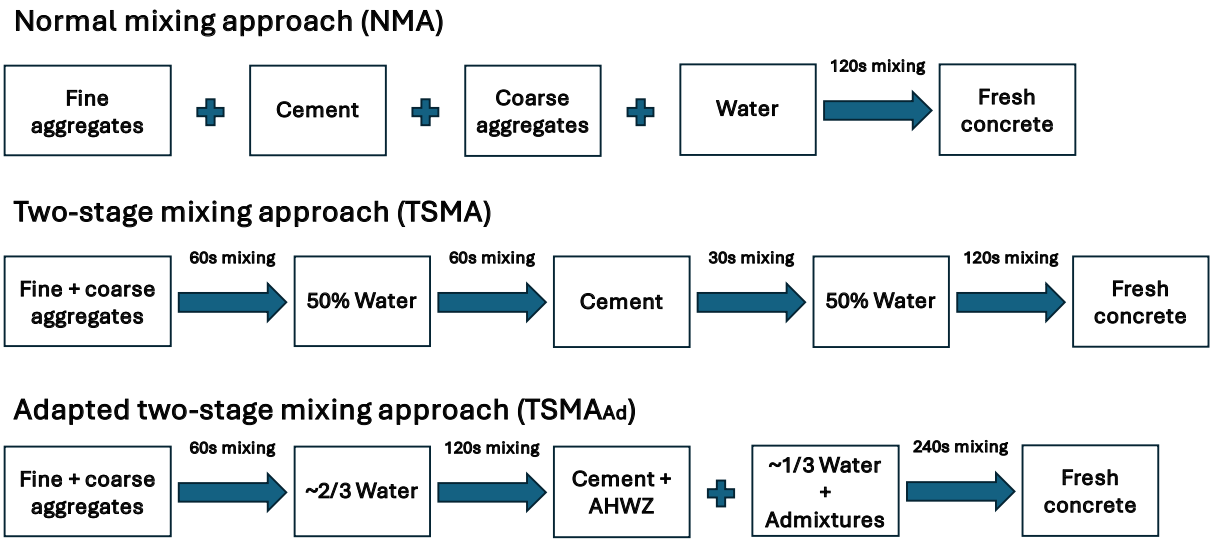

Fig. 16: Flow diagram with the stages of the different mixing approaches: NMA [13], TSMA [13], $TSMA_{Ad}$ used in this study

The strength and durability of the RAC are decreased due to the cracks and pores in the old ITZ, which increase the aggregates' water absorption and thereby decrease the quantity of hydration water available for cement hydration, especially in the new ITZ that forms between the RA and the mortar. The cracks and pores in the old ITZ increase the water absorption of the aggregates, which reduces the water available for cement hydration, particularly in the new ITZ formed between the RA and the mortar and thereby reduces the strength and durability of the RAC. During the first phase of the TSMA, when RCA is mixed with water, a thin layer of cement slurry forms on the aggregate surface, penetrating the cracks and pores in the old ITZ and effectively sealing them. Scanning electron microscopy images show that, when using the TSMA, the cracks in the RA are filled, and sufficient water is available in the new ITZ between the RA and the mortar. As a result, both the new and old ITZs are stronger and denser when using the TSMA [13]. Other studies conducted on the effects of the TSMA on RAC have confirmed an improvement of the compressive strength of concrete produced of up to 20% using the TSMA when compared to the same concrete produced with the NMA [37], [38].

Tab. 6: Mixing stages and durations for the $TSMA_{Ad}$

Mixing stage	Duration
mixing coarse and fine aggregates	1 min
adding 2/3 of the mixing water	-
mixing	2 min
adding binder	-
adding 1/3 of the mixing water + Superplasticiser and Air-entraining Agent	-
mixing	4 min

Die approbierte gedruckte Originalversion dieser Diplomarbeit ist an der TU Wien Bibliothek verfügbar
The approved original version of this thesis is available in print at TU Wien Bibliothek.

3.5 Specimen Preparation

During the experimental campaign, the compressive strength, the chloride resistance, the freeze-thaw-resistance, the depth of penetration, and the carbonation of the concrete have been experimentally investigated. For each test, the corresponding standards specify the size, form and other specifications required for the tested specimens and the casting moulds. An overview of the specimens needed for each test is presented in **Tab. 7**.

Tab. 7: Specimens required for the experimental campaign

Test	Number of Specimens	Specimen size [mm*mm*mm]
Compressive strength	11	150x150x150
Chloride resistance Air void analysis	2	150x150x150
Freeze-thaw-resistance	4	150x150x150
Depth of penetration	3	200x200x120
Carbonation	2	100x100x400

For all the specimens, calibrated steel moulds (**Fig. 17**) were used, as they are watertight and non-absorbent, and meet stricter tolerances. The inside of the moulds was coated with a thin layer of mould-oil to avoid the adhesion of the concrete from to the mould and seal the joints.

Fig. 17: Steel moulds used to cast the specimens [photo by author]

After filling the moulds with the prepared concrete using a scoop, the concrete was immediately compacted using the *Beckel B3000* concrete vibrating table (**Fig. 18**) for a duration of 12 seconds. This time was found to be adequate to achieve complete compaction of the concrete without loss of entrained air or segregation. Using a trowel, the extra concrete was removed, and the surface was carefully levelled.

Die approbierte gedruckte Originalversion dieser Diplomarbeit ist an der TU Wien Bibliothek verfügbar
The approved original version of this thesis is available in print at TU Wien Bibliothek.
TU Bibliothek Your knowledge hub WIEN

(a) (b)

Fig. 18: (a) Vibrating table, (b) steel moulds [photo by author]

The filled moulds were placed on a pallet, covered with a PE construction film to avoid rapid dehydration, and stored in a safe place in the lab with an ambient temperature of 22±2 °C.

With the concrete sufficiently hardened after 24 h, the specimens were removed from the moulds. After labelling two sides of each specimen with the type of concrete and the production date (**Fig. 19**), they were placed in a tank filled with tap water with a temperature of 20±2 °C (**Fig. 20**). The duration of water curing varies for the specimens depending on the conducted tests.

Fig. 19: B7_0-0 and B7_30-15 concrete specimens after demoulding and labelling [photo by author]

Die approbierte gedruckte Originalversion dieser Diplomarbeit ist an der TU Wien Bibliothek verfügbar
The approved original version of this thesis is available in print at TU Wien Bibliothek.

Fig. 20: Curing of the specimens in a water tank [photo by author]

In addition to the investigation of the mechanical properties and durability of the concrete mixtures, we analysed the structure of the air void system of the hardened concrete. For this, it was necessary to cut one specimen of each concrete mixture after curing and prepare the cut surface for the digital analysis process. The surface preparation and editing process are described in detail in section 3.6.

3.6 Experimental Methods

3.6.1 Fresh Concrete Properties

3.6.1.1 Temperature

The initial concrete temperature is a crucial factor in the setting time of concrete, as the hydration rate decreases noticeably at low concrete temperatures. This is particularly the case, when part of the cement is substituted for supplementary cementitious materials (SCMs).

The substitution of OPC with GGBFS typically results in an increase in setting time. The replacement percentage, the fresh concrete temperature, the water-binder ratio, and the characteristics of the cement and additives employed all have an impact on this delay. The concrete temperature plays a crucial role in determining the setting time of GGBFS-based composites, with a more significant delay observed at lower temperatures [2]. However, the lower concrete temperatures result in higher concrete strengths at later ages [28].

During the manufacturing process, the temperature of the fresh concrete was determined directly after mixing using a digital thermometer with a cable sensor. The ÖNORM B 4710-1 limits the temperature of fresh concrete under normal conditions between +5 °C and +27 °C, the permissible temperature range guarantees an adequate setting period with an admissible progress of the heat of hydration and without excessive water evaporation and serves as a quality control feature.

Die approbierte gedruckte Originalversion dieser Diplomarbeit ist an der TU Wien Bibliothek verfügbar
The approved original version of this thesis is available in print at TU Wien Bibliothek.

3.6.1.2 Consistency – Flow Table Test

The flow table test according to ÖNORM EN 12350-5 “Testing fresh concrete - Part 5: Flow table test” [39] determines the consistence of fresh concrete for flow values between 340 mm and 620 mm. The consistency represents a measure of the stiffness of the concrete and defines its workability, i.e. the ease with which it can be mixed, poured, compacted, and finished to a homogeneous condition [40].

With the difference in aggregate type and composition, differences in the workability of the three concrete mixtures are expected. Due to the higher porosity and water absorption capacity of the RCA, part of the mixing water, notably around the RCA in the new ITZ, can be absorbed, and the hydration process disturbed.

In addition to that, fine recycled concrete aggregates require more water and generally reduce the workability of concrete. The angular shape, surface roughness, and open porosity of fine RCA particles increase internal friction and water demand and consequently reduce the flowability. The initial moisture content of fine RCA also plays a critical role, higher pre-wetting levels can improve workability by reducing the aggregate’s tendency to absorb mixing water [41]. With the partial pre-saturation of the added RB LSB 0-4 and RB LSB 4-16, the increased water demand for the B7_30-15 and B7_100-15 concrete was accounted for.

Fig. 21: Flow table test equipment

The first flow table test was carried out for all mixtures directly after mixing using samples taken directly from the concrete mixer. For the subsequent tests after 45 min and 90 min from mixing, a sample from each mixture was stored in a dampened plastic bucket, covered with a PE construction film and sealed.

Die approbierte gedruckte Originalversion dieser Diplomarbeit ist an der TU Wien Bibliothek verfügbar
The approved original version of this thesis is available in print at TU Wien Bibliothek.

3.6.1.3 Fresh Density

The density of the compacted fresh concrete was determined according to ÖNORM 12350-6 "Testing fresh concrete - Part 6: Density" [42]. The test was performed simultaneously to the air content test, as the container used for the air content test complies with the requirements specified for the density test. The container with the known volume was filled and compacted alternately until it was full to the top. The full container was then weighed, and the fresh density was calculated using the equation 3-1.

$$d_{fresh} = \frac{m_{Total} - m_{Container}}{V_{container}} \qquad 3\text{-}1$$

Where according to ÖNORM 12350-6 [42]:

d_{fresh}: *„density of fresh concrete;"*

m_{Total}: *„mass of filled container;"*

$m_{Container}$: *„mass of empty container;"*

$V_{Container}$: *„internal volume of container;"*

3.6.1.4 Air Content

The air content of the fresh concrete was determined with the pressure gauge method described in ÖNORM 12350-7 "Testing fresh concrete - Part 7: Air content - Pressure methods" [43]. The standard is suitable for concrete made with normal weight or relatively dense aggregate but does not apply to concretes made with lightweight aggregates. This will later prove to be relevant for the recycled concrete aggregate and will be discussed in more detail in the relevant sections of the thesis.

According to ÖNORM B 4710-1 [44], the allowed air content range for B7 concrete with a maximum aggregate size of 16 mm is 4,5% to 8,5%. This increases the resistance of concrete to freeze-thaw cycles and ensures its endurance in harsh environments. With the addition of an air-entraining agent into the mixture design, the percentage of air voids can be adjusted.

Die approbierte gedruckte Originalversion dieser Diplomarbeit ist an der TU Wien Bibliothek verfügbar
The approved original version of this thesis is available in print at TU Wien Bibliothek.

Fig. 22: Air content testing equipment

3.6.1.5 Water Content

The water content of the concrete was determined through the rapid heating method using a microwave as described in ÖNORM B 4710-3 [45]. A sample of at least 2000g was taken from each fresh concrete mixture immediately after mixing and weighed on a paper plate. The sample was then dried in the microwave for a sufficient amount of time until reaching a constant mass. The sample was weighed once more, and the water content was calculated based on the mass loss during the drying process using equation 3-2.

$$w = \frac{m_f - t_f - m_d + t_d}{m_f - t_f} \times 100 \qquad 3\text{-}2$$

Where according to ÖNORM B 4710-3 [45]:

w: *„Total water content of the sample in mass-%;"*

m_f: *„Mass of the weighed sample quantity and the paper plate before testing;"*

t_f: *„Mass of the paper plate before testing;"*

m_d: *„Mass of the dried sample and the paper plate after drying;"*

t_d: *„Mass of the paper plate after drying;"*

3.6.2 Density of hardened Concrete

The concrete density is crucial in determining the mechanical and physical properties of the hardened concrete. A higher density generally means a denser concrete structure and fewer air voids, which increases the compressive strength.

The density of normal concrete is about 2400 kg/m^3. As a result of the increased air content in B7 concrete, its density is generally lower. However, the density of RAC is not only

Die approbierte gedruckte Originalversion dieser Diplomarbeit ist an der TU Wien Bibliothek verfügbar
The approved original version of this thesis is available in print at TU Wien Bibliothek.

affected by the mixture design, i.e. the quantity of air-entraining agents, but also by the quality and constitution of the recycled aggregates used. Recycled concrete aggregates possess a lower density than natural aggregates, this means that a higher aggregate replacement ratio leads to a lower concrete density and thereby to a lower compressive strength.

The density of the hardened concrete was determined 24 h after casting the concrete by measuring the exact dimensions of the 150 x 150 x 150 cm^3 cubic samples used for the compressive strength test with an accuracy of ±0,1 mm using a digital calliper, and then weighing the surface dry specimens as specified in ÖNORM EN 12390-7 "Testing hardened concrete - Part 7: Density of hardened concrete" [46].

3.6.3 Compressive Strength

The strength of the concrete was evaluated through its compressive strength as it constitutes an easily identifiable, yet essential measure of the mechanical performance and quality of concrete. It indicates the material's capacity to withstand axial loading and offers a solid reference for evaluating other mechanical characteristics such as elastic modulus and tensile strength.

The test specimens used for the compressive strength test following ÖNORM EN 12390-3 "Testing hardened concrete – Part 3: Compressive strength of test specimens" [47] were prepared in accordance with the requirements of ÖNORM EN 12390-1 "Testing hardened concrete - Part 1: Shape, dimensions and other requirements for specimens and moulds" [48]. The compressive strength was evaluated at a concrete age of 1d, 2d, 7d, and 28d.

3.6.4 Chloride Resistance

When reinforced concrete is exposed to saline environments –through de-icing salts or through seawater - its durability is strongly dependent on its containment of chloride ions ingress. Chloride ions disrupt the passivation layer surrounding the steel bars and cause expansive corrosion products to accumulate on their surface. This results in cracking, spalling and eventually a loss of the concrete's structural integrity.

Chloride ions penetration in solid concrete happens through different mechanisms, including diffusion, permeation, migration, and capillary suction [49], the penetration rate depends on concrete porosity, permeability, water-to-cement ratio, curing conditions, and the presence of SCMs. Due to the presence of residual old mortar with a higher porosity on its aggregates, RAC typically is more prone to chloride damage

Die approbierte gedruckte Originalversion dieser Diplomarbeit ist an der TU Wien Bibliothek verfügbar
The approved original version of this thesis is available in print at TU Wien Bibliothek.
TU Bibliothek Your knowledge hub WIEN

The chloride resistance of concrete was determined through experimental testing of the hardened concrete according to ÖNORM EN 12390-11 “Determination of the chloride resistance of concrete, unidirectional diffusion” [50], on two cubic specimens with a nominal size d=150 mm.

The concrete specimens were cast as previously described and cured in water for a period of 28 days. After that, they were divided into two sub-specimens: a reference sub-specimen for determining the initial chloride level Ci and a "profile-specimen" for determining the chloride profile following exposure to unidirectional chloride ingress.

The profile specimens were placed in a saturated calcium hydroxide solution for 18 hours after being vacuum-saturated with demineralised water and covered with an epoxy covering on all but the sawn face. The specimens were then moved to the inversion exposure apparatus, where the exposure surface was submerged in a 3% NaCl solution. The specimens were taken out of the exposure solution after 90 days, and 8 parallel layers of the profile specimen were dry ground, with the thickness of each layer corresponding to the suggested intervals in the ÖNORM EN 12390-11 [51] (**Fig. 23**).

Water/cement ratio [a]	0,30	0,35	0,40	0,50	0,60	0,70
Layer 1	0~1	0~1	0~1	0~1	0~1	0~1
Layer 2	1~2	1~2	1~2	1~3	1~3	1~3
Layer 3	2~3	2~3	2~3	3~5	3~5	3~6
Layer 4	3~4	3~4	3~5	5~7	5~8	6~10
Layer 5	4~5	4~6	5~7	7~10	8~12	10~15
Layer 6	5~6	6~8	7~9	10~13	12~16	15~20
Layer 7	6~8	8~10	9~12	13~16	16~20	20~25
Layer 8	8~10	10~12	12~16	16~20	20~25	25~30

[a] Where the concrete contains a Type II addition, the w/c ratio is replaced with a w/(c + k.a) ratio.

Fig. 23: Recommended depth intervals of profile grinding for concrete containing GGBFS, fly ash or silica fume [51]

The initial chloride content and the acid-soluble chloride content of each ground layer was then determined according to ÖNORM EN 14629 [52] using the potentiometric titration method. Through non-linear regression analysis of the measured chloride profile, the calculated chloride content at the exposed concrete surface (C_s) and the non-steady chloride diffusion coefficient (D_{nss}) have been determined using the formula:

$$C_x = C_i + (C_s - C_i) * \left(1 - \mathrm{erf}\left(\frac{x}{\sqrt{D_{nss}^t}}\right)\right) \qquad 3\text{-}3$$

Die approbierte gedruckte Originalversion dieser Diplomarbeit ist an der TU Wien Bibliothek verfügbar
The approved original version of this thesis is available in print at TU Wien Bibliothek.

Where according to ÖNORM EN 14629 [52]:

C_x: *„chloride content measured at average depth x and exposure time t;"*

C_s: *„calculated chloride content at the exposed surface;"*

C_i: *„initial chloride content;"*

x: *„depth below the exposed surface to the mid-point of the ground-layer;"*

D_{nss}: *„non-steady state chloride diffusion coefficient;"*

t: *„exposure time."*

with a coefficient of determination (R^2) greater than 0,950.

3.6.5 Freeze-Thaw Resistance - Scaling

Freeze-thaw resistance is the ability of concrete to withstand damage from repeated cycles of freezing and thawing, this characteristic is especially crucial in climates where temperatures fluctuate around the freezing point. The water within the pore system of the concrete generates internal stresses when it expands during the freezing phase and creates fissures within the concrete, these fissures in turn fill up with water during the thawing phase and get larger when the water freezes again, causing surface scaling, and an overall loss of durability. The use of de-icing salts aggravates this process by increasing moisture penetration and introducing chemical reactions that accelerate the deterioration. The water-cement ratio, the degree of saturation, the overall porosity, and the air-void system (i.e. the size, spacing, and distribution of entrained air) all have a significant impact on the capacity of concrete to resist freeze-thaw cycles. An adequate system of entrained air voids lowers internal pressure by providing freezing water relief space. Whereas poorly distributed or overly saturated pores increase vulnerability to freeze-thaw damage.

Under freeze-thaw attacks, concrete is exposed to two forms of damage: scaling, which is the near-surface detachment of concrete bits, and internal structural damage. During our experimental campaign, we evaluated the scaling resistance through experimental testing of the hardened concrete according to ONR CEN/TS 12390-9 "Part 9: Freeze-thaw resistance with de-icing salts – scaling" [53] and ÖNORM B 4710-3 "Part 3: National application of testing standards for concrete and its source" [45]. The tests for all concrete mixtures were carried out by *Mapei*.

Die approbierte gedruckte Originalversion dieser Diplomarbeit ist an der TU Wien Bibliothek verfügbar
The approved original version of this thesis is available in print at TU Wien Bibliothek.
TU Bibliothek Your knowledge hub WIEN

The testing method assesses the deterioration of concrete surfaces due to cyclic freezing and thawing in the presence of de-icing agents, simulating real environmental conditions for infrastructure exposed to winter maintenance treatments.

After casting and curing the concrete specimens in water for a period of 7 days as described in section 3.5, the specimens were stored in the climate chamber at (20 ± 2) °C and a relative humidity of (65 ± 5)%. When the concrete age reached 28 days, the samples were re-saturated for a period of 3 days, after which the freeze-thaw cycles started. The exposed surface of each specimen was subjected to a 3% sodium chloride (NaCl) solution, replicating the effect of de-icing salts.

The specimens were placed in a climate chamber programmed to follow a standardised freeze-thaw cycle:

- The freezing phase involved lowering the temperature to (-18) – (-22) °C over a defined period.
- The thawing phase raised the temperature to (+16) – (+24) °C, ensuring complete thawing of the specimens.

3.6.6 Depth of Penetration

Permeability plays a crucial role in the durability of concrete. It regulates the ingress of potentially hazardous materials like chlorides, sulphates, and carbon dioxide. Low permeability contributes to an enhanced resistance to freeze-thaw cycles, carbonation and chemical attack. The permeability of concrete is affected by various factors including water-cement ratio, curing, age of concrete and aggregate properties [54].

To evaluate the permeability of hardened concrete, the depth of water penetration under pressure was determined in accordance with ÖNORM B 4710-3 “Part 3: National application of testing standards for concrete and its source” [45]. The testing method proposed involves a two-phase process to assess the permeability of hardened concrete and subsequently measure the maximum depth of water penetration.

The specimens used for this test with dimensions of 200 × 200 × 120 mm, complied with the minimum size requirements indicated in the standard. Before testing, a circular area with a 10 cm diameter was roughened at the surface exposed to water pressure to promote uniform permeability. The test procedure involved applying water pressure in two phases:

- First phase: from 1st to 3rd day with a water pressure of 1,75 bar
- Second phase: from 4th to 14th day with a water pressure of 7,0 bar

Die approbierte gedruckte Originalversion dieser Diplomarbeit ist an der TU Wien Bibliothek verfügbar
The approved original version of this thesis is available in print at TU Wien Bibliothek.
TU Bibliothek Your knowledge hub WIEN

Throughout the test, the specimens were continuously monitored for signs of moisture penetration on the non-exposed surfaces, which could compromise the validity of the results.

After the test duration, each specimen was split perpendicular to the exposed surface, and the water penetration front was visually identified once the split face had dried sufficiently. The level of water penetration was marked, and the side length of a rectangle with an equivalent penetrated area was calculated to determine the average penetration depth(**Fig. 24**).

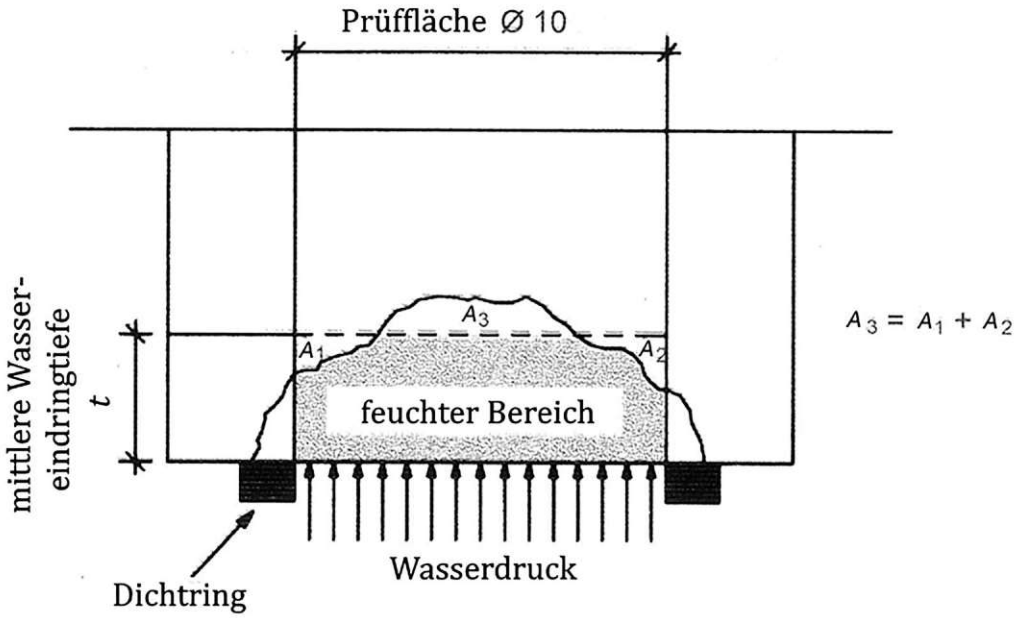

Fig. 24: The determination of water penetration depth

The final test result was reported as the mean penetration depth of three test specimens, rounded to the nearest millimetre, providing a quantified evaluation of the concrete's permeability properties.

The tests were carried out by *Rohdorfer* for all concrete mixtures. After casting and curing the concrete specimens for a period of 28 days as described in section 3.5, the specimens were readied and transported to the testing facilities.

3.6.7 Carbonation Resistance

Carbonation is a chemical reaction in which atmospheric carbon dioxide (CO_2) penetrates the concrete matrix and mostly combines with calcium hydroxide ($Ca(OH)_2$) to produce calcium carbonate ($CaCO_3$). This slow process gradually lowers the alkalinity of the concrete, which can compromise the protective passivation layer around steel reinforcement and in-crease the risk of corrosion. Porosity, moisture content, CO2 concentration, and exposure duration are some of the variables that affect carbonation, which usually moves inward from the surface.

Die approbierte gedruckte Originalversion dieser Diplomarbeit ist an der TU Wien Bibliothek verfügbar
The approved original version of this thesis is available in print at TU Wien Bibliothek.

Carbonation typically progresses inward from the surface and is affected by porosity, moisture content, CO_2 concentration, and exposure time.

The carbonation resistance of the concrete mixtures was evaluated through experimental testing of the hardened concrete according to ÖNORM EN 12390-12 "Part 12: Determination of the carbonation resistance of concrete – Accelerated carbonation method" [55]. This method, which is intended to speed up the carbonation process, describes the depth of carbonation and carbonation rate under controlled settings.

The test specimens consisted of two prisms with dimensions of $100 \times 100 \times 400\,mm$, which were cast and cured in accordance with ÖNORM EN 12390-2 [56]. After an initial water curing period of 28 days, the specimens underwent a 14-day preconditioning phase in an environmental chamber (18 – 25 °C, relative humidity of 50 – 65%). They were then stored in a controlled carbonation chamber with a carbon dioxide concentration of (3,0 ± 0,5)% at (20 ± 2) °C and (57 ± 3)% relative humidity for 70 days.

To assess carbonation ingress over time, a 50 mm slice was split from each prism after 7-, 28-, and 70-days storage in the carbonation chamber. The depth of the carbonation reaction was determined by applying a phenolphthalein indicator solution on the split surface, which changes colour to distinguish carbonated and non-carbonated areas. The carbonation depth was then measured at twelve points of the sprayed surface on each slice, and the mean depth (Dk) was calculated for each exposure period. The carbonation rate was then determined in $mm/d^{0,5}$ based on these measurements.

The tests were carried out by *Rohdorfer*.

3.6.8 Air Void Analysis

The analysis of the air void system in the hardened concrete was done using digital image processing in MATLAB. The preparation of the specimens and the analytical procedure were based on ÖNORM EN 480-11 "Admixtures for concrete, mortar and grout – Test methods. Part 11: Determination of air void characteristics in hardened concrete" [57], with some modifications depending on the equipment available. Instead of a manually conducted measurement procedure as described in ÖNORM EN 480-11, we opted for an automated digital image analysis based on the work of Fonseca and Scherer [58].

In this, the air-void structure is described through the following parameters:

- **Total air content:** *„proportion of the total volume of air voids by volume percentage"* [57]

Die approbierte gedruckte Originalversion dieser Diplomarbeit ist an der TU Wien Bibliothek verfügbar
The approved original version of this thesis is available in print at TU Wien Bibliothek.

- **Specific surface of air void system:** *„total surface area of the air voids divided by their volume"* [57]
- **Spacing factor:** *„maximum distance of any point in the cement paste from the periphery of an air void"* [57]
- **Air-void size distribution:** *„number of air voids of various diameters within the hardened cement paste"* [57]
- **Micro air content:** *„air content attributed to air voids of 0,3 mm diameter or less"* [57]

To obtain a clear representation of the air voids, the specimen surfaces were first wet ground using a diamond grinding wheel and then polished to achieve a smooth, flat surface. This step helped minimise surface roughness, which would interfere with the image analysis. After polishing, the specimens were thoroughly cleaned with deionised water and compressed air to remove any dust or debris. The achieved surface quality is shown in **Fig.** .

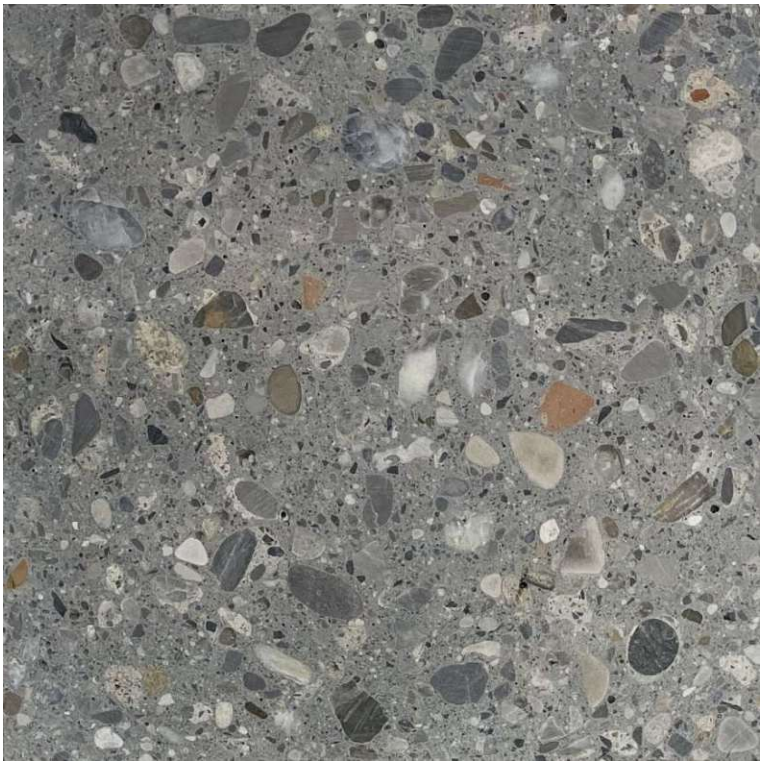

(a)

Fig. 25 (part 1): Ground and polished surfaces of (a) B7_0-0, (b) B7_30-15 and (c) B7_100-15 concrete

Die approbierte gedruckte Originalversion dieser Diplomarbeit ist an der TU Wien Bibliothek verfügbar
The approved original version of this thesis is available in print at TU Wien Bibliothek.

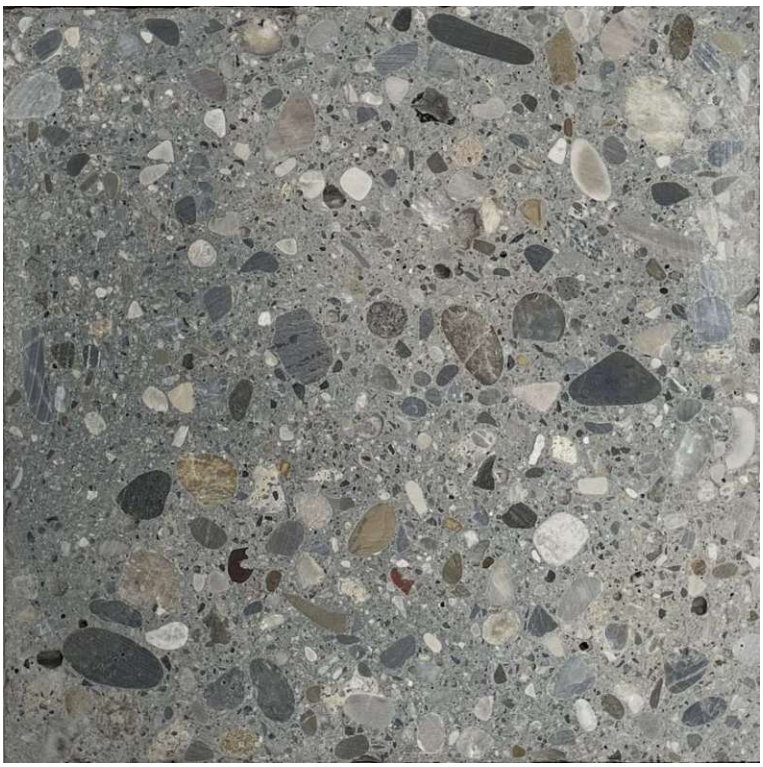

(b)

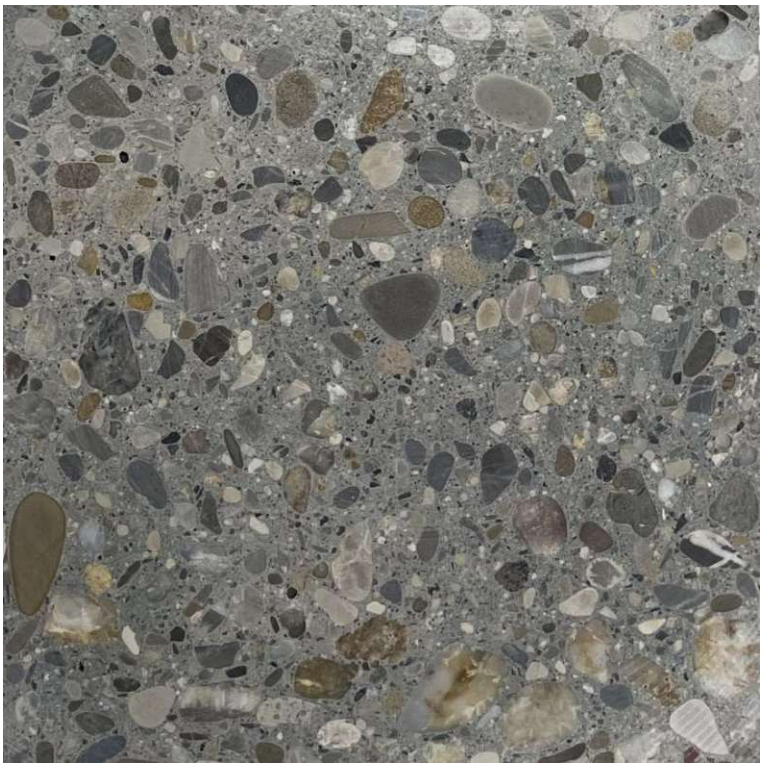

(c)

Fig. 26 (part 2): Ground and polished surfaces of (a) B7_0-0, (b) B7_30-15 and (c) B7_100-15 concrete

To enhance the contrast between the air voids and the solid concrete, a mixture of gypsum and colour pigments was applied to the surface. The mixture was spread evenly using a scraper, ensuring that all air voids were completely filled. Any excess gypsum was then removed with the scraper to maintain an even coating.

Die approbierte gedruckte Originalversion dieser Diplomarbeit ist an der TU Wien Bibliothek verfügbar
The approved original version of this thesis is available in print at TU Wien Bibliothek.
TU Bibliothek Your knowledge hub WIEN

The specimens were then placed in an oven at 40°C until the gypsum was fully dried. Once dried, any residual gypsum on the surface was carefully sanded down, leaving the filled air voids clearly visible while exposing the solid concrete matrix for optimal imaging conditions.

These preparation steps ensured a well-defined air void structure, allowing for accurate and reliable image analysis using MATLAB.

The images were taken under bright natural lighting conditions with the digital microscope *DigiMicro Profi* from *dnt*. With each image depicting an area of around 600 mm².

The digital image analysis was then conducted in two steps:

1. Image editing and processing
2. Image analysis

3.6.8.1 Image Editing and Processing in *ImageJ*

Firstly, the images taken with the digital microscope were edited with the image editing and image processing software *ImageJ*. The editing of the images was necessary to eliminate the light-green film that remained on the prepared specimen surface after the removal of the dried gypsum residues. It helped improve the visibility of the filled air voids and further enhance the contrast with the solid concrete matrix, facilitating the setting of a colour threshold and the segmentation of the image. Setting the correct colour threshold however, remained a manual operator-dependent task that required a certain level of precision and fine tuning, switching back and forth between the original and segmented image, verifying that all air voids are filtered and none of the solid matrix is. Once the results were satisfying, a binary mask was created.

Through the process of creating a binary image and due to the colour thresholding and the image resolution, the segmented air voids (white) could take irregular shapes, with isolated white pixels and/or enclosed black pixels (holes). These were removed using the following processing tools available in *ImageJ*:

- *Close-*: *„Performs a dilation operation, followed by erosion. This smoothens objects and fills in small holes"* [59].
- *Fill Holes*: *„This command fills holes (4–connected background elements) in objects by filling the background"* [59].

Another issue we encountered during the process, was the merging of smaller air voids to one large pore due to their proximity. This issue was reversed using the command:

Die approbierte gedruckte Originalversion dieser Diplomarbeit ist an der TU Wien Bibliothek verfügbar
The approved original version of this thesis is available in print at TU Wien Bibliothek.
TU Bibliothek Your knowledge hub WIEN

- *Watershed*: *„Watershed segmentation is a way of automatically separating or cutting apart particles that touch. It first calculates the Euclidian distance map (EDM) and finds the ultimate eroded points (UEPs). It then dilates each of the UEPs (the peaks or local maxima of the EDM) as far as possible – either until the edge of the particle is reached, or the edge touches a region of another (growing) UEP. Watershed segmentation works best for smooth convex objects that don't overlap too much"* [59].

The resulting binary images from the editing and processing were saved as a *.tif* file, to be then used during the second step of the analysis.

3.6.8.2 Image Analysis in *MATLAB*

The second step was an automated analysis of the created binary images using MATLAB. The analysis was based on the work of Fonseca and Scherer [58], which aimed at developing an automatic image analysis using a customisable MATLAB script.

The source script was written to analyse sample images obtained by scanning the specimen surfaces with a flatbed scanner. Since we are using an already binarised images obtained with a digital microscope, we edited the script to work with the given input data, and added a scale, which was already determined and set in ImageJ, as an additional input parameter. The other argument taken in when running the code is the paste to solids ratio of the concrete mixtures.

The MATLAB script - provided in the attachment - consists of three main functions, which can be described as follows:

- **Image Import and Scaling (readimage_adapted.m):**
  This function loads an image of the concrete cross-section, determines whether the image is binary or grayscale and assigns it to the base workspace as either *bw2* for binary images or *grayimage* for grayscale images. It allows the user to set a scaling factor in pixels per millimetre (px/mm). It then calculates the pixel size in micrometres and stores it in the base workspace.

- **Basic Image Analysis (basicanalysis_adapted.m):**
  This function performs a basic analysis of a binary image or a grayscale image from the base workspace. It requires the user to input the paste-to-solids ratio and optionally a threshold for binarization of grayscale images, if no threshold is provided, Otsu's method is used to determine it automatically. It then removes small objects and identifies connected pore regions. The function then calculates:
    - The **total air void content** as a percentage of the total volume

Die approbierte gedruckte Originalversion dieser Diplomarbeit ist an der TU Wien Bibliothek verfügbar
The approved original version of this thesis is available in print at TU Wien Bibliothek.
TU Bibliothek Your knowledge hub WIEN

- The **specific surface area** of the voids (mm^{-1})
- The **paste-to-air ratio**
- The **Powers spacing factor**, which describes the average void distribution

- **3D Pore Structure Reconstruction (reconstructspheres.m):**
  This function applies the Saltykov method to estimate a 3D distribution of air voids from 2D profile sections. It first calculates the histogram distribution of observed pore radii. Then, these data points are converted into a sphere distribution, determining the mean sphere radius and the total void volume density. An optional bin width for histogram representation is provided.

As mentioned, the paste-to-solids ratio is required as an input parameter for the evaluation of the air void system when performing the basicanalysis_adapted.m function. It was calculated based on the recipe of the respective concrete mixtures as follows:

$$paste\ to\ solids\ ratio = \frac{Volume\ of\ cement, water\ and\ SCM}{Volume\ of\ paste\ and\ aggregates}$$

Tab. 8: Paste-to-solids ratio based on the concrete recipes

			B7_0-0		B7_30-15		B7_100-15	
	Material	**Density**	**Mass**	**Volume**	**Mass**	**Volume**	**Mass**	**Volume**
Paste	Cement	3100	378	0,122	378	0,122	378	0,122
	AHWZ	2710	42	0,015	42	0,015	42	0,015
	Water	1000	180	0,180	180	0,180	180	0,180
Aggregate	NA 0-4	2460	871	0,354	741	0,301	739	0,300
	NA 4-16	2820	761	0,270	534	0,189	0	0,000
	RA 0-4	2310	0	0,000	109	0,047	104	0,045
	RA 4-16	2470	0	0,000	199	0,081	636	0,257
Paste/solids ratio			**0,34**		**0,34**		**0,34**	

The paste to solids ratio is equal to 0,34 for all mixtures.

Die approbierte gedruckte Originalversion dieser Diplomarbeit ist an der TU Wien Bibliothek verfügbar
The approved original version of this thesis is available in print at TU Wien Bibliothek.

4 Results and Interpretation

This section presents the results obtained during the experimental program, followed by an analysis and a graphical interpretation of these results. While the preceding chapter introduced the testing program and methodologies, the focus here is placed exclusively on the outcomes of the investigations and the performance of the RAC in comparison to NAC.

4.1 Fresh Concrete Properties

During the mixing and casting of the different concrete mixtures, the development of certain characteristics of the fresh concrete, that provide an insight into the quality and workability of the product, were monitored and investigated. These parameters are described in detail in this section.

4.1.1 Temperature

As can be seen in **Tab. 9**, the fresh concrete temperature is within the permitted range as described in section 3.6.1.1, and the hydration rate is therefore satisfactory. The recorded temperatures for all three concrete mixtures are quite similar and are not expected to influence their early strength.

Tab. 9: Fresh concrete temperatures

Mixture Code	Fresh Concrete Temperature [°C]
B7-0-0	24,2
B7-30-15	23,8
B7-100-15	24,4

4.1.2 Consistency

During the testing, the consistency of concrete was measured directly after mixing (initial), at 45 min and at 90 min after the first measurement. **Fig. 27** provides a comparison of the development of concrete consistencies over time.

Die approbierte gedruckte Originalversion dieser Diplomarbeit ist an der TU Wien Bibliothek verfügbar
The approved original version of this thesis is available in print at TU Wien Bibliothek.

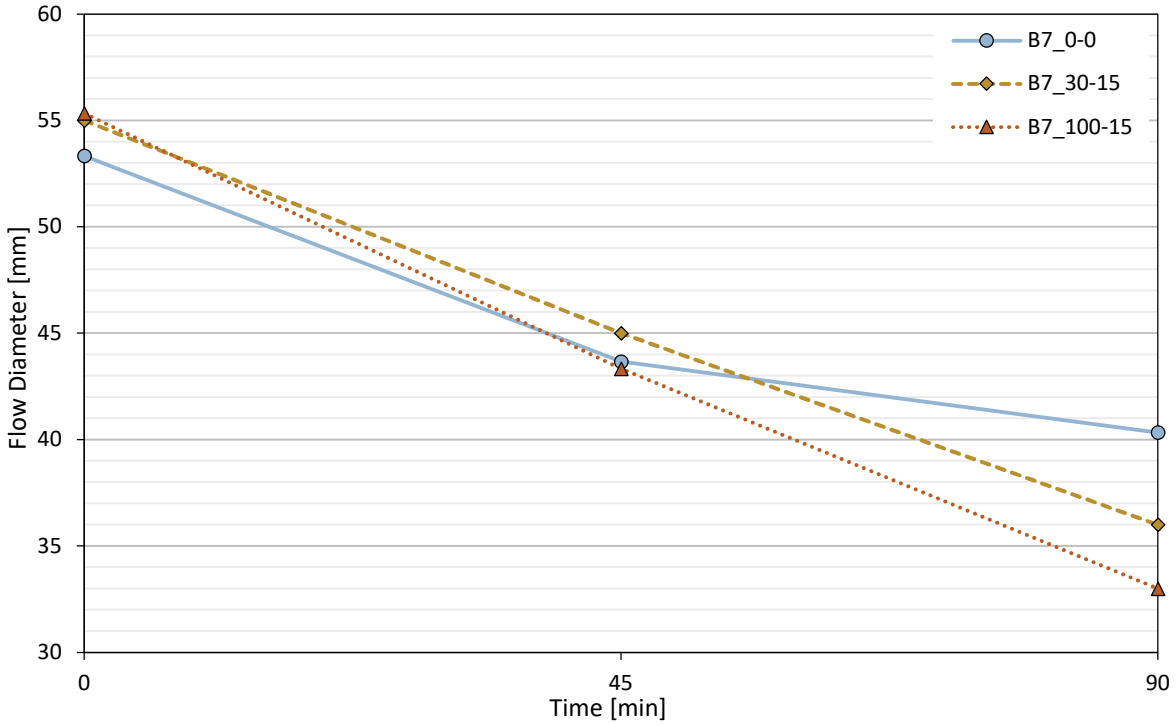

Fig. 27: flow diameter of the fresh concrete mixtures over time (initial, after 45 min and after 90 min)

The initial flow diameter varies between 53 and 55 cm and corresponds to the consistency class F52 (soft concrete). The concrete mixtures with RCAs, B7_30-15 and B7_100-15, have a slightly larger flow diameter compared to the concrete mixture with NA. These values were targeted during the design of the mixtures and are attained primarily through the addition of a superplasticiser (see **Tab. 5**), to counter the expected poorer performance in terms of workability of the RAC. In addition to that, various studies have observed a positive impact of aggregate pre-saturation and the two-stage-mixing approach on the consistency of the concrete [13], [17], [60], [61], [62], [63]. As the pre-saturation of aggregates limits the absorption of mixing water and helps improve the consistency of fresh concrete and maintain it over time.

The flow diameter after 45 min was fairly identical for all concrete mixtures with RAC reaching consistency values similar to those of NAC even with 100% coarse RCA used, although it can be noticed that B7_30-15 maintained its consistencies slightly better than the B7_100-15 mixture, with a relative drop of the flow diameter of around 18% for B7_30-15 compared to 22% for B7_100-15 (**Fig. 28**).

The largest discrepancy was observed after 90 min. The line chart in **Fig. 27** illustrates a steady decline of the flow diameter for the concrete mixtures with RCAs, with B7_100-15 concrete recording the sharpest decline in workability, dropping below the lowest consistency class F38 as defined in ÖNORM B 4710-1 [44]. Meanwhile, the consistency change for the NAC was less pronounced, with a drop of only 7,6% relative to its consistency after 45 min.

Die approbierte gedruckte Originalversion dieser Diplomarbeit ist an der TU Wien Bibliothek verfügbar
The approved original version of this thesis is available in print at TU Wien Bibliothek.
TU Bibliothek Your knowledge hub WIEN

Fig. 28 shows the relative change of consistency between the first, second and third measurement for all mixtures.

The quasi-linear decline of workability of the B7_30-15 and B7_100-15 concrete mixtures during the 90 minutes of testing is likely linked to the increased amount of fine aggregate fractions in the RAC mixture. As can be seen in section 3.3, the share of aggregates with a particle size between 0,5 mm and 4,0 mm increases with increasing replacement ratio of coarse aggregates due to the distinctive sieve curves of NA and RA fractions. A higher amount of fine RCA means a higher specific surface area and a higher water sorption, and in addition to that, the angular shape of the RCA particles leads to stronger interlocking between the particles and by that to a reduced flowability.

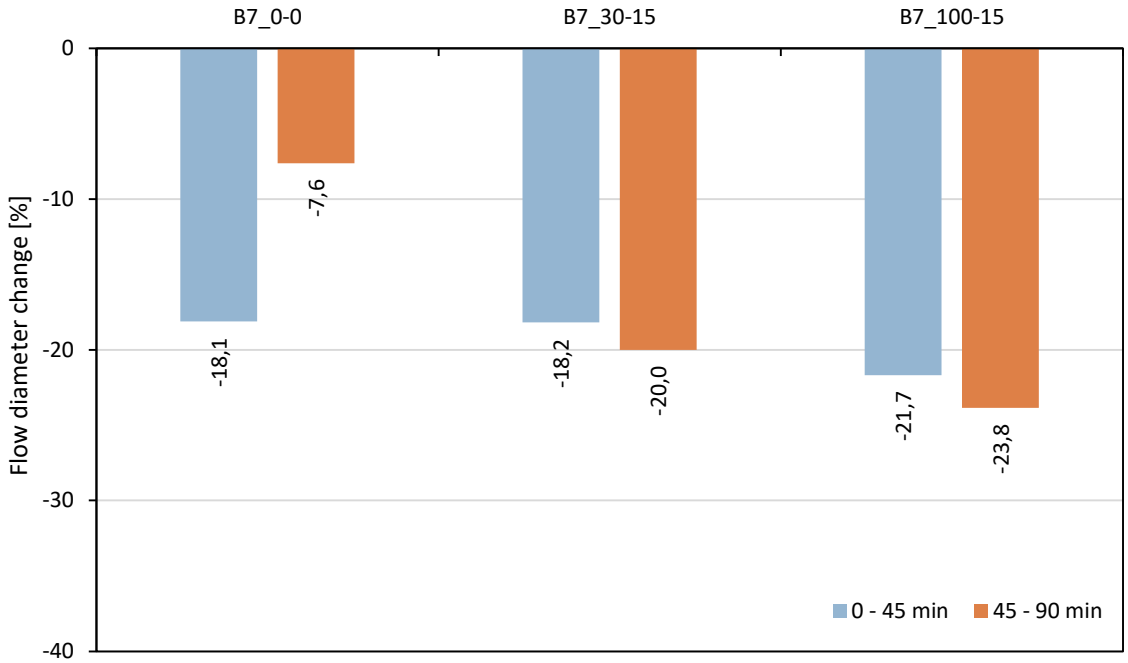

Fig. 28: Development of flow diameter change between measurement intervals

4.1.3 Fresh Density

The resulting values for the concrete fresh densities are detailed in **Tab. 10**, with the theoretical densities calculated as the sum of the masses of all concrete components as described in **Tab. 5**, divided by the sum of their total volume plus the volume of the theoretical air content.

The measured densities of the RAC mixtures are higher than the theoretically calculated densities and almost equal to or higher than the density of the NAC mixture. These results do not concur with the state of knowledge on the influence of RCA on concrete density. The porous mortar attached to the aggregate should lead to a decrease of the concrete density. This deviation could be the result of different levels of compaction of the mixtures during the testing.

Die approbierte gedruckte Originalversion dieser Diplomarbeit ist an der TU Wien Bibliothek verfügbar
The approved original version of this thesis is available in print at TU Wien Bibliothek.
TU Bibliothek Your knowledge hub WIEN

Tab. 10: Theoretical and measured density of the fresh concrete

Fresh Concrete Density [kg/m³]		
Mixture Code	**Theoretical**	**Measured**
B7_0-0	2236	2173
B7_30-15	2187	2202
B7_100-15	2084	2165

4.1.4 Air Content

The air content was, as previously mentioned, determined in agreement with the requirements of ÖNORM EN 12350-7 [64] using the pressure gauge method. The results of the measurements are provided in **Tab. 11**. The determined values are all within the required limits defined by the ÖNORM B 4710-1.

Tab. 11: Air content measured with the pressure gauge method

Mixture Code	Air Content [%]
B7_0-0	7,0
B7_30-15	7,2
B7_100-15	7,0

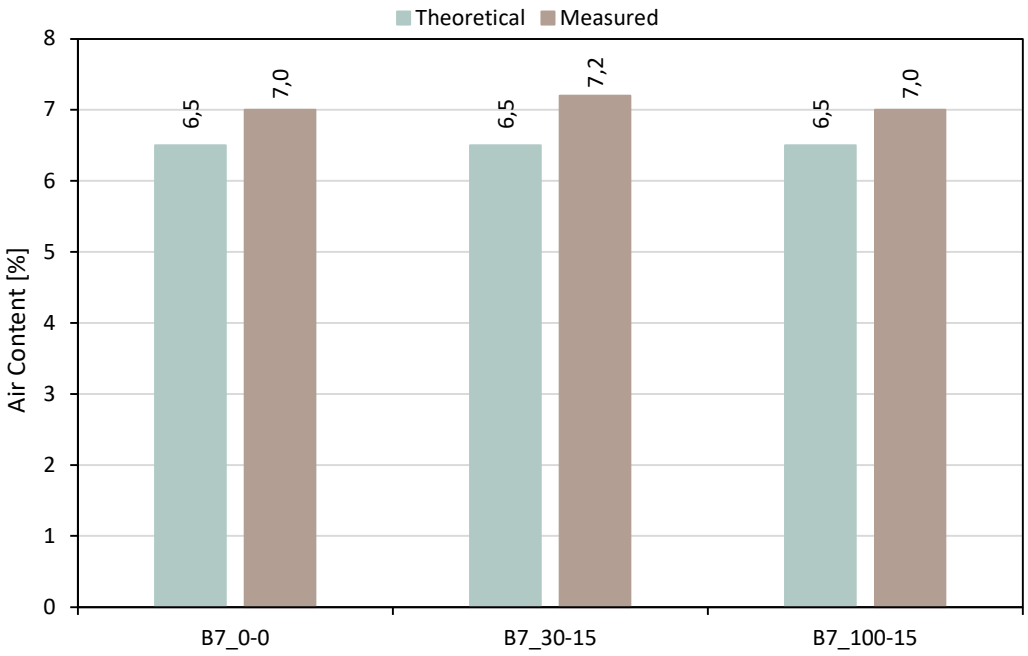

Fig. 29: Theoretical and measured air content

Fig. 29 compares the theoretical and measured air contents of the tested mixtures. The measured air content is expected to differentiate marginally from the theoretical one, since it is dependent on many variables such as concrete compaction, amount of air entraining agent and more.

Die approbierte gedruckte Originalversion dieser Diplomarbeit ist an der TU Wien Bibliothek verfügbar
The approved original version of this thesis is available in print at TU Wien Bibliothek.

The measured values are nearly identical for all mixtures, ranging from 7,0 to 7,2%. These results are somewhat unexpected, given that similar amounts of air-entraining agent were incorporated in the three mixtures (**Tab. 5**) and that RCA exhibits a higher intrinsic porosity. The results are likely caused by the limitations of the applied testing method (see section 4.8.2).

4.1.5 Water Content

With the water content determined through rapid heating of fresh concrete samples in a microwave, we were able to calculate the effective water-binder ratio of the mixtures. **Fig. 30** shows the results of the calculations and compares them to the theoretical w/b-ratio.

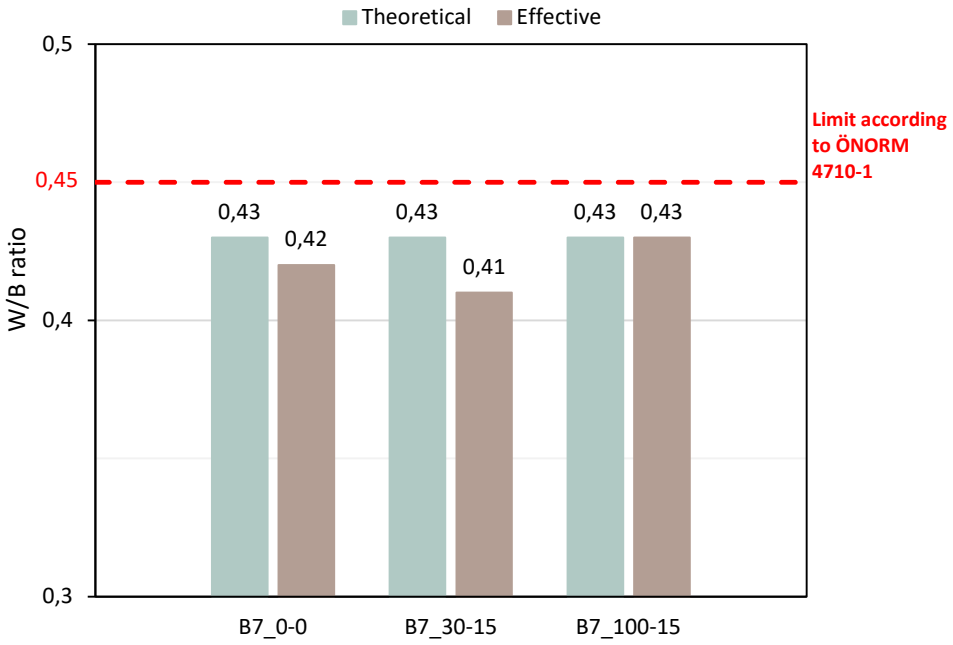

Fig. 30: Water/Binder ratio of concrete mixtures

The effective w/b-ratio is lower than the maximum permitted value of 0,45 according to ÖNORM B 4710-1 and therefore complies with the requirements for B7-concrete in all mixtures.

The values for the theoretical and effective w/b-ratios are very similar, suggesting that the assumed water content of the aggregate is correct.

4.2 Hardened Density

For each concrete mixture, 3 specimens were measured and weighed to determine their mass and volume and thereof calculate their densities. The results are presented in **Tab. 12**.

Die approbierte gedruckte Originalversion dieser Diplomarbeit ist an der TU Wien Bibliothek verfügbar
The approved original version of this thesis is available in print at TU Wien Bibliothek.

Tab. 12: Hardened density of the concrete specimens

Hardened Concrete Density [kg/m³]					
Mixture Code	**Specimen 1**	**Specimen 2**	**Specimen 3**	**Mean**	**Std. dev.**
B7_0-0	2252	2306	2299	2286	29
B7_30-15	2268	2283	2287	2279	10
B7_100-15	2200	2219	2209	2209	9

As anticipated, the hardened concrete density drops with increasing aggregate replacement ratios. However, the table shows that the decrease between the B7_0-0 and B7_30-15 concrete is marginal. Meanwhile, the decrease in density between the B7_0-0 and B7_100-15 mixtures is clearer (**Fig. 31**).

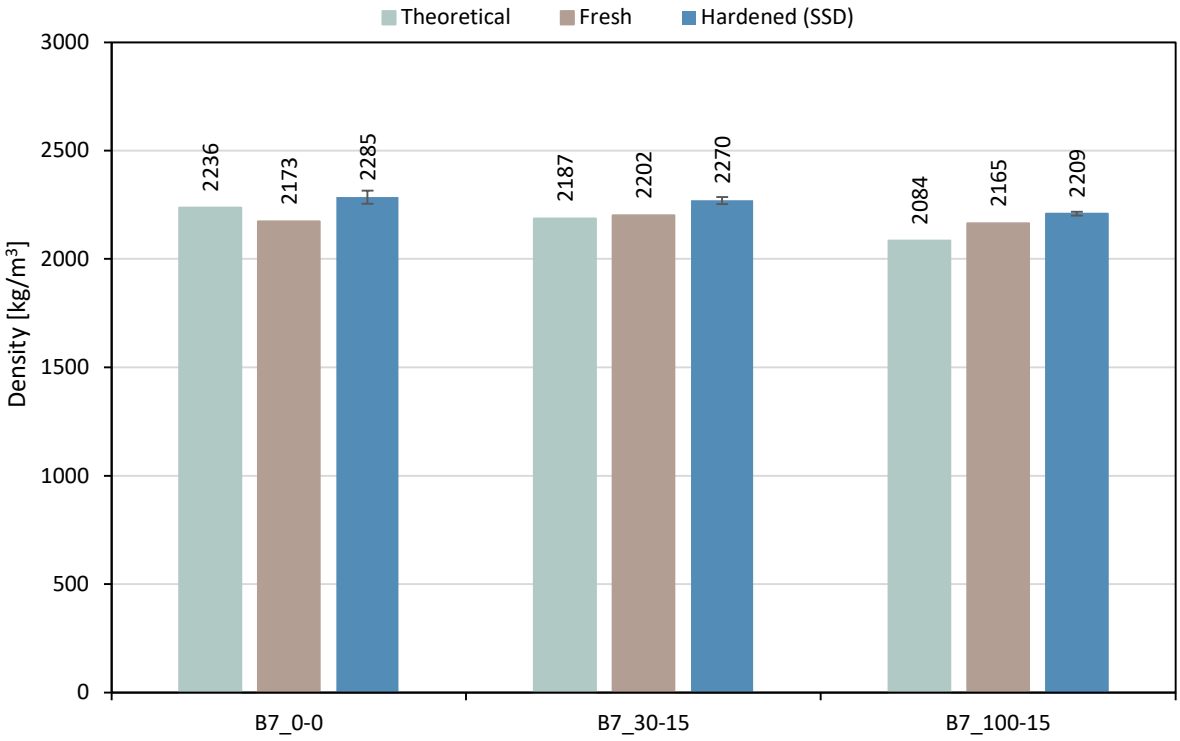

Fig. 31: Fresh and hardened density of concrete mixtures

Generally, the measured densities on the hardened concrete are higher than the theoretical and fresh densities. This might be due to the water curing of the samples, which promotes the formation of hydration products creating a denser microstructure and thus, resulting in a higher density of the hardened concrete.

4.3 Compressive Strength

The compressive strength of the concrete was evaluated after 1, 2, 7 and 28 days, using 1, 1, 3 and 3 cubic specimens for each age, respectively. **Fig. 33** shows some of the fracture patterns of the tested specimens which were all satisfactory according to the description in the

Die approbierte gedruckte Originalversion dieser Diplomarbeit ist an der TU Wien Bibliothek verfügbar
The approved original version of this thesis is available in print at TU Wien Bibliothek.

ÖNORM EN 12390-3 [65]. The individual values as well as the mean values of the compressive strength for B7_0-0, B7_30-15 and B7_100-15 are expressed in **Tab. 13**.

Fig. 32: Compressive strength test

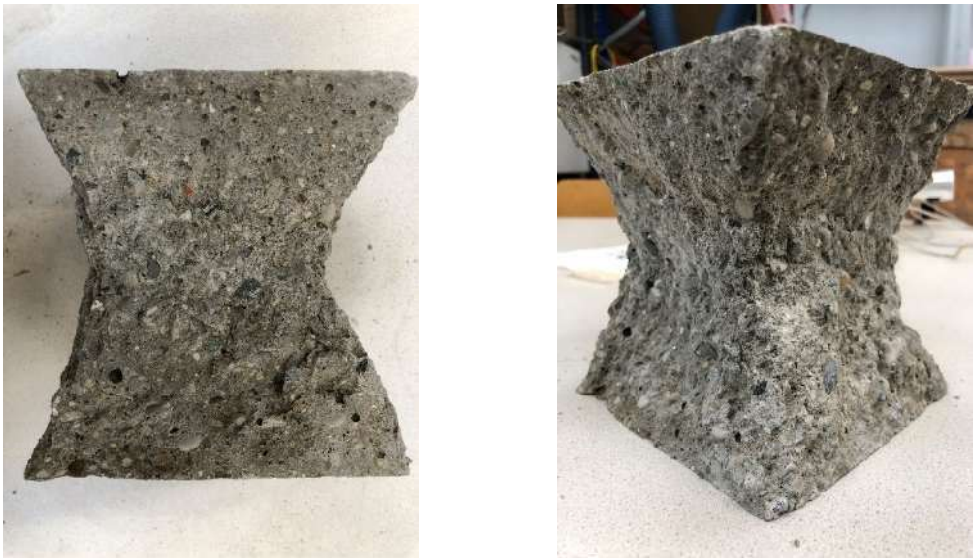

Fig. 33: Concrete specimens after compressive strength failure and removal of loose material

Tab. 13: Compressive strength test results

Compressive Strength [MPa]					
Curing time	**Specimen 1**	**Specimen 2**	**Specimen 3**	**Mean**	**Std. Dev.**
B7_0-0					
1 d	20,1	-	-	**20,1**	-
2 d	26,9	-	-	**26,9**	-
7 d	45,4	43,7	41,8	**43,6**	1,8
28 d	64,1	55,4	53,2	**57,6**	5,8
B7_30-15					
1 d	24,1	-	-	**24,1**	-
2 d	29,8	-	-	**29,8**	-
7 d	43,9	39,3	46,4	**43,2**	3,6
28 d	52,7	57,9	54,0	**55,9**	2,7
B7_100-15					
1 d	24,0	-	-	**24,0**	-
2 d	27,9	-	-	**27,9**	-
7 d	39,0	40,9	41,9	**40,6**	1,4
28 d	50,3	48,9	50,0	**49,7**	0,7

Die approbierte gedruckte Originalversion dieser Diplomarbeit ist an der TU Wien Bibliothek verfügbar
The approved original version of this thesis is available in print at TU Wien Bibliothek.

The initial compressive strength after demoulding (1 day) is distinctly higher for the concrete mixtures with RCA compared to the NAC mixture, with a relative improvement of around 19% for both RAC mixtures. The superior early strength performance of the RAC mixtures was affirmed with the specimens tested after an additional day of curing in water, with the compressive strength values surpassing the NAC strength by 10,7% and 3,9% for B7_30-15 and B7_100-15, respectively. The superior compressive strength of the RAC is likely related to the internal curing taking place with the incorporation of partially saturated RAs. It is also important to consider, that the compressive strength tests after 1 day and after 2 days were carried out on one specimen only for each mixture, and therefore the statistical dispersion of the values is not known.

At the age of 7 days, it is observed, that the disparity between the three mixtures has developed in the opposite direction, with B7_0-0 reaching the highest compressive strength at 43,6 MPa, B7-30-15 at a similar level, and B7_100-15 reaching 40,9 MPa, which represents a relative difference of 7,0% in comparison to the reference concrete B7_0-0.This trend continues after 28 days, with the B7_30-15 mix and the B7_100-15 mix reaching a compressive strength 4,0% and 13,2% lower than the B7_0-0 mix respectively (**Fig. 35**).

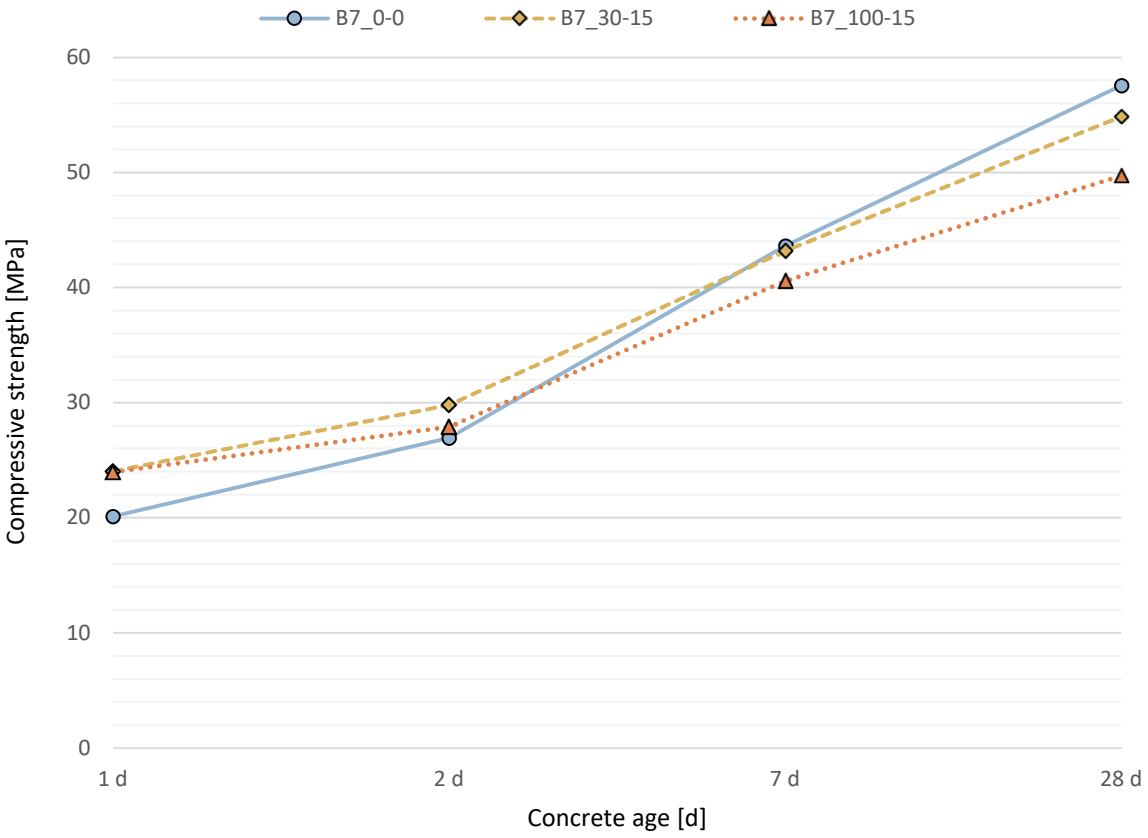

Fig. 34: Compressive strength results

Die approbierte gedruckte Originalversion dieser Diplomarbeit ist an der TU Wien Bibliothek verfügbar
The approved original version of this thesis is available in print at TU Wien Bibliothek.

As previously mentioned, the use of RCA was expected to cause a decrease of the compressive strength due to the attached mortar on the RCA and the presence of two ITZs. Previous studies indicate that an increase in the replacement ratio generally decreased the compressive strength of RAC with the compressive strength of concrete with 100% coarse RCA reported to be 20% to 30% lower than that of the corresponding natural aggregate concrete [66], [67]. These findings are consistent with our experimental results. Although replacement of NA with RCA resulted in a clear reduction in compressive strength after 28 days, the strength levels achieved for all mixtures were satisfactory. Thus, confirming that the pre-saturation of the RCA and the use of the adapted TSMA positively impact the RAC and help mitigate the decrease of the concrete strength with increased aggregates replacement levels. This is also supported by the findings of Brand et al. [17] and Tam et al. [38] who identified a correlation between the improvement of the compressive strength and the use of a TSMA and/or pre-saturation of RCA. Tam et al. state that the application of both methods leads to an increase in compressive strength of up to 30% in comparison to RAC with oven-dried aggregates produced using a normal mixing approach.

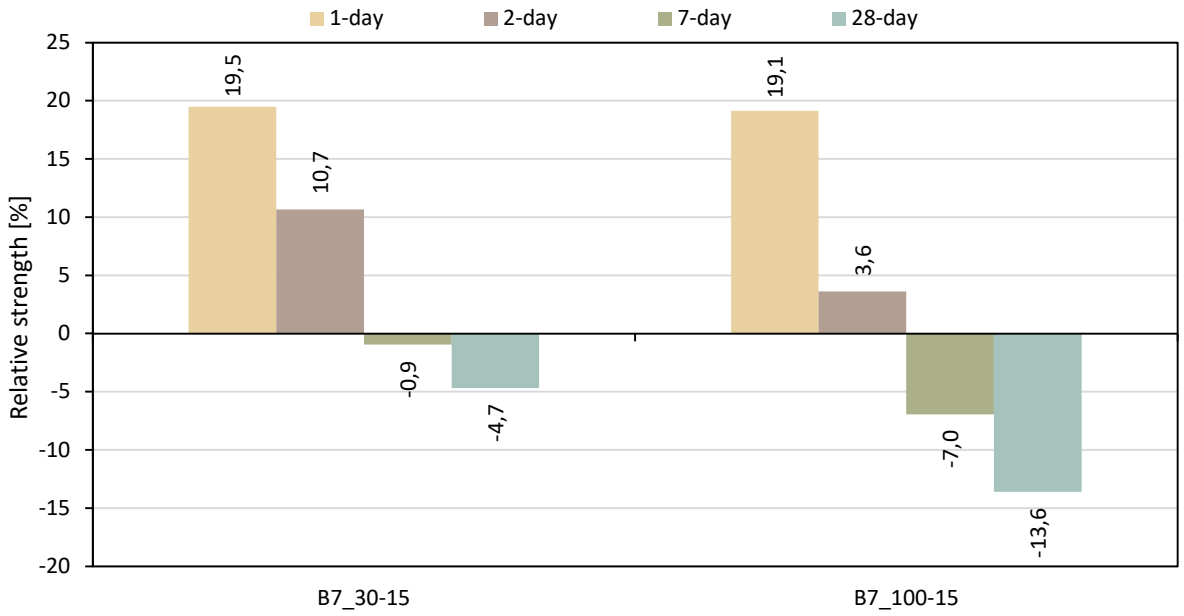

Fig. 35: Strength development of the RAC mixtures in comparison to the NAC (B7_0-0)

4.4 Chloride Resistance

Tab. 14 shows the acid-soluble chloride content of each layer ground from the profile-specimen as described in section 3.6.4, the chloride content was determined with the potentiometric titration method.

Die approbierte gedruckte Originalversion dieser Diplomarbeit ist an der TU Wien Bibliothek verfügbar
The approved original version of this thesis is available in print at TU Wien Bibliothek.

Tab. 14: Acid-soluble chloride content per layer determined through potentiometric titration

	Layer Depth [mm]	C_x [Mass-%]	Layer depth [mm]	C_x [Mass-%]
	Specimen 1		Specimen 2	
B7_0-0	1,52	0,555391	1,7	0,492936
	2,78	0,471209	3,54	0,372747
	3,91	0,375334	5,18	0,319154
	6,89	0,205742	5,99	0,214070
	8,9	0,141111	7,47	0,164803
	12,09	0,032939	11,67	0,014590
	15,22	0,005897	15,91	0,005676
	17,5	0,006026	18,58	-0,010809
B7_30-15	1,83	0,486515	1,74	0,532522
	4,49	0,404680	3,94	0,441000
	5,22	0,360357	4,92	0,335086
	6,42	0,310072	6,24	0,268406
	7,34	0,240745	8,21	0,193690
	11,29	0,075406	11,97	0,067787
	14,34	0,009910	15,64	0,023265
	18,32	0,000000	18,25	0,002911
B7_100-15	1,98	0,684117	1,98	0,594128
	2,76	0,578518	2,85	0,538398
	3,9	0,510377	4,02	0,431010
	5,48	0,380581	5,66	0,374468
	7,26	0,312631	7,8	0,274942
	11,62	0,102166	11,66	0,110579
	14,82	0,019165	15,46	0,033201
	18,61	0,015399	18,45	0,015655

The results of the regression analysis are presented in **Tab. 15**, and the graphical illustration is shown in **Fig. 36**.

Tab. 15: results of the regression analysis of chloride profile

Specimen	D_{nss}	C_s	R^2
$B7_0\text{-}0_{Specimen\ 1}$	2,88207E-12	0,68229	0,998
$B7_0\text{-}0_{Specimen\ 2}$	2,77835E-12	0,63552	0,985
$B7_30\text{-}15_{Specimen\ 1}$	4,32970E-12	0,64206	0,970
$B7_30\text{-}15_{Specimen\ 2}$	3,71118E-12	0,67011	0,993
$B7_100\text{-}15_{Specimen\ 1}$	3,67579E-12	0,84080	0,995
$B7_100\text{-}15_{Specimen\ 2}$	4,48602E-12	0,72733	0,995

In accordance with the existing literature, the results from our conducted test, as seen in **Fig. 36**, show higher chloride contents in the RAC mixtures compared to the reference concrete. The gap between the three concrete types diminishes with greater depths until it reaches

Die approbierte gedruckte Originalversion dieser Diplomarbeit ist an der TU Wien Bibliothek verfügbar
The approved original version of this thesis is available in print at TU Wien Bibliothek.
TU Bibliothek Your knowledge hub WIEN

similar chloride contents around 1,85 cm depth. The higher chloride content in the RAC is due to higher chloride diffusion through the cracked old mortar, as the porosity of the RCA allows for higher penetration of chloride ions.

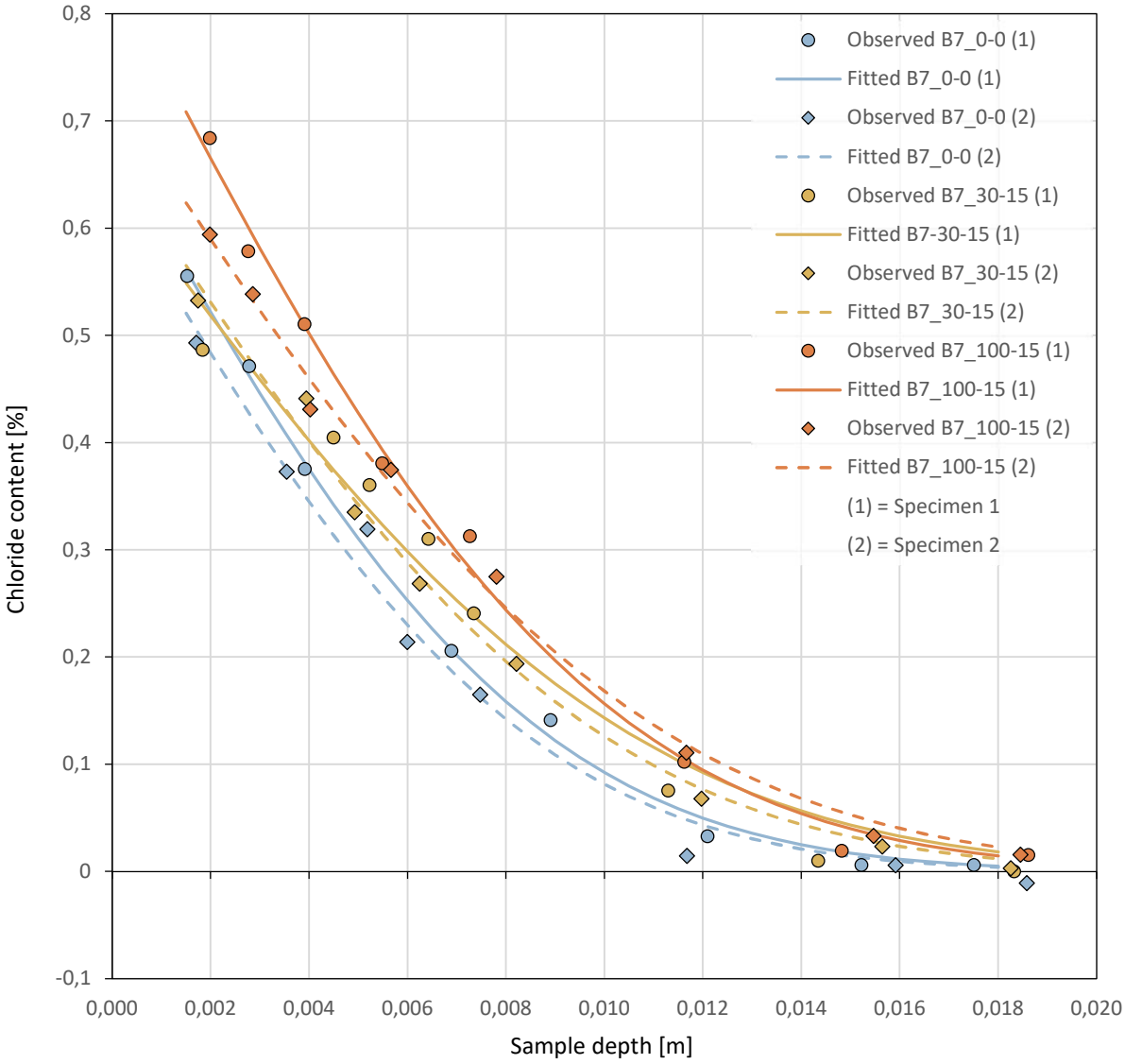

Fig. 36: Illustration of the regression for B7_0-0, B7_30-15 and B7_100-15

4.5 Freeze-thaw Resistance – Scaling

As stated in section 3.6.5, the freeze-thaw resistance was evaluated through scaling measurement, which quantifies the material loss due to surface degradation.

After a specified number of freeze-thaw cycles (i.e. (7±1), (14±1), (28±1), (42±1) and 56 cycles), the detached particles from the examined specimens were collected, dried, and weighed. The cumulative mass of scaled material per unit area (g/m²) was recorded and is presented in **Tab. 16**.

Die approbierte gedruckte Originalversion dieser Diplomarbeit ist an der TU Wien Bibliothek verfügbar
The approved original version of this thesis is available in print at TU Wien Bibliothek.

Tab. 16: Cumulative mass of scaled material after 56 cycles

Mixture	Scaling [kg/m²]
Reference concrete	0,05
B7_0-0	0,14
B7_30-15	0,31
B7_100-15	0,48

According to the acceptance criteria for XF4 exposure, a tested concrete mixture demonstrates equivalent freeze-thaw resistance to the reference concrete if the total surface scaling after 56 cycles does not exceed that of the reference by more than 100 g/m² [45]. From the test results, as presented in **Tab. 16**, it is evident that only the B7_0-0 concrete mixture meets this criterion, with a cumulative mass of scaled material of 140 g/m². The material loss in B7-30-15 concrete was over 120% more than what it was in the B7_0-0 concrete, and with increasing incorporation of RCA, the material loss increased by around 240% compared to B7_0-0 concrete. The B7_30-15 and B7_100-15 concrete mixtures both exceeded the threshold of 150 g/m² considerably and, therefore, did not meet the required freeze-thaw resistance.

The significantly higher scaling observed in the RCA-containing mixtures suggests that the properties of RCA play a critical role in freeze-thaw resistance. The microcracks inflicted during the crushing process likely contribute to increased water absorption and ice formation within the old mortar, leading to higher internal stresses and micro-cracking during freeze-thaw cycles.

This hypothesis is supported by multiple studies. Kazmi et al. [68] found that RCA concrete exhibited higher weight loss after freeze-thaw cycles due to increased water ingress through additional open pores, leading to greater internal pressure and micro-cracking.

It has been reported that the presence of RCA and the increase in the total volume of cement paste increases the open porosity of concrete, making it susceptible to freeze-thaw cycles and increasing the negative impact on its mechanical properties [69]. Verian [5] further emphasised that RCA concrete generally has lower freeze-thaw resistance than concrete with natural aggregates due to its greater porosity, which results in higher water absorption and poorer mechanical properties.

However, contradictory findings exist as well. Smith [70] found no significant difference between RAC and NAC in terms of freeze-thaw resistance. While Gokce et al. [71] demonstrated that RCA concrete can achieve high frost resistance if the recycled coarse aggregate originates from air-entrained concrete, highlighting the importance of the original concrete properties.

Die approbierte gedruckte Originalversion dieser Diplomarbeit ist an der TU Wien Bibliothek verfügbar
The approved original version of this thesis is available in print at TU Wien Bibliothek.
TU Bibliothek Your knowledge hub WIEN

In accordance with the literature and the test results, we can conclude that the used RCA has a low freeze-thaw-resistance due to inner cracks and its open porosity and is likely produced from a non-air-entrained concrete.

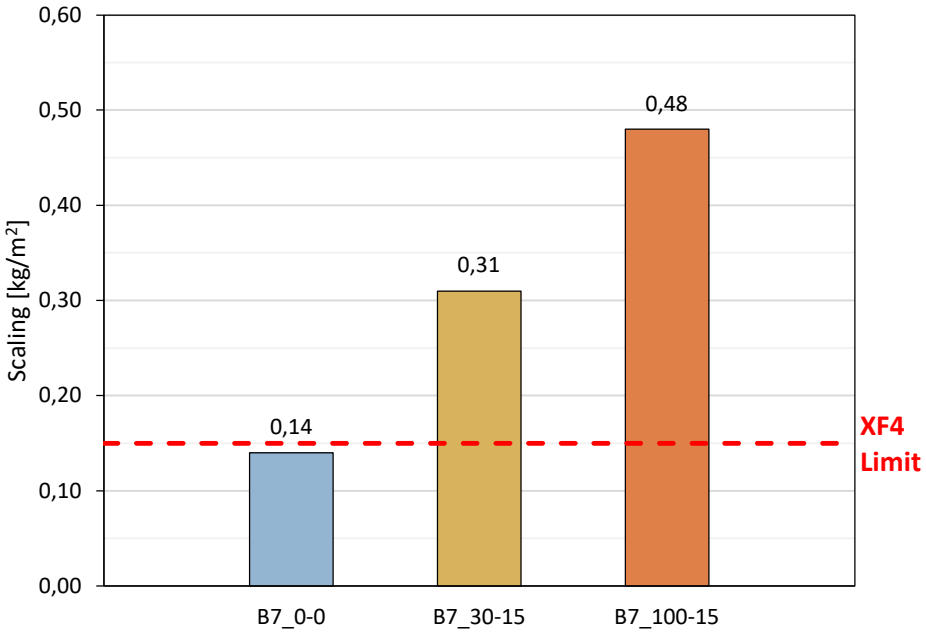

Fig. 37: Concrete scaling after 56 cycles

4.6 Depth of Penetration

The results obtained from the water penetration test are shown in **Fig. 38**.

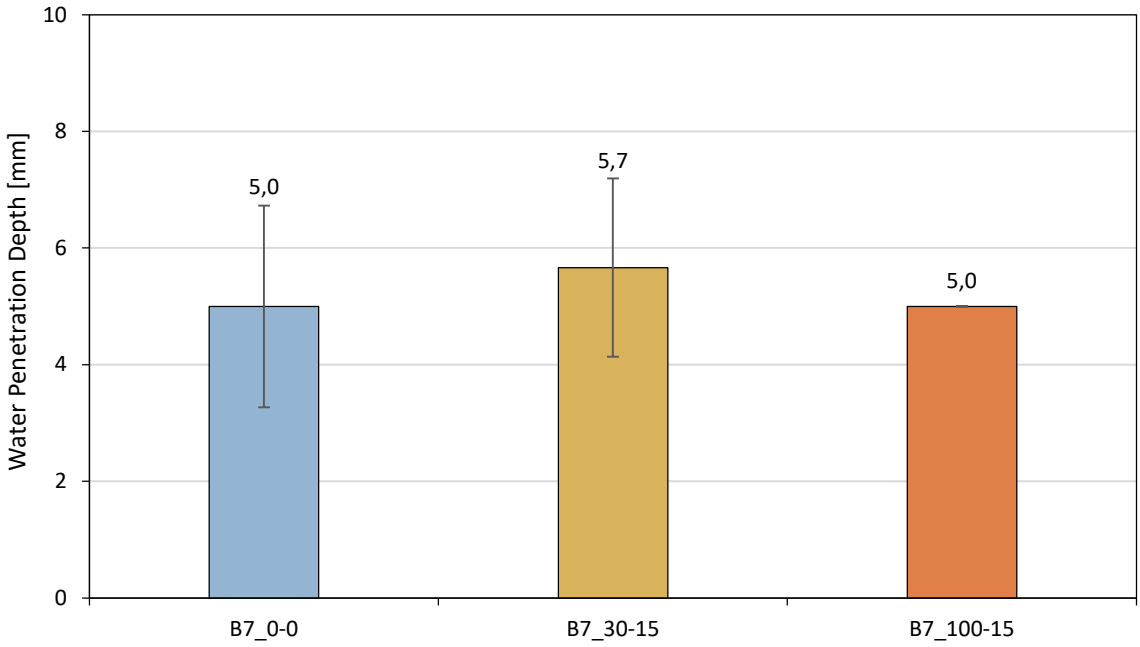

Fig. 38: Water penetration depth

Die approbierte gedruckte Originalversion dieser Diplomarbeit ist an der TU Wien Bibliothek verfügbar
The approved original version of this thesis is available in print at TU Wien Bibliothek.

The results of the water penetration depth test show that all tested concrete mixtures, B7_0-0, B7_30-15 and B7_100-15, exhibit similar water permeability with penetration depths ranging from 5,0 mm to 5,7 mm. These findings suggest that the incorporation of recycled concrete aggregates did not significantly impact the permeability of the hardened concrete, even at a 100% replacement ratio.

The literature provides varying insights into the relationship between RCA content and concrete permeability. Guo et al. [72] reported that the permeability of RAC increased with increasing RCA content, with water absorption by capillarity up to 1,70 times higher than that of NAC. However, they also noted some opposite trends, which could be due to variations in RCA quality.

Lage et al. [73] reported that in many cases, higher RCA replacement led to lower water penetration, potentially due to unsoaked RCA absorbing more water internally rather than allowing water penetration through the concrete matrix. This process is not likely to occur in our mixtures since the incorporated RCA were 80% pre-saturated. Additionally, Thomas et al. [74] demonstrated that water permeability of concrete mixtures with different degrees of substitution tend to converge on similar water penetration values at low water-cement ratios, which aligns with our results, as our mixtures had a controlled w/b ratio below 0,45.

The permeability of concrete is mainly influenced by its open porosity, which in turn is influenced by aggregate properties, the quality of the cement paste, and the curing conditions. In this study, the penetration depth did not exceed 6 mm for any of the concrete types, suggesting that the aggregate substitution had little effect on the permeability. The low water penetration values indicate that water absorption was largely confined to the surface zone, where the concrete structure may be dominated by the new cement paste. Since the properties of this new paste vary only slightly between the mixes and the low water binder ratio limits water intake, the permeability remained low across all specimens.

4.7 Carbonation Resistance

The test results as seen in **Tab. 17** show that the carbonation depth increased over time for all tested concrete mixtures, with overall higher carbonation depths observed in RCA mixtures. After reaching an average carbonation of 3,8 cm after 7 days, the B7_0-0 concrete exhibited a relatively stable progression, reaching 5,5 mm after 70 days. In contrast, both the B7_30-15 and the B7_100-15 mixtures exhibited a lower carbonation depth after 7 days, with B7_100-15 showing the highest carbonation resistance. The gradient of the carbonation between 7 and 70 days however is higher than that of the NAC, with the carbonation depth after 70 days

Die approbierte gedruckte Originalversion dieser Diplomarbeit ist an der TU Wien Bibliothek verfügbar
The approved original version of this thesis is available in print at TU Wien Bibliothek.
TU Bibliothek Your knowledge hub WIEN

reaching 8,7 mm and 7,5 mm for B7_30-15 and B7_100-15, respectively (**Fig. 39**). When 15% of fine aggregates and 30% of coarse aggregates are made up of RCA, the carbonation depth after 70 days was approximately 1,6 times higher than in the reference concrete. Conversely, a further increase in the proportion of coarse RCA to 100% resulted in a smaller increase in carbonation depth, with the carbonation depth reaching approximately 1,4 times that of the reference concrete.

Tab. 17: Carbonation depth after 7, 28 and 70 days

Carbonation Depth [cm]						
Mixture Code	**Day 7**		**Day 28**		**Day 70**	
	Average	Std Dev	Average	Std Dev	Average	Std Dev
B7_0-0	**3,8**	0,97	**4,5**	0,67	**5,5**	2,4
B7_30-15	**2,9**	0,94	**5,6**	1,34	**8,7**	1,59
B7_100-15	**2,2**	0,66	**4,5**	1,16	**7,5**	1,65

With a noticeable tendency of continuous carbonation over time in RCA mixtures, these results imply that the use of RCA affects the carbonation resistance of concrete. Reports from a number of studies analysed by Silva et al. [75] demonstrate similar outcomes, with higher RCA incorporation leading to higher carbonation depths, up to twice as deep as those of the corresponding NAC mixes when employing 100% coarse RCA.

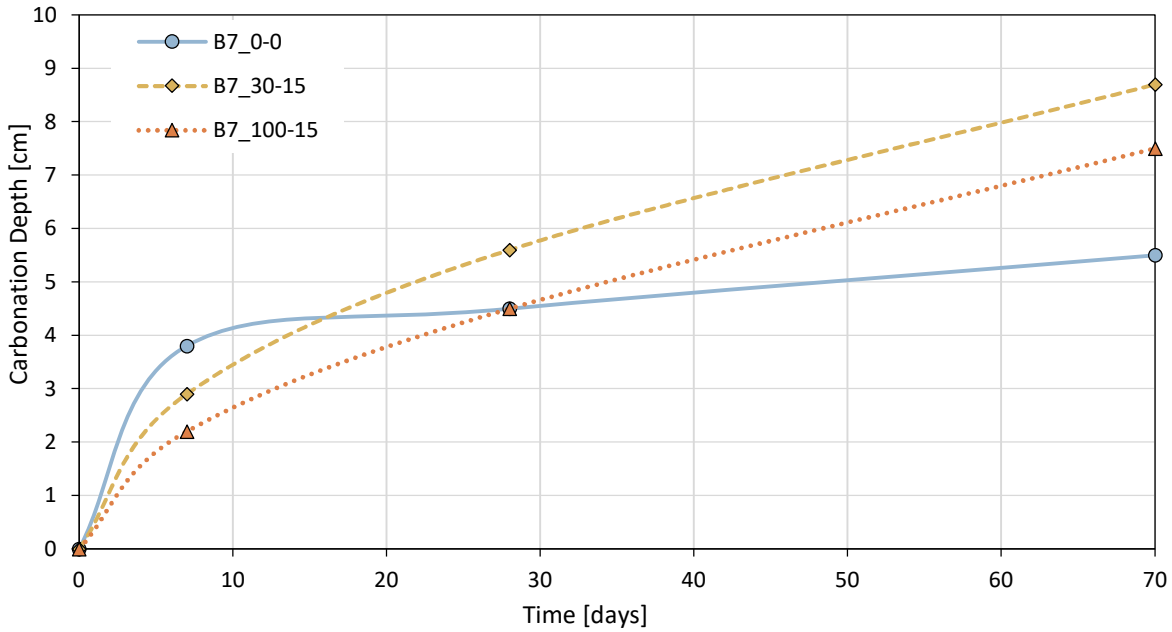

Fig. 39: Progression of the carbonation depth with time

The results can be caused by several factors. One major influencing factor is the increased porosity and permeability of RCA compared to NAC, which facilitates the diffusion of CO_2 into the concrete matrix. Literature supports this observation, as studies have shown that RCA has a higher intrinsic porosity, allowing for greater gas penetration and accelerating the car-

Die approbierte gedruckte Originalversion dieser Diplomarbeit ist an der TU Wien Bibliothek verfügbar
The approved original version of this thesis is available in print at TU Wien Bibliothek.

bonation process [76]. Additionally, the ITZ within RCA tends to be weaker and more porous than that in NAC, further enhancing carbon dioxide diffusion [77].

It was also notable that, the RCA mixtures experienced a continuous growth of the carbonated area over time. Whereas the B7_0-0 mixture showed a stabilisation of carbonation depth at an early stage (**Fig. 39**).

4.8 Air Void Analysis

4.8.1 Image Editing and Processing in *ImageJ*

The results of the image editing and processing as described in section 3.6.8 are presented below in several step. On the left side are the edited images, the images filtered after a set colour threshold are shown in the middle, and on the right are the final processed binary images used in the following step.

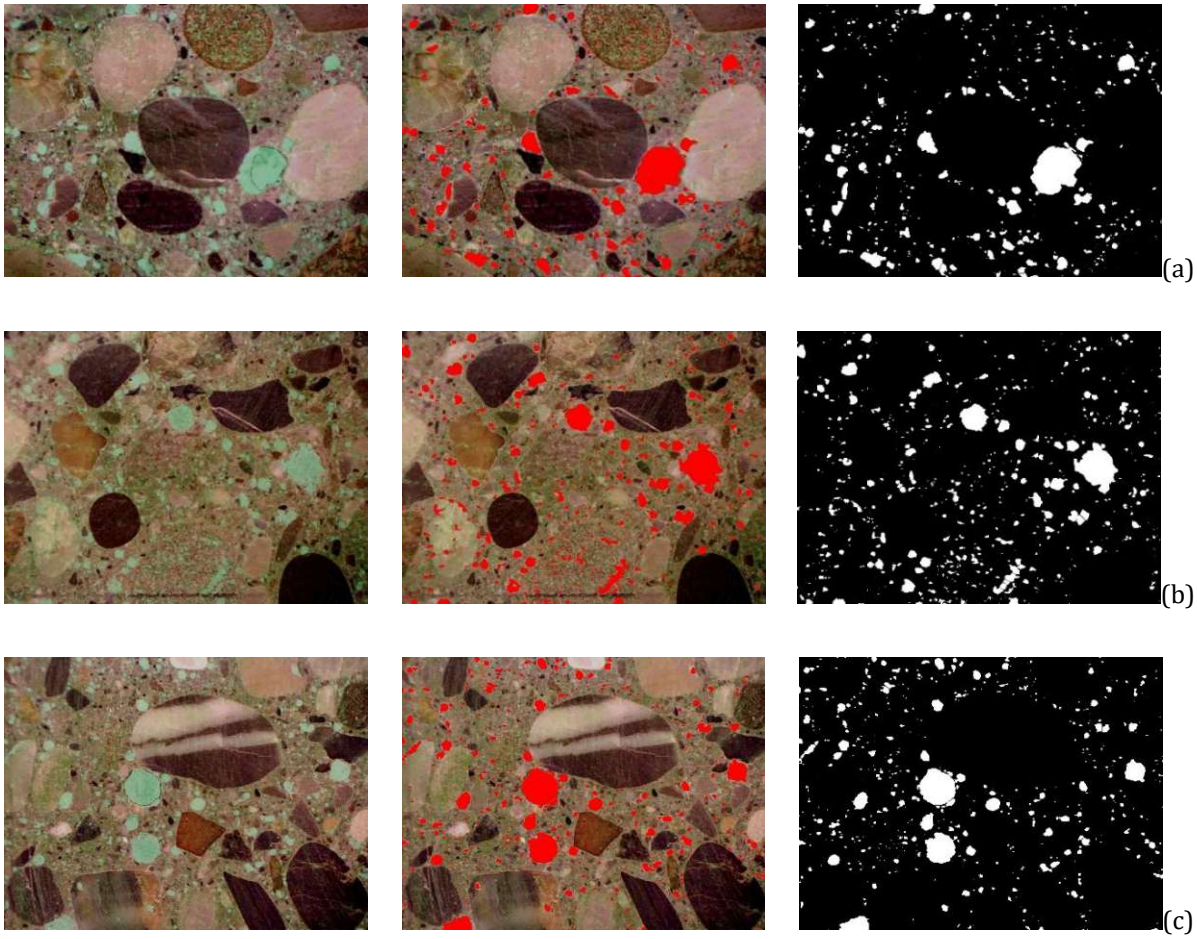

Fig. 40 (part 1): B7_0-0: Edited image (left), filtered image after applying colour threshold (centre), binary image (right)

Die approbierte gedruckte Originalversion dieser Diplomarbeit ist an der TU Wien Bibliothek verfügbar
The approved original version of this thesis is available in print at TU Wien Bibliothek.

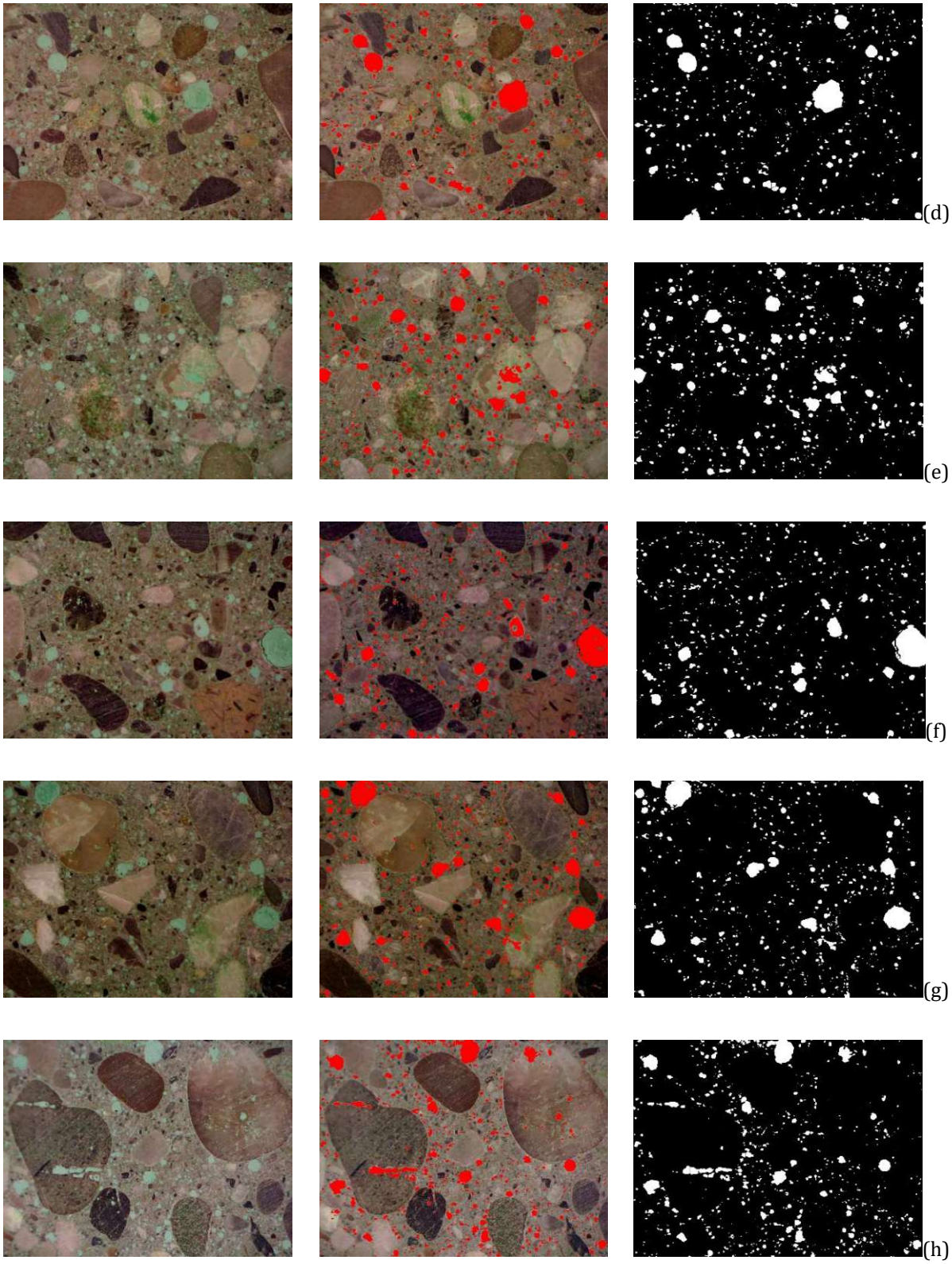

Fig. 41 (part 2): B7_0-0: Edited image (left), filtered image after applying colour threshold (centre), binary image (right)

Die approbierte gedruckte Originalversion dieser Diplomarbeit ist an der TU Wien Bibliothek verfügbar
The approved original version of this thesis is available in print at TU Wien Bibliothek.
TU Bibliothek Your knowledge hub WIEN

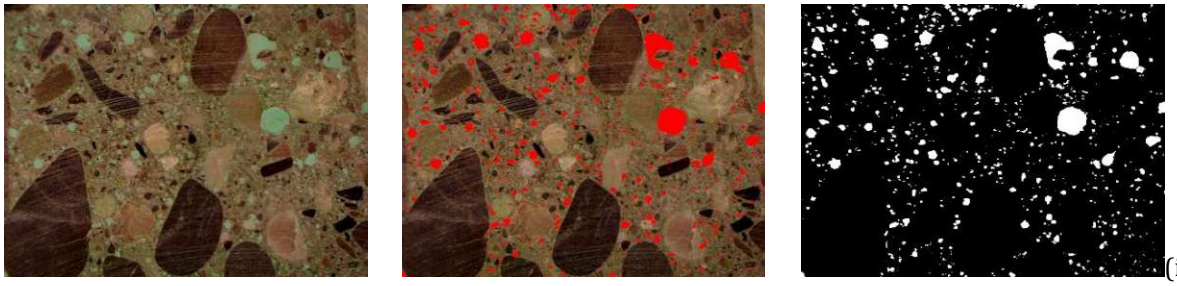
(i)

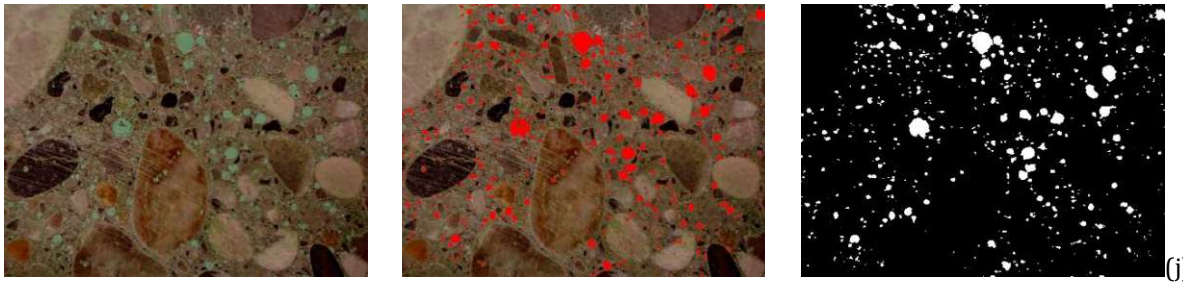
(j)

Fig. 42 (part 3): B7_0-0: Edited image (left), filtered image after applying colour threshold (centre), binary image (right)

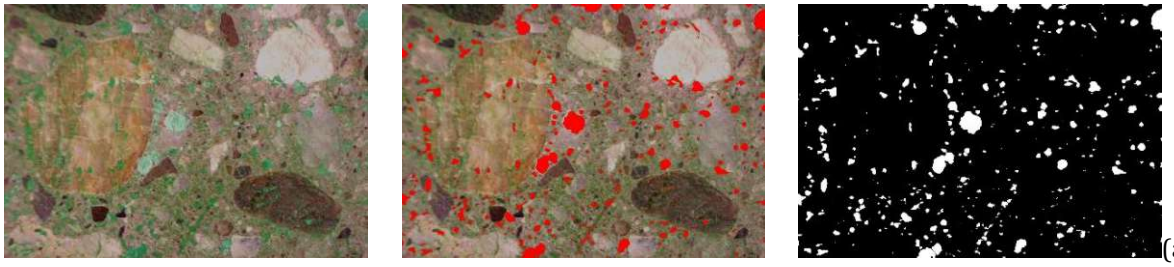
(a)

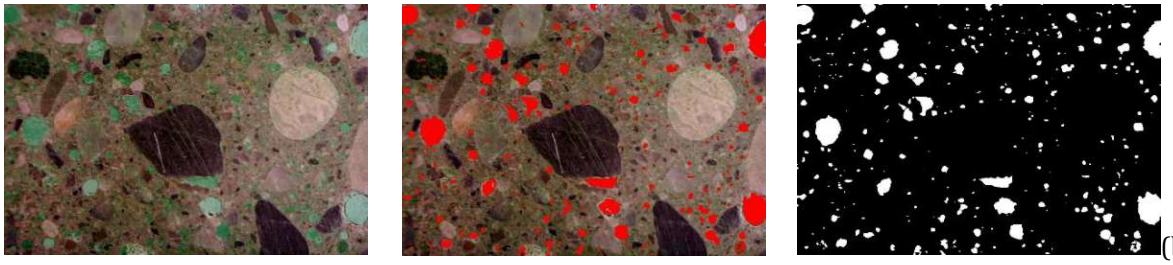
(b)

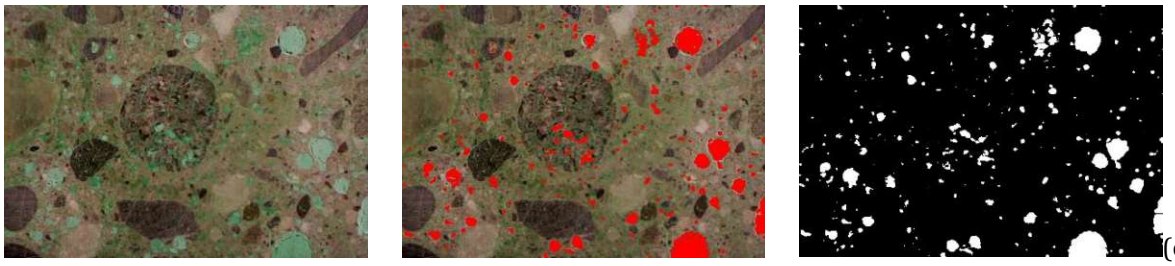
(c)

Fig. 43 (part 1): B7_30-15: Edited image (left), filtered image after applying colour threshold (centre), binary image (right)

Die approbierte gedruckte Originalversion dieser Diplomarbeit ist an der TU Wien Bibliothek verfügbar
The approved original version of this thesis is available in print at TU Wien Bibliothek.
TU Bibliothek Your knowledge hub WIEN

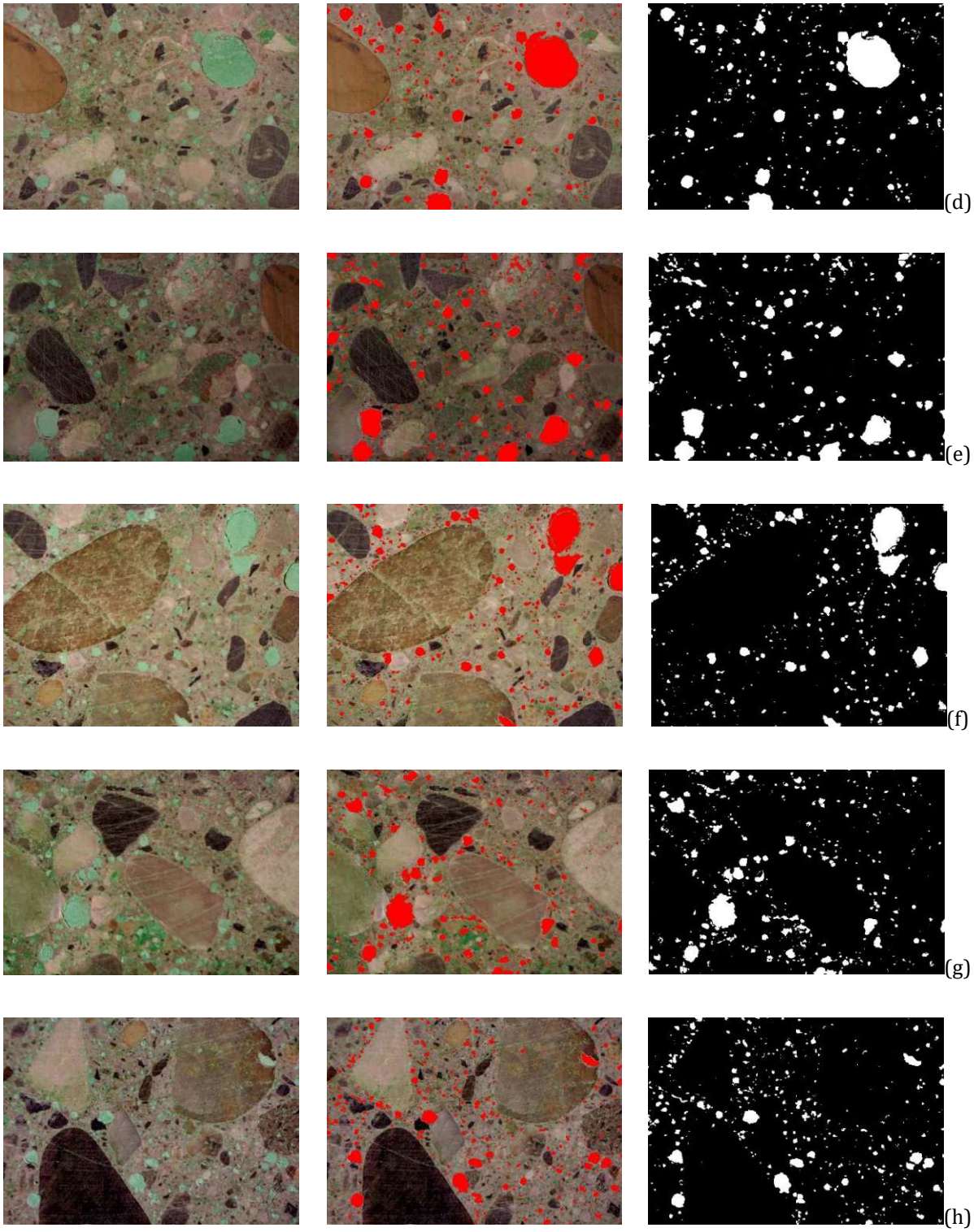

Fig. 44 (part 2): B7_30-15: Edited image (left), filtered image after applying colour threshold (centre), binary image (right)

Die approbierte gedruckte Originalversion dieser Diplomarbeit ist an der TU Wien Bibliothek verfügbar
The approved original version of this thesis is available in print at TU Wien Bibliothek.

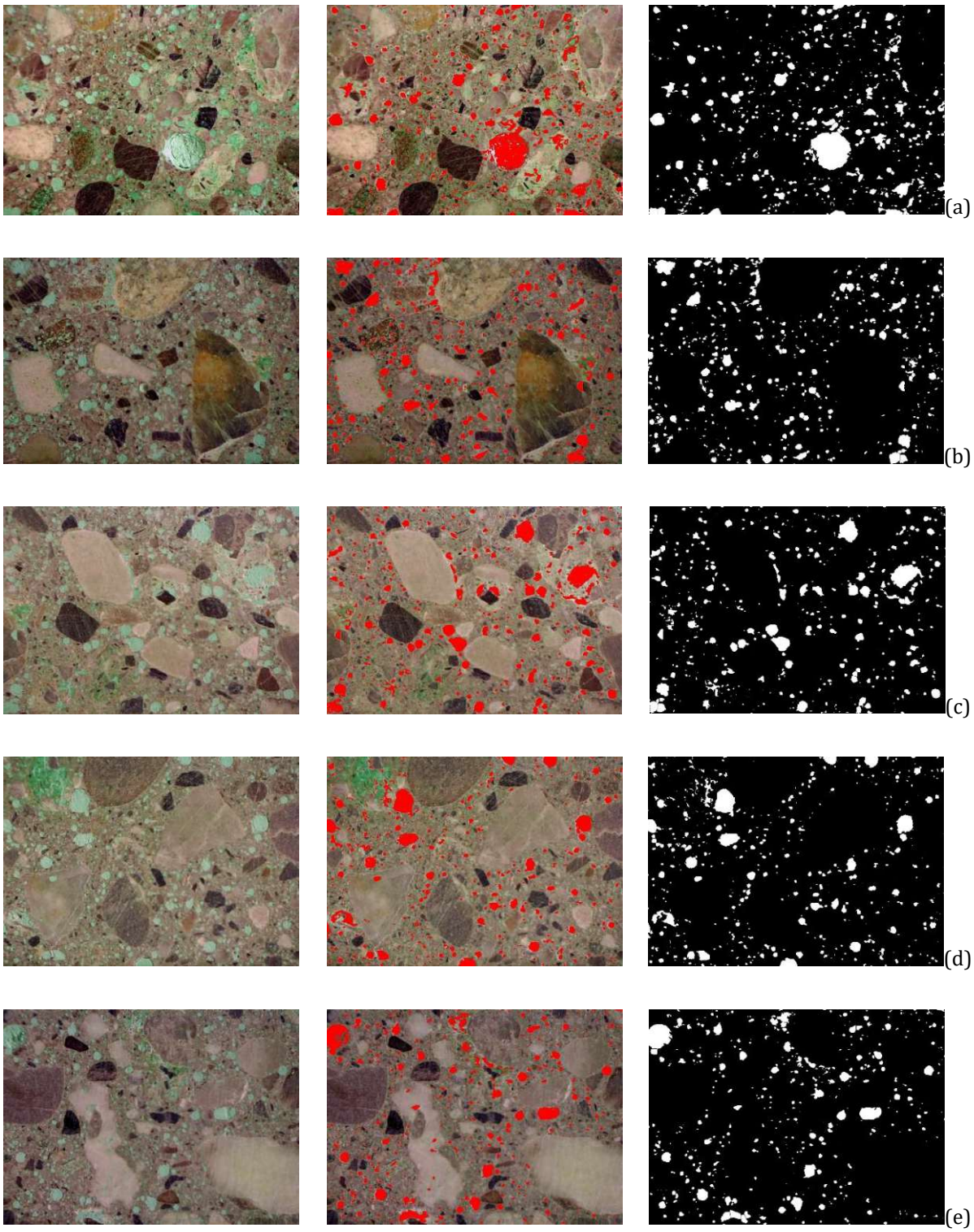

Fig. 45 (part 1): B7_100-15: Edited image (left), filtered image after applying colour threshold (centre), binary image (right)

Die approbierte gedruckte Originalversion dieser Diplomarbeit ist an der TU Wien Bibliothek verfügbar
The approved original version of this thesis is available in print at TU Wien Bibliothek.

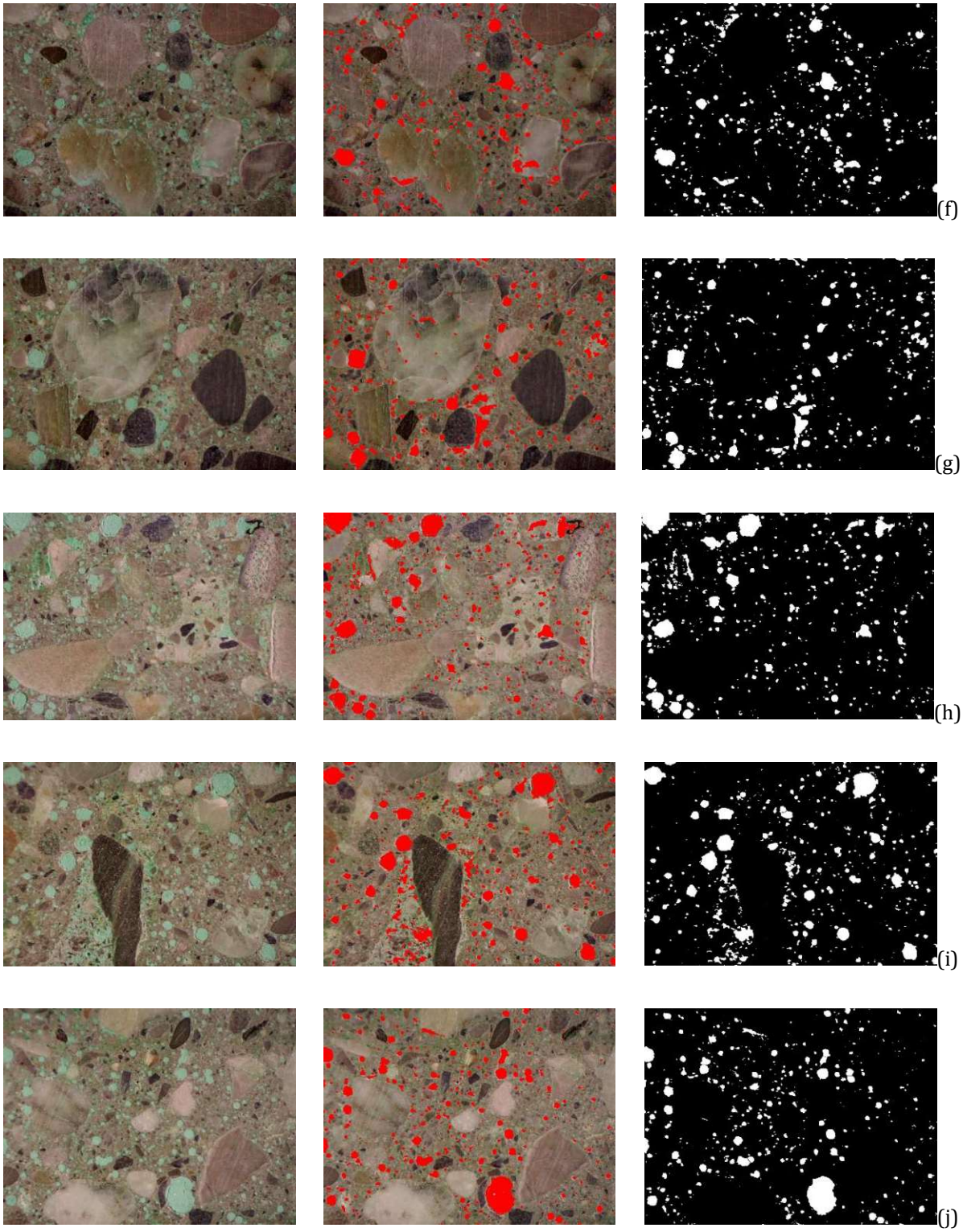

Fig. 46 (part 2): B7_100-15: Edited image (left), filtered image after applying colour threshold (centre), binary image (right)

Die approbierte gedruckte Originalversion dieser Diplomarbeit ist an der TU Wien Bibliothek verfügbar
The approved original version of this thesis is available in print at TU Wien Bibliothek.

(a)

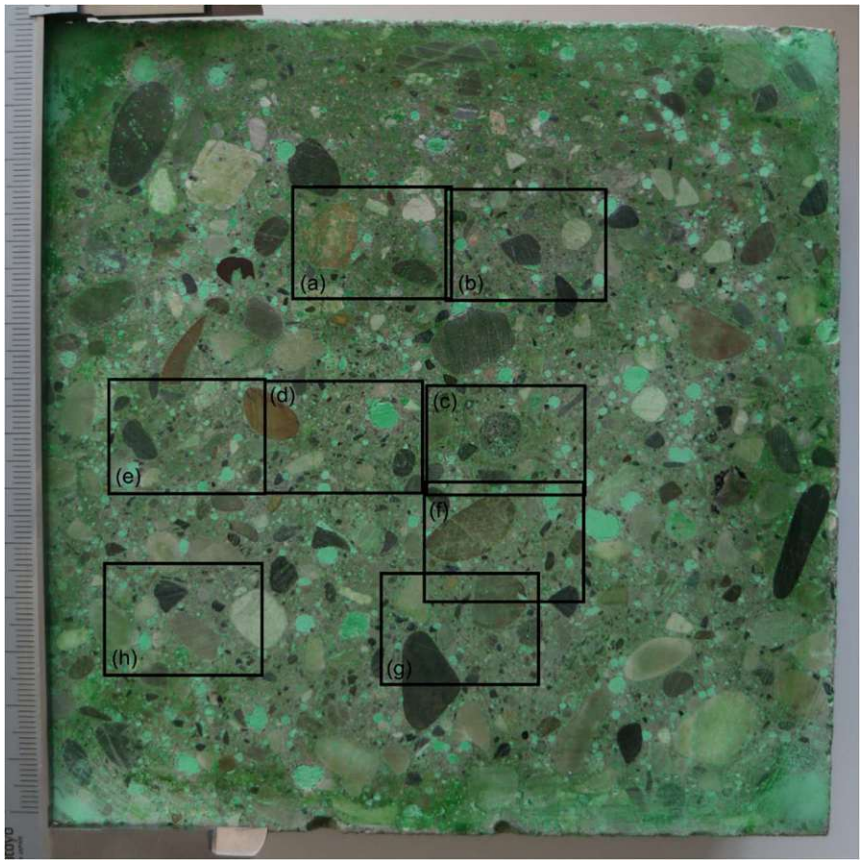

(b)

Fig. 47 (part 1): Positions of the captured images on the surface of (a) B7_0-0, (b) B7_30-15 and (c) B7_100-15 concrete

Die approbierte gedruckte Originalversion dieser Diplomarbeit ist an der TU Wien Bibliothek verfügbar
The approved original version of this thesis is available in print at TU Wien Bibliothek.

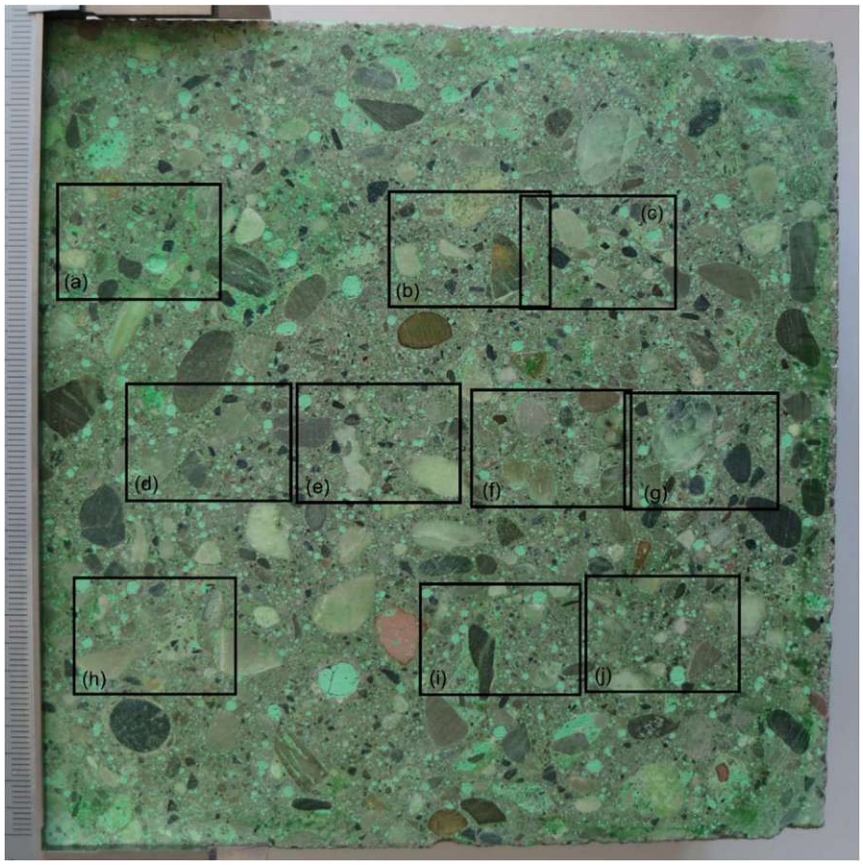

(c)

Fig. 48 (part 2): Positions of the captured images on the surface of (a) B7_0-0, (b) B7_30-15 and (c) B7_100-15 concrete

During the editing and processing of the images in *ImageJ*, we were also able to obtain valuable information about the captured images as seen in **Tab. 18**. The image area was calculated through the set scale, and the air void count indicates the number of air voids on the captured surface. The air void distribution per millimetre was then calculated from these two values. We used the air void distribution as a reference value to verify the plausibility of the results and thus of the colour thresholding procedure.

Die approbierte gedruckte Originalversion dieser Diplomarbeit ist an der TU Wien Bibliothek verfügbar
The approved original version of this thesis is available in print at TU Wien Bibliothek.

Tab. 18: Properties of the images edited and processed in *ImageJ*

	Image	Scale	Image area	Air void count	Air void/mm²	Perimeter
		[px/mm]	[mm²]	[-]	[mm⁻²]	[mm]
B7_0-0	(a)	45	606,6252	587	0,968	0,700
	(b)	45	606,6252	673	1,109	0,696
	(c)	45	606,6252	583	0,961	0,698
	(d)	45	604,636	608	1,006	0,691
	(e)	45	606,6252	685	1,129	0,73
	(f)	45	604,636	670	1,108	0,681
	(g)	45	606,6252	704	1,161	0,651
	(h)	45	604,636	720	1,191	0,702
	(i)	45	606,6252	880	1,451	0,642
	(j)	45	606,6252	689	1,136	0,679
	Mean values	-	-	6799	1,122	0,687
	Total area	-	6060,2844	-	-	-
B7_30-15	(a)	45	560,332	472	0,842	0,880
	(b)	45	557,208	346	0,621	1,010
	(c)	45	559,764	354	0,632	0,947
	(d)	45	563,681	355	0,630	0,880
	(e)	45	569,136	331	0,582	1,030
	(f)	45	606,625	483	0,796	0,767
	(g)	45	561,121	547	0,975	0,761
	(h)	45	562,888	564	1,002	0,716
	Mean values	-	-	-	0,760	0,874
	Total area	-	4540,755	-	-	-
B7_100-15	(a)	45	572,544	598	1,044	0,910
	(b)	45	561,184	556	0,991	0,846
	(c)	45	564,308	469	0,831	0,943
	(d)	45	569,988	530	0,930	0,816
	(e)	45	587,028	475	0,809	0,836
	(f)	45	586,176	588	1,003	0,754
	(g)	45	581,348	517	0,889	0,86
	(h)	45	569,988	529	0,928	0,859
	(i)	45	560,332	550	0,982	0,854
	(j)	45	594,412	560	0,942	0,768
	Mean values	-	-	6417	0,928	0,852
	Total area	-	6917,388	-	-	-

4.8.2 Image Analysis in *MATLAB*

After generating a binary image, we analysed it in *MATLAB* by running the previously described functions in order. We generated a histogram for each image with the computed size distribution of the air voids, using Saltykov's method for non-parametric sphere reconstruc-

Die approbierte gedruckte Originalversion dieser Diplomarbeit ist an der TU Wien Bibliothek verfügbar
The approved original version of this thesis is available in print at TU Wien Bibliothek.
TU Bibliothek Your knowledge hub WIEN

tion to estimate the 3D size distribution based on the apparent sizes on a 2D plane. The reconstruction approach is described in more detail by Fonseca and Scherer [58].

Prior to that, the examined air void properties were calculated and output by the script. We have summarised these in **Tab. 19** for the respective concrete mixtures.

The results presented in **Tab. 19** show large discrepancies between the individual photographs, these differences can be attributed to several causes. As already mentioned, the photos depict an area of around 5,5 to 6 cm² (approx. 3 cm x 2 cm), and with an aggregate size of 0 to 22mm, the proportion of cement paste is lower in photographed areas where larger aggregates are present, and the air void content is therefore also lower. To the same extent, the proportion of cement paste is higher in photographed areas with smaller aggregates and therefore the air void content is also higher. Another reason is the occurrence of entrapped air pockets in the concrete; these are generally larger than the air voids introduced and can noticeably increase the air void content of the analysed images.

The table shows that the air void content increases with increasing aggregate replacement rate. It reaches a value of 7,3% for B7_30-15 concrete and even 7,68% for B7_100-15 concrete. Both values are higher than the air content determined on the fresh concrete. The difference between these results and the results from the air content determination through the pressure gauge method is likely due to the fact that the pressure gauge method is not applicable to concretes made with lightweight aggregates or aggregates with high porosity, which applies to recycled aggregate. This can lead to a deviation of up to 0,6% when using recycled concrete [5]. Therefore, the results from the air void analysis performed are more accurate and can be assumed to reflect the actual air void content of the concrete.

A close examination of the processed images reveals that in some places in the old mortar, unlike in the new mortar, the air voids have a non-circular shape, this could be due to a combination of the manufacturing process of RCA and the surface preparation method (see section 3.6.8). Microcracks occurring in the matrix during the crushing of the concrete cause the material to become brittle along the pore spaces, and this brittleness affects the quality of the surface preparation, resulting in some cases in larger highly porous areas being identified as one single large air pore (**Fig. 49**).

Die approbierte gedruckte Originalversion dieser Diplomarbeit ist an der TU Wien Bibliothek verfügbar
The approved original version of this thesis is available in print at TU Wien Bibliothek.
TU Bibliothek Your knowledge hub WIEN

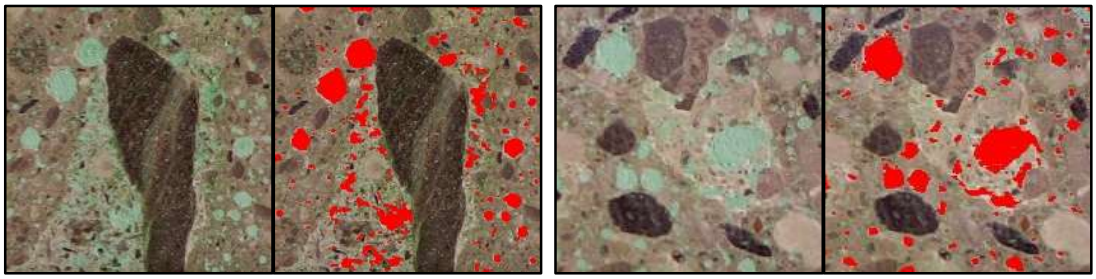

Fig. 49: Examples of RCA with large porous areas

Tab. 19: Air void properties of the images analysed in *MATLAB*

	Image	Air content	Specific surface	Volumetric Paste/Air ratio	Spacing factor
		Vol.- [%]	[mm^{-1}]	[-]	[mm]
B7_0-0	(a)	7,103	10,736	4,447	0,409
	(b)	7,692	12,462	4,080	0,327
	(c)	6,922	11,102	4,572	0,400
	(d)	6,554	12,143	4,848	0,376
	(e)	7,160	13,216	4,408	0,331
	(f)	6,745	12,839	4,701	0,351
	(g)	6,920	12,462	4,573	0,357
	(h)	6,878	14,020	4,603	0,318
	(i)	7,227	14,677	4,364	0,297
	(j)	5,888	14,994	5,434	0,321
	mean	**6,909**	**12,865**	**4,603**	**0,349**
B7_30-15	(a)	6,425	13,430	4,952	0,343
	(b)	7,922	9,283	3,952	0,426
	(c)	6,929	10,136	4,567	0,438
	(d)	8,933	7,221	3,466	0,480
	(e)	7,922	8,874	3,952	0,445
	(f)	7,247	9,747	4,352	0,446
	(g)	7,182	11,907	4,394	0,367
	(h)	5,847	14,108	5,475	0,342
	mean	**7,301**	**10,588**	**4,389**	**0,411**
B7_100-15	(a)	9,651	11,483	3,183	0,277
	(b)	7,191	13,566	4,388	0,342
	(c)	8,182	11,205	3,186	0,341
	(d)	7,239	12,163	4,357	0,358
	(e)	6,585	11,936	4,823	0,382
	(f)	6,252	13,945	5,098	0,335
	(g)	7,003	12,692	4,515	0,348
	(h)	8,453	10,977	3,682	0,335
	(i)	8,957	10,878	3,456	0,318
	(j)	7,285	11,478	4,327	0,377
	mean	**7,680**	**12,032**	**4,102**	**0,341**

Die approbierte gedruckte Originalversion dieser Diplomarbeit ist an der TU Wien Bibliothek verfügbar
The approved original version of this thesis is available in print at TU Wien Bibliothek.
TU Bibliothek Your knowledge hub WIEN

In order to combine the results from the individual photos and obtain meaningful values for the concrete mixtures, we created a function using MATLAB (see Appendix) that allows us to combine the air void distribution of the individual sections and create a histogram that reflects the total air void system determined. The function also indicates the volume fraction of micro air voids, i.e. the volume fraction of all air voids with a diameter of less than or equal to 300 microns.

4.8.3 Computed Sphere Distribution

- B7_0-0

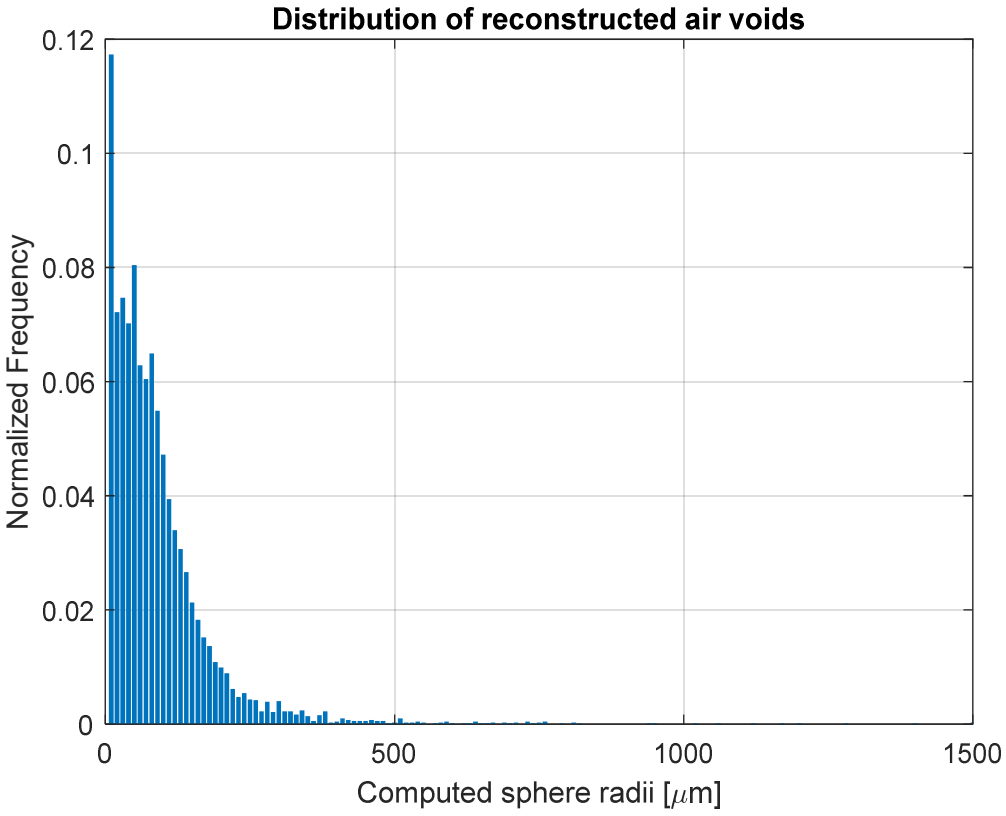

Fig. 50: Air void distribution of computed spheres for B7_0-0

Die approbierte gedruckte Originalversion dieser Diplomarbeit ist an der TU Wien Bibliothek verfügbar
The approved original version of this thesis is available in print at TU Wien Bibliothek.

- B7_30-15

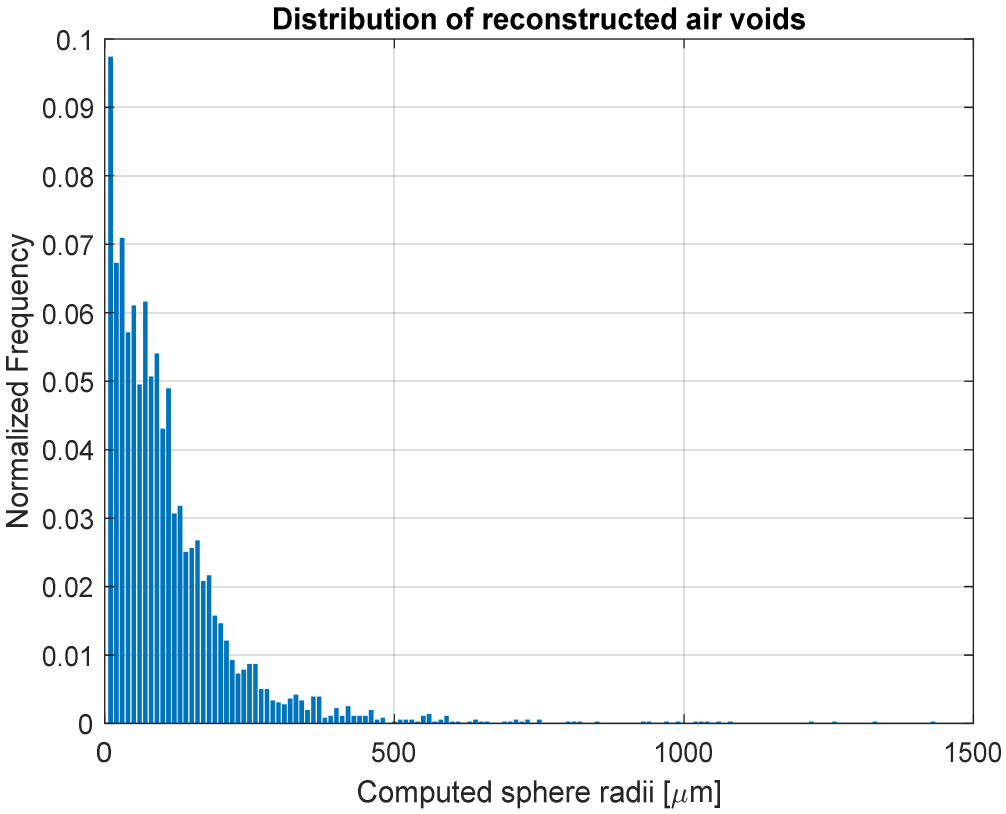

Fig. 51: Air void distribution of computed spheres for B7_30-15

- B7_100-15

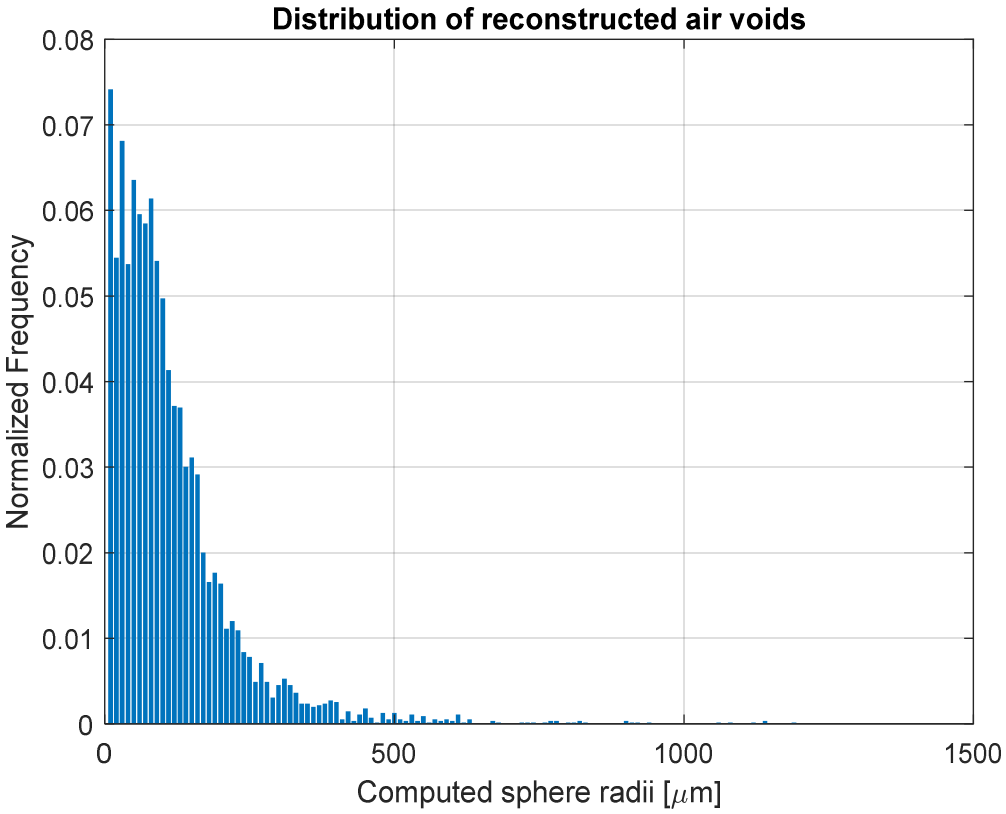

Fig. 52: Air void distribution of computed spheres for B7_100-15

Die approbierte gedruckte Originalversion dieser Diplomarbeit ist an der TU Wien Bibliothek verfügbar
The approved original version of this thesis is available in print at TU Wien Bibliothek.

The comparison of the air void distribution for B7_0-0 and B7_30-15 (**Fig. 53**), as well as for B7_0-0 and B7_100-15 (**Fig. 54**), reveals a clear trend. In the concrete with natural aggregate, the proportion of smaller air voids (at approx. 100 microns) is higher than in the concrete mixtures with RCA, while the proportion of pores larger than 100 microns is higher in RAC than in NAC. This trend is a bit less obvious in the comparison between B7_30-15 and B7_100-15 (**Fig. 55**). The difference in the air void distribution between RCA and NCA suggests that the recycled aggregates increase the number of larger pores, these pores exist in the old, adhered mortar. This is likely the result of different factors. On the one hand, the origin of the concrete from which the aggregate was obtained may have an influence. Compared to ordinary concrete, air-entrained concrete contains not only a higher total volume of air voids but also a larger proportion of micropores, which are beneficial for the durability properties of the concrete. In contrast, the air voids in ordinary concrete tend to be larger, irregularly shaped, unevenly distributed, and are often the result of insufficient compaction. These generally have a negative effect on the properties of concrete. The results of this analysis suggest that the original concrete was not air entrained. Another factor is the deterioration of the interfacial transition zone as a result of weathering during the service life of the concrete, as well as the crushing process during the production process.

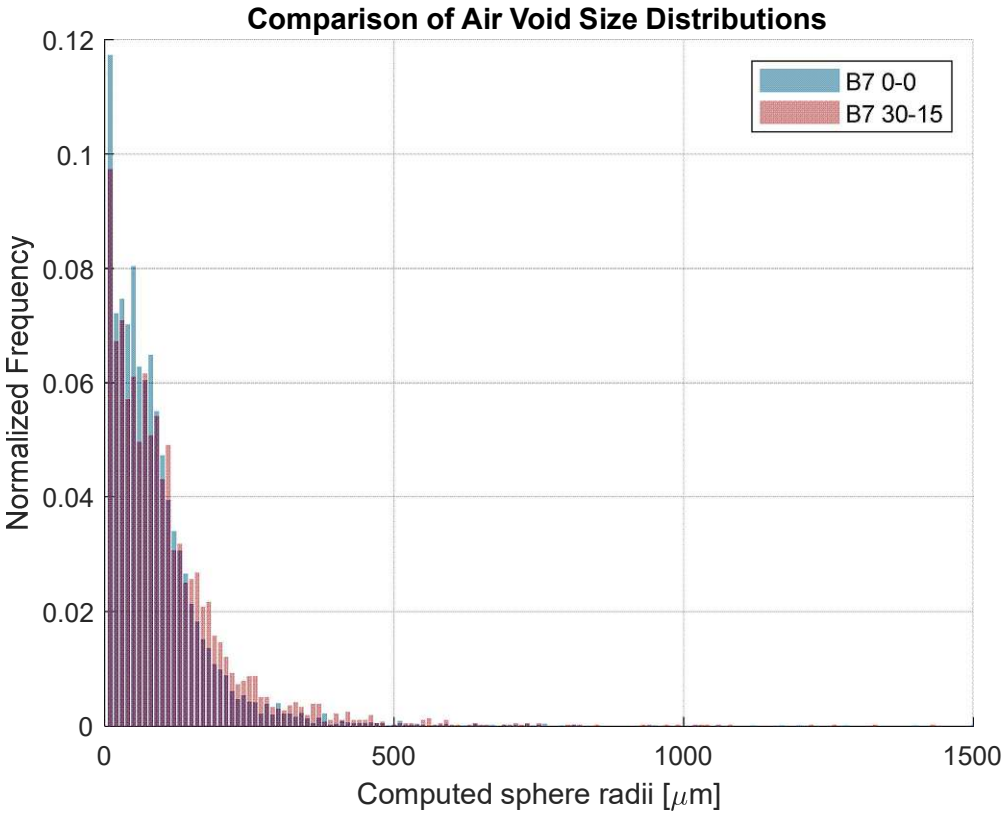

Fig. 53: Comparison of air void distribution of B7_0-0 and B7_30-15

Die approbierte gedruckte Originalversion dieser Diplomarbeit ist an der TU Wien Bibliothek verfügbar
The approved original version of this thesis is available in print at TU Wien Bibliothek.

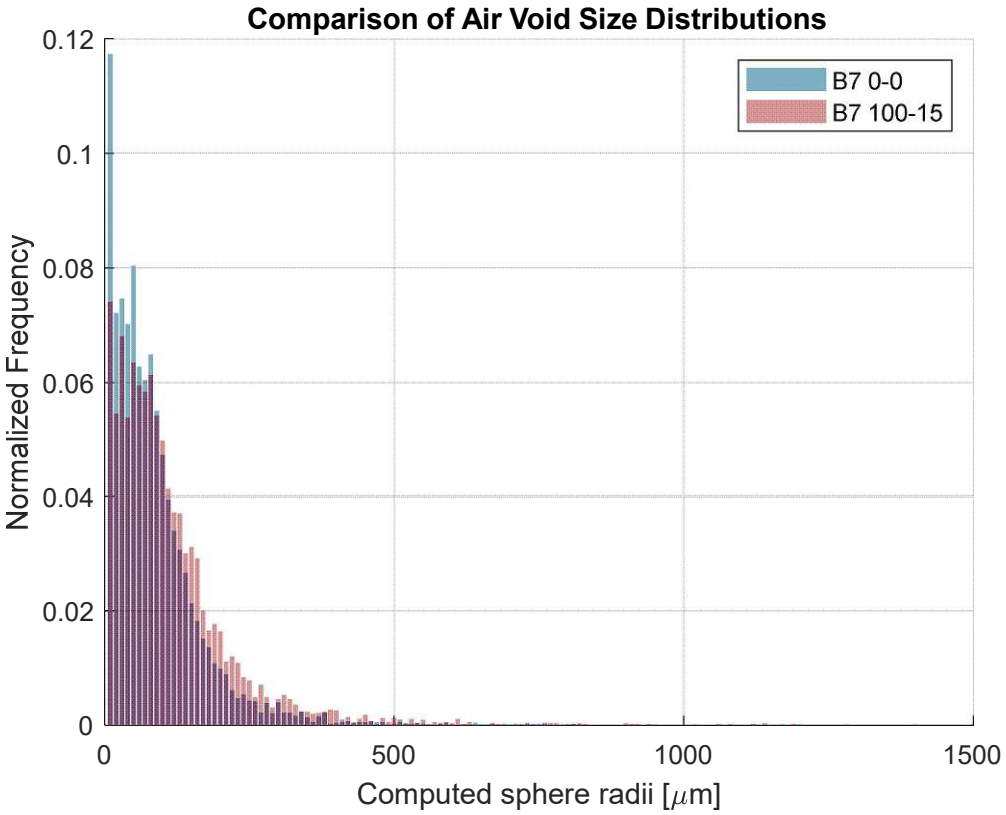

Fig. 54: Comparison of air void distribution of B7_0-0 and B7_100-15

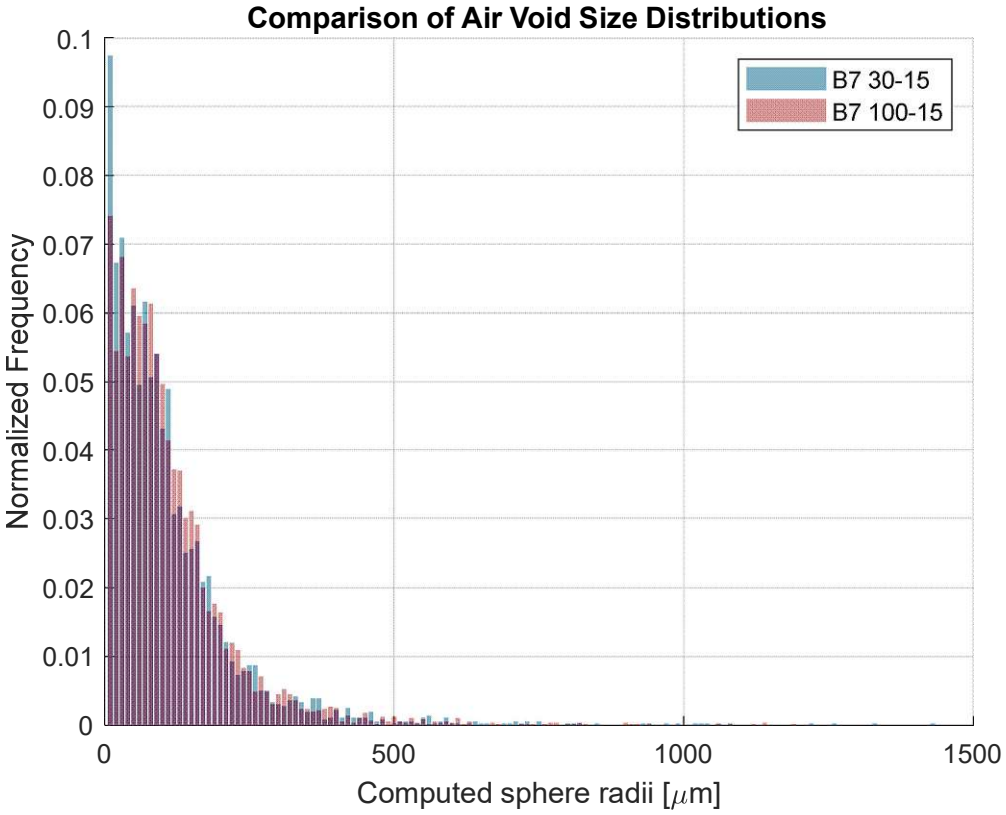

Fig. 55: Comparison of air void distribution of B7_30-15 and B7_100-15

Die approbierte gedruckte Originalversion dieser Diplomarbeit ist an der TU Wien Bibliothek verfügbar
The approved original version of this thesis is available in print at TU Wien Bibliothek.
TU Bibliothek Your knowledge hub WIEN

5 Conclusion

5.1 Summary of Findings

This study investigated the mechanical and durability performance of recycled aggregate concrete incorporating varying replacement ratios of NA with RCA. The results demonstrate that, with appropriate mix design adjustments and aggregate treatment, RAC can achieve satisfactory performance in several key aspects, although some durability properties remain critical limitations.

The presence of porous mortar was identified as a fundamental factor influencing the strength and durability of RAC. The quality of the recycled aggregates, the applied mixing approach and the aggregate pre-treatment therefore play a decisive role in the resulting concrete performance.

5.2 Fresh Concrete Properties

By adjusting the superplasticiser dosage, applying the adapted two-stage mixing approach, and pre-saturating the RCA to 80% of their water absorption capacity, three mixtures with targeted equivalent consistencies were successfully produced. All maintained satisfactory workability values after 45 minutes. However, a decrease in workability after 90 minutes was observed with increasing RCA content, primarily due to the higher share of fine aggregate fractions (0,250 to 4 mm) and the associated increase in surface area and water absorption. Through the optimisation of the particle size distribution design in RAC mixtures, an improvement of concrete consistency could be reached.

Through the addition of air-entraining agents in the mixing design, all mixtures exhibited air contents around 7%, remaining within the permissible range for concrete exposed to severe environmental conditions. The substitution of NA with RCA did not significantly affect the air content measured on fresh concrete, though the used pressure gauge method may not accurately capture the air content in concrete containing porous aggregates, as stated in the corresponding norm. The incorporation of RCA led to a reduction in concrete density of up to approximately 4% compared to the reference concrete, consistent with the lower specific gravity of RCA.

5.3 Mechanical Properties

An increase in RCA content led to a reduction in compressive strength, which is attributed to the presence of two ITZs. Nevertheless, the partial pre-saturation of RCA and the use of the

Die approbierte gedruckte Originalversion dieser Diplomarbeit ist an der TU Wien Bibliothek verfügbar
The approved original version of this thesis is available in print at TU Wien Bibliothek.
TU Bibliothek Your knowledge hub WIEN

adapted TSMA mitigated this negative effect, resulting in RAC with overall satisfactory strength levels. In particular, RAC exhibited higher early-age compressive strength than NAC, likely due to internal curing provided by water stored within the porous RCA. After 56 days, the mixture with 30% coarse and 15% fine RCA showed no significant strength loss compared to the reference, while the mixture with 100% coarse and 15% fine RCA displayed a moderate reduction. Overall, RAC mixtures achieved adequate mechanical performance for structural applications.

5.4 Durability Properties

Chloride Resistance:

Chloride ingress increased with higher RCA content due to the greater porosity of recycled aggregates. This trend aligns with expectations and literature findings, confirming that higher permeability of RCA facilitates chloride-ion transport within the concrete matrix.

Freeze–Thaw Resistance:

RAC mixtures showed substantially higher surface scaling under freeze–thaw conditions with de-icing salts, failing to meet the standard requirements for XF4 exposure class (freeze-thaw attack under high water saturation with de-icing agent). The B7_30-15 and B7_100-15 mixtures exceeded the allowable scaling limit by 120% and 240%, respectively. The poor freeze–thaw performance suggests that the RCA used in this study is obtained from non-air-entrained concrete. Improvements may be achieved through more rigorous selection of RCA based on source quality and the use of air-entrained parent concrete.

Depth of Water Penetration:

Contrary to some literature, the incorporation of RCA even up to 100% did not increase water permeability under pressure. All mixtures exhibited very low penetration depths (5,0 to 5,7 mm), largely due to the low water–binder ratio. This suggests that the chosen mix design effectively limited permeability. However, the standard test method (ÖNORM B 4710-3 [45]) is imprecise and may not be well suited for low w/b-ratio concretes with high air content.

Carbonation Depth:

The inclusion of RCA increased carbonation depth, consistent with existing studies attributing this to the higher porosity. The results confirm that carbonation progresses more rapidly in RAC than in NAC, although the extent depends on RCA characteristics, replacement ratio, and exposure conditions. The use of supplementary cementitious materials, such as fly ash or slag, may help reduce carbonation depth and improve long-term durability.

Die approbierte gedruckte Originalversion dieser Diplomarbeit ist an der TU Wien Bibliothek verfügbar
The approved original version of this thesis is available in print at TU Wien Bibliothek.
TU Bibliothek Your knowledge hub WIEN

Digital Air-Void Analysis:

The digital air-void analysis showed that the total air-void volume increased with higher RCA content, while the micropore content decreased. This finding explains the poor freeze–thaw performance observed experimentally and highlights the need for stricter selection of RCA with appropriate air-void structure for the utilisation in severe conditions.

5.5 Overall Assessment

Overall, the results indicate that recycled aggregate concrete can achieve comparable mechanical performance to conventional concrete when properly designed and produced. However, durability remains the primary limitation, particularly with respect to freeze–thaw resistance and carbonation depth. These shortcomings seem to be primarily linked to the porosity and microstructural characteristics of the recycled aggregates rather than the mixing process itself. Consequently, RAC in applications requiring high durability, is only implementable with careful selection and pre-treatment of aggregates.

Future research should focus on enhancing RAC durability through improved aggregate pre-treatment, quality-based aggregate classification, and optimised mix designs. Particular attention should be given to the use of RCA derived from air-entrained parent concrete, as such aggregates may provide improved freeze–thaw resistance and overall durability performance. Further investigation of curing techniques and aggregate processing methods may also contribute to the sustainable and widespread use of recycled concrete aggregates in structural concrete.

Die approbierte gedruckte Originalversion dieser Diplomarbeit ist an der TU Wien Bibliothek verfügbar
The approved original version of this thesis is available in print at TU Wien Bibliothek.
TU Bibliothek Your knowledge hub WIEN

Bibliography

[1] 'Über UP!crete – UP!crete'. Accessed: Oct. 24, 2025. [Online]. Available: https://up-crete.project.tuwien.ac.at/ueber-upcrete/

[2] Österreichischer Baustoff-Recycling Verband, 'Die 10 Qualitätsbaustoffe nach der neuen Recycling-Baustoffverordnung und typische Anwendungsmöglichkeiten'. [Online]. Available: https://brv.at/recycling-baustoffe/

[3] M. Khan and M. Dominic, 'Sustainability of concrete using recycled aggregate: a review', *Sustain. Agri Food Environ. Res.*, vol. 10, Apr. 2021, doi: 10.7770/safer-V10N1-art2508.

[4] A. Müller, 'Aufbereitung von Bauabfällen', in *Baustoffrecycling: Entstehung - Aufbereitung - Verwertung*, A. Müller, Ed., Wiesbaden: Springer Fachmedien, 2018, pp. 61–124. doi: 10.1007/978-3-658-22988-7_4.

[5] K. P. Verian, 'Using recycled concrete as coarse aggregate in pavement concrete', Purdue University, 2012.

[6] M. Etxeberria, E. Vázquez, A. Marí, and M. Barra, 'Influence of amount of recycled coarse aggregates and production process on properties of recycled aggregate concrete', *Cem. Concr. Res.*, vol. 37, no. 5, pp. 735–742, May 2007, doi: 10.1016/j.cemconres.2007.02.002.

[7] K. P. Verian, W. Ashraf, and Y. Cao, 'Properties of recycled concrete aggregate and their influence in new concrete production', *Resour. Conserv. Recycl.*, vol. 133, pp. 30–49, June 2018, doi: 10.1016/j.resconrec.2018.02.005.

[8] 'Einsatz von Recyclingbeton im Hochbau.pdf'. Accessed: May 28, 2025. [Online]. Available: https://hochbauamt.tg.ch/public/upload/assets/111211/Einsatz%20von%20Recyclingbeton%20im%20Hochbau.pdf

[9] R. Kurda, J. Brito, and J. Silvestre, 'Indirect evaluation of the compressive strength of recycled aggregate concrete with high fly ash ratios', *Mag. Concr. Res.*, vol. 70, pp. 204–216, Sept. 2017, doi: 10.1680/jmacr.17.00216.

[10] A. G. Khoshkenari, P. Shafigh, M. Moghimi, and H. B. Mahmud, 'The role of 0–2 mm fine recycled concrete aggregate on the compressive and splitting tensile strengths of recycled concrete aggregate concrete', *Mater. Des.*, vol. 64, pp. 345–354, Dec. 2014, doi: 10.1016/j.matdes.2014.07.048.

[11] P. Zhu, Y. Hao, H. Liu, D. Wei, S. Liu, and L. Gu, 'Durability evaluation of three generations of 100% repeatedly recycled coarse aggregate concrete', *Constr. Build. Mater.*, vol. 210, pp. 442–450, June 2019, doi: 10.1016/j.conbuildmat.2019.03.203.

[12] H. Luo, J. Aguiar, X. Wan, Y. Wang, S. Cunha, and Z. Jia, 'Application of Aggregates from Construction and Demolition Wastes in Concrete: Review', *Sustainability*, vol. 16, no. 10, Art. no. 10, Jan. 2024, doi: 10.3390/su16104277.

[13] V. W. Y. Tam, X. F. Gao, and C. M. Tam, 'Microstructural analysis of recycled aggregate concrete produced from two-stage mixing approach', *Cem. Concr. Res.*, vol. 35, no. 6, pp. 1195–1203, June 2005, doi: 10.1016/j.cemconres.2004.10.025.

[14] K. L. Scrivener, A. K. Crumbie, and P. Laugesen, 'The Interfacial Transition Zone (ITZ) Between Cement Paste and Aggregate in Concrete', *Interface Sci.*, vol. 12, no. 4, pp. 411–421, Oct. 2004, doi: 10.1023/B:INTS.0000042339.92990.4c.

[15] B. Wang, L. Yan, Q. Fu, and B. Kasal, 'A Comprehensive Review on Recycled Aggregate and Recycled Aggregate Concrete', *Resour. Conserv. Recycl.*, vol. 171, p. 105565, Aug. 2021, doi: 10.1016/j.resconrec.2021.105565.

[16] S. Mindess, J. F. Young, and D. Darwin, *Concrete*. in Prentice-Hall civil engineering and engineering mechanics series. Prentice Hall, 2003. [Online]. Available: https://books.google.at/books?id=euMXnwEACAAJ

[17] A. S. Brand, J. R. Roesler, and A. Salas, 'Initial moisture and mixing effects on higher quality recycled coarse aggregate concrete', *Constr. Build. Mater.*, vol. 79, pp. 83–89, Mar. 2015, doi: 10.1016/j.conbuildmat.2015.01.047.

[18] I. F. Sáez del Bosque, W. Zhu, T. Howind, A. Matías, M. I. Sánchez de Rojas, and C. Medina, 'Properties of interfacial transition zones (ITZs) in concrete containing recycled mixed ag-

Die approbierte gedruckte Originalversion dieser Diplomarbeit ist an der TU Wien Bibliothek verfügbar
The approved original version of this thesis is available in print at TU Wien Bibliothek.
TU Bibliothek Your knowledge hub WIEN

gregate', *Cem. Concr. Compos.*, vol. 81, pp. 25–34, Aug. 2017, doi: 10.1016/j.cemconcomp.2017.04.011.
[19] F. Trebut and B. Pfefferer, 'Anforderungen an die Kreislauffähigkeit von Massivbaustoffen'.
[20] Austrian Standards International, *ÖNORM B 4710-1:2018 01 01: Concrete - Specification, performance, production, use and conformity - Part 1: Rules for the implementation of ÖNORM EN 206 for normal and heavy concrete*, Wien., 01 2018.
[21] W. Matthes *et al.*, 'Ground Granulated Blast-Furnace Slag', in *Properties of Fresh and Hardened Concrete Containing Supplementary Cementitious Materials: State-of-the-Art Report of the RILEM Technical Committee 238-SCM, Working Group 4*, N. De Belie, M. Soutsos, and E. Gruyaert, Eds, Cham: Springer International Publishing, 2018, pp. 1–53. doi: 10.1007/978-3-319-70606-1_1.
[22] Austrian Standards International, *ÖNORM EN 197-1:2011 10 15: Cement - Part 1: Composition, specifications and conformity criteria for common cements*, Wien., 15 2011.
[23] Austrian Standards International, *ÖNORM B 3309-1:2010 12 01: Processed hydraulic additions for concrete prduction - Part 1: Combination products (GC/GC-HS)*, Wien., 01 2010.
[24] J.W. Meusel and J.H. Rose, 'Production of Granulated Blast Furnace Slag at Sparrows Point, and the Workability and Strength Potential of Concrete Incorporating the Slag', *ACI Symp. Publ.*, vol. 79, Jan. 1983, doi: 10.14359/6730.
[25] P. L. Domone and M. N. Soutsos, 'Properties of high-strength concrete mixes containing PFA and ggbs', *Mag. Concr. Res.*, vol. 47, no. 173, pp. 355–367, 1995, doi: 10.1680/macr.1995.47.173.355.
[26] R. Demirboğa, 'Influence of mineral admixtures on thermal conductivity and compressive strength of mortar', *Energy Build.*, vol. 35, no. 2, pp. 189–192, Feb. 2003, doi: 10.1016/S0378-7788(02)00052-X.
[27] G. Xu and X. Shi, 'Characteristics and applications of fly ash as a sustainable construction material: A state-of-the-art review', *Resour. Conserv. Recycl.*, vol. 136, pp. 95–109, Sept. 2018, doi: 10.1016/j.resconrec.2018.04.010.
[28] K. Sideris, H. Justnes, M. Soutsos, and T. Sui, 'Fly Ash', in *Properties of Fresh and Hardened Concrete Containing Supplementary Cementitious Materials: State-of-the-Art Report of the RILEM Technical Committee 238-SCM, Working Group 4*, N. De Belie, M. Soutsos, and E. Gruyaert, Eds, Cham: Springer International Publishing, 2018, pp. 55–98. doi: 10.1007/978-3-319-70606-1_2.
[29] L. Courard, D. Herfort, and Y. Villagrán, 'Limestone Powder', in *Properties of Fresh and Hardened Concrete Containing Supplementary Cementitious Materials: State-of-the-Art Report of the RILEM Technical Committee 238-SCM, Working Group 4*, N. De Belie, M. Soutsos, and E. Gruyaert, Eds, Cham: Springer International Publishing, 2018, pp. 123–151. doi: 10.1007/978-3-319-70606-1_4.
[30] Austrian Standards International, *ÖNORM EN 12620:2014 02 15: Aggregates for concrete*, Wien., 15 2014.
[31] Austrian Standards International, *ÖNORM B 3140:2020 11 01: Recycled aggregates for unbound and hydraulically bound applicaions as well as for concrete*, Wien., 01 2020.
[32] Austrian Standards International, *ÖNORM EN 1097-6:2022 05 01: Tests for mechanical and physical properties of aggregates - Part 6: Determination of particle density and water absortion*, Wien., 01 2022.
[33] J. García-González, D. Rodríguez-Robles, A. Juan-Valdes, J. Pozo, and M. Guerra-Romero, 'Pre-Saturation Technique of the Recycled Aggregates: Solution to the Water Absorption Drawback in the Recycled Concrete Manufacture', *Materials*, vol. 7, pp. 6224–6236, Sept. 2014, doi: 10.3390/ma7096224.
[34] A. S. Brand, J. R. Roesler, and A. Salas, 'Initial moisture and mixing effects on higher quality recycled coarse aggregate concrete', *Constr. Build. Mater.*, vol. 79, pp. 83–89, Mar. 2015, doi: 10.1016/j.conbuildmat.2015.01.047.
[35] C. S. Poon, Z. H. Shui, L. Lam, H. Fok, and S. C. Kou, 'Influence of moisture states of natural and recycled aggregates on the slump and compressive strength of concrete', *Cem. Concr. Res.*, vol. 34, no. 1, Art. no. 1, Jan. 2004, doi: 10.1016/S0008-8846(03)00186-8.

Die approbierte gedruckte Originalversion dieser Diplomarbeit ist an der TU Wien Bibliothek verfügbar
The approved original version of this thesis is available in print at TU Wien Bibliothek.
TU Bibliothek Your knowledge hub WIEN

[36] J. Plank, E. Sakai, C. W. Miao, C. Yu, and J. X. Hong, 'Chemical admixtures — Chemistry, applications and their impact on concrete microstructure and durability', *Cem. Concr. Res.*, vol. 78, pp. 81–99, Dec. 2015, doi: 10.1016/j.cemconres.2015.05.016.

[37] N. Kisku, P. Rajhans, S. K. Panda, V. Pandey, and S. Nayak, 'Microstructural investigation of recycled aggregate concrete produced by adopting equal mortar volume method along with two stage mixing approach', *Structures*, vol. 24, pp. 742–753, Apr. 2020, doi: 10.1016/j.istruc.2020.01.044.

[38] V. W. Y. Tam, X. F. Gao, and C. M. Tam, 'Microstructural analysis of recycled aggregate concrete produced from two-stage mixing approach', *Cem. Concr. Res.*, vol. 35, no. 6, Art. no. 6, June 2005, doi: 10.1016/j.cemconres.2004.10.025.

[39] Austrian Standards International, *ÖNORM EN 12350-5:2019 08 15: Testing fresh concrete - Part 5: Flow table test*, Wien., 15 2019.

[40] 'Workability of Concrete – Types and Effects on Concrete Strength', theconstructor.org. Accessed: Apr. 11, 2025. [Online]. Available: https://theconstructor.org/concrete/workability-of-concrete-types-strength/11739/

[41] M. Nedeljković, J. Visser, B. Šavija, S. Valcke, and E. Schlangen, 'Use of fine recycled concrete aggregates in concrete: A critical review', *J. Build. Eng.*, vol. 38, p. 102196, June 2021, doi: 10.1016/j.jobe.2021.102196.

[42] Austrian Standards International, *ÖNORM EN 12350-6:2019 09 15: Testing fresh concrete - Part 6: Density*, Wien., 15 2019.

[43] Austrian Standards International, *ÖNORM EN 12350-7:2023 02 15: Testing fresh concrete - Part 7: Air content - Pressure methods (consolidated version)*, Wien., 15 2023.

[44] Austrian Standards International, *ÖNORM B 4710-1:2018 01 01: Concrete - Specification, performance, production, use and conformity - Part 1: Rules for the implementation of ÖNORM EN 206 for normal and heavy concrete*, Wien., 01 2018.

[45] Austrian Standards International, *ÖNORM B 4710-3:2023 01 01: Concrete - Specification, performance, production, use and conformity - Part 3: National applicaion of testing standards for concrete and its source materials*, Wien., 01 2023.

[46] Austrian Standards International, *ÖNORM EN 12390-7:2021 01 15: Testing hardened concrete - Part 7: Density of hardened concrete*, Wien., 15 2021. Accessed: Apr. 06, 2025. [Online]. Available: https://lesesaal.austrian-standards.at/action/de/private/details/692080/OENORM_EN_12390-7_2021_01_15

[47] Austrian Standards International, *ÖNORM EN 12390-3:2019 11 15: Testing hardened concrete - Part 3: Compressive strength of test specimens*, Wien., 15 2019.

[48] Austrian Standards International, *ÖNORM EN 12390-1:2021 11 01: Testing hardened concrete - Part 1: Shape, dimensions and other requirements for specimens and moulds*, Wien., 01 2021.

[49] H. Ye, C. Fu, Y. Tian, and N. Jin, 'Chloride Ingress in Cracked Concrete', in *Chloride-Induced Steel Corrosion in Concrete Under Service Loads*, H. Ye, C. Fu, Y. Tian, and N. Jin, Eds, Singapore: Springer, 2020, pp. 43–60. doi: 10.1007/978-981-15-4108-7_3.

[50] Austrian Standards International, *ÖNORM EN 12390-13:2015 12 01: Testing hardened concrete - Part 11: Determination of the chloride resistance of concrete, unidirectional diffusion*, Wien., 01 2015.

[51] Austrian Standards Institut, *ÖNORM EN 12390-11_2015-12, Testing hardened concrete, Part 11: Determination of the chloride resistance of concrete, unidirectional diffusion*.

[52] Austrian Standards International, *ÖNORM EN 14629:2007 06 01: Products and systems for the protection and repair of concrete structures - Test methods - Determination of chloride content in hardened concrete*, Wien., 01 2007. Accessed: Apr. 15, 2025. [Online]. Available: https://lesesaal.austrian-standards.at/action/de/private/details/264428/OENORM_EN_14629_2007_06_01

[53] Austrian Standards International, *ONR CEN/TS 12390-9:2017 02 15: Testing hardened concrete - Part 9: Freeze-thaw resistance with de-icing salts - Scaling (CEN/TS 12390-9:2016)*, Wien., 15 2017.

[54] J. Chen, S. Yu, W. Huang, and H. Wang, 'Two-Dimensional Microstructure-Based Model for Evaluating the Permeability Coefficient of Heterogeneous Construction Materials', *Materials*, vol. 16, no. 17, p. 5892, Aug. 2023, doi: 10.3390/ma16175892.

Die approbierte gedruckte Originalversion dieser Diplomarbeit ist an der TU Wien Bibliothek verfügbar
The approved original version of this thesis is available in print at TU Wien Bibliothek.
TU Bibliothek Your knowledge hub WIEN

[55] Austrian Standards International, *ÖNORM EN 12390-12:2020 03 01: Testing hardened concrete - Part 12: Determination of the carbonation resistance of concrete - Accelerated carbonation method*, Wien., 01 2020.

[56] Austrian Standards International, *ÖNORM EN 12390-2:2019 11 15: Testing hardened concrete - Part 2: Making and cuing specimens for strength tests*, Wien., 15 2019. Accessed: Apr. 13, 2025. [Online]. Available: https://lesesaal.austrian-standards.at/action/de/private/details/664990/OENORM_EN_12390-2_2019_11_15

[57] Austrian Standards International, *ÖNORM EN 480-11:2005 12 01: Admixtures for concrete, mortar and grout . Test methods - Part 11: Determination of air voids characteristics in hardened concrete*, Wien., 01 2005.

[58] P. C. Fonseca and G. W. Scherer, 'An image analysis procedure to quantify the air void system of mortar and concrete', *Mater. Struct.*, vol. 48, no. 10, pp. 3087–3098, Oct. 2015, doi: 10.1617/s11527-014-0381-9.

[59] T. Ferreira and W. S. Rasband, 'ImageJ User Guide - IJ 1.46r'. Accessed: Mar. 28, 2025. [Online]. Available: https://imagej.net/ij/docs/guide/

[60] C. S. Poon, Z. H. Shui, L. Lam, H. Fok, and S. C. Kou, 'Influence of moisture states of natural and recycled aggregates on the slump and compressive strength of concrete', *Cem. Concr. Res.*, vol. 34, no. 1, pp. 31–36, Jan. 2004, doi: 10.1016/S0008-8846(03)00186-8.

[61] J. García-González, D. Rodríguez-Robles, A. Juan-Valdes, J. Pozo, and M. Guerra-Romero, 'Pre-Saturation Technique of the Recycled Aggregates: Solution to the Water Absorption Drawback in the Recycled Concrete Manufacture', *Materials*, vol. 7, pp. 6224–6236, Sept. 2014, doi: 10.3390/ma7096224.

[62] A. Nealen and S. Schenk, 'The influence of recycled aggregate core moisture on freshly mixed and hardened concrete properties', *Darmstadt Concr*, vol. 13, no. 5, 1998.

[63] R. V. Silva, J. de Brito, and R. K. Dhir, 'Fresh-state performance of recycled aggregate concrete: A review', *Constr. Build. Mater.*, vol. 178, pp. 19–31, July 2018, doi: 10.1016/j.conbuildmat.2018.05.149.

[64] Austrian Standards International, *ÖNORM EN 12350-7:2023 02 15: Testing fresh concrete - Part 7: Air content - Pressure methods (consolidated version)*, Wien., 15 2023.

[65] Austrian Standards International, *ÖNORM EN 12390-3:2019 11 15: Testing hardened concrete - Part 3: Compressive strength of test specimens*, Wien., 15 2019.

[66] R. V. Silva, de Brito ,J., and R. K. and Dhir, 'The influence of the use of recycled aggregates on the compressive strength of concrete: a review', *Eur. J. Environ. Civ. Eng.*, vol. 19, no. 7, pp. 825–849, Aug. 2015, doi: 10.1080/19648189.2014.974831.

[67] B. Wang, L. Yan, Q. Fu, and B. Kasal, 'A Comprehensive Review on Recycled Aggregate and Recycled Aggregate Concrete', *Resour. Conserv. Recycl.*, vol. 171, p. 105565, Aug. 2021, doi: 10.1016/j.resconrec.2021.105565.

[68] S. M. S. Kazmi, M. J. Munir, Y.-F. Wu, I. Patnaikuni, Y. Zhou, and F. Xing, 'Effect of different aggregate treatment techniques on the freeze-thaw and sulfate resistance of recycled aggregate concrete', *Cold Reg. Sci. Technol.*, vol. 178, p. 103126, Oct. 2020, doi: 10.1016/j.coldregions.2020.103126.

[69] C. Rangel, M. Amario, M. Pepe, E. Martinelli, and R. Toledo Filho, 'Durability of Structural Recycled Aggregate Concrete Subjected to Freeze-Thaw Cycles', *Sustainability*, vol. 12, p. 6475, Aug. 2020, doi: 10.3390/su12166475.

[70] J. T. Smith, 'Recycled Concrete Aggregate – A Viable Aggregate Source For Concrete Pavements', University of Waterloo, 2009. Accessed: Mar. 29, 2025. [Online]. Available: http://hdl.handle.net/10012/4900

[71] A. Gokce, S. Nagataki, T. Saeki, and M. Hisada, 'Freezing and thawing resistance of air-entrained concrete incorporating recycled coarse aggregate: The role of air content in demolished concrete', *Cem. Concr. Res.*, vol. 34, no. 5, pp. 799–806, May 2004, doi: 10.1016/j.cemconres.2003.09.014.

[72] H. Guo *et al.*, 'Durability of recycled aggregate concrete – A review', *Cem. Concr. Compos.*, vol. 89, pp. 251–259, May 2018, doi: 10.1016/j.cemconcomp.2018.03.008.

[73] I. Martínez-Lage, F. Martínez-Abella, C. Vázquez-Herrero, and J. L. Pérez-Ordóñez., 'Properties of plain concrete made with mixed recycled coarse aggregate', *Constr. Build. Mater.*, vol. 37, pp. 171–176, Dec. 2012, doi: 10.1016/j.conbuildmat.2012.07.045.

Die approbierte gedruckte Originalversion dieser Diplomarbeit ist an der TU Wien Bibliothek verfügbar
The approved original version of this thesis is available in print at TU Wien Bibliothek.
TU Bibliothek Your knowledge hub WIEN

[74] C. Thomas, J. Setién, J. A. Polanco, P. Alaejos, and M. Sánchez de Juan, 'Durability of recycled aggregate concrete', *Constr. Build. Mater.*, vol. 40, pp. 1054–1065, Mar. 2013, doi: 10.1016/j.conbuildmat.2012.11.106.

[75] R. V. Silva, R. Neves, J. de Brito, and R. K. Dhir, 'Carbonation behaviour of recycled aggregate concrete', *Cem. Concr. Compos.*, vol. 62, pp. 22–32, Sept. 2015, doi: 10.1016/j.cemconcomp.2015.04.017.

[76] C. Chen, R. Liu, P. Zhu, H. Liu, and X. Wang, 'Carbonization Durability of Two Generations of Recycled Coarse Aggregate Concrete with Effect of Chloride Ion Corrosion', *Sustainability*, vol. 12, p. 10544, Dec. 2020, doi: 10.3390/su122410544.

[77] I. F. Sáez del Bosque, P. Van den Heede, N. De Belie, M. I. Sánchez de Rojas, and C. Medina, 'Carbonation of concrete with construction and demolition waste based recycled aggregates and cement with recycled content', *Constr. Build. Mater.*, vol. 234, p. 117336, Feb. 2020, doi: 10.1016/j.conbuildmat.2019.117336.

Die approbierte gedruckte Originalversion dieser Diplomarbeit ist an der TU Wien Bibliothek verfügbar
The approved original version of this thesis is available in print at TU Wien Bibliothek.
TU Bibliothek Your knowledge hub WIEN

List of Figures

Fig. 1: Image of RCA in the concrete matrix taken from the produced samples [photo by author] 4
Fig. 2: Microscopic image under UV light of NA (a) and RCA (b) [8] 5
Fig. 3: Illustration of the formation of the ITZ along the aggregate surface from Wang et al. [15] 7
Fig. 4: Illustration of RA in RAC from Wang et al. [15] 7
Fig. 5: Image of cement bag used for concrete production during the experimental campaign [photo by author] 11
Fig. 6: General grading requirements for aggregates as specified in ÖNORM EN 12620 [30] 13
Fig. 7: Images of (a) fine natural aggregates NA 0-4, and (b) coarse natural aggregates NA 4-16 [photo by author] 14
Fig. 8: Images of (a) recycled fine concrete aggregates RB LSB 0-4 and (b) recycled coarse concrete aggregates RB LSB 4-16 [photo by author] 15
Fig. 9: Aggregate particle size distribution of NA 0-4, NA 4-16, RB LSB 0-4 and RB LSB 4-16 15
Fig. 10: Water absorption capacity of NA 0-4, NA 4-16, RB LSB 0-4 and RB LSB 4-16 18
Fig. 11: Image of the superplasticiser *MAPEI Dynamon SF 14S* [photo by author] 20
Fig. 12: Image of the Superplasticiser *MAPEI Dynamon RC 910* [photo by author] 20
Fig. 13: Image of air-entraining-agent *MAPEI Mapeair LP X9* [photo by author] 21
Fig. 14: Aggregate replacement ratios for the concrete mixtures 21
Fig. 15: Particle size distribution of aggregates used for B7_0-0, B7_30-15, and B7_100_15 22
Fig. 16: Flow diagram with the stages of the different mixing approaches: NMA [13], TSMA [13], $TSMA_{Ad}$ used in this study 24
Fig. 17: Steel moulds used to cast the specimens [photo by author] 25
Fig. 18: (a) Vibrating table, (b) steel moulds [photo by author] 26
Fig. 19: B7_0-0 and B7_30-15 concrete specimens after demoulding and labelling [photo by author] 26
Fig. 20: Curing of the specimens in a water tank [photo by author] 27
Fig. 21: Flow table test equipment 28
Fig. 22: Air content testing equipment 30
Fig. 23: Recommended depth intervals of profile grinding for concrete containing GGBFS, fly ash or silica fume [51] 32
Fig. 24: The determination of water penetration depth 35
Fig. 25 (part 1): Ground and polished surfaces of (a) B7_0-0, (b) B7_30-15 and (c) B7_100-15 concrete 37
Fig. 26 (part 2): Ground and polished surfaces of (a) B7_0-0, (b) B7_30-15 and (c) B7_100-15 concrete 38
Fig. 27: flow diameter of the fresh concrete mixtures over time (initial, after 45 min and after 90 min) 43
Fig. 28: Development of flow diameter change between measurement intervals 44
Fig. 29: Theoretical and measured air content 45
Fig. 30: Water/Binder ratio of concrete mixtures 46
Fig. 31: Fresh and hardened density of concrete mixtures 47
Fig. 32: Compressive strength test 48
Fig. 33: Concrete specimens after compressive strength failure and removal of loose material 48
Fig. 34: Compressive strength results 49
Fig. 35: Strength development of the RAC mixtures in comparison to the NAC (B7_0-0) 50
Fig. 36: Illustration of the regression for B7_0-0, B7_30-15 and B7_100-15 52
Fig. 37: Concrete scaling after 56 cycles 54
Fig. 38: Water penetration depth 54
Fig. 39: Progression of the carbonation depth with time 56
Fig. 40 (part 1): B7_0-0: Edited image (left), filtered image after applying colour threshold (centre), binary image (right) 57
Fig. 41 (part 2): B7_0-0: Edited image (left), filtered image after applying colour threshold (centre), binary image (right) 58

Die approbierte gedruckte Originalversion dieser Diplomarbeit ist an der TU Wien Bibliothek verfügbar
The approved original version of this thesis is available in print at TU Wien Bibliothek.
TU Bibliothek Your knowledge hub WIEN

Fig. 42 (part 3): B7_0-0: Edited image (left), filtered image after applying colour threshold (centre), binary image (right) 59
Fig. 43 (part 1): B7_30-15: Edited image (left), filtered image after applying colour threshold (centre), binary image (right) 59
Fig. 44 (part 2): B7_30-15: Edited image (left), filtered image after applying colour threshold (centre), binary image (right) 60
Fig. 45 (part 1): B7_100-15: Edited image (left), filtered image after applying colour threshold (centre), binary image (right) 61
Fig. 46 (part 2): B7_100-15: Edited image (left), filtered image after applying colour threshold (centre), binary image (right) 62
Fig. 47 (part 1): Positions of the captured images on the surface of (a) B7_0-0, (b) B7_30-15 and (c) B7_100-15 concrete 63
Fig. 48 (part 2): Positions of the captured images on the surface of (a) B7_0-0, (b) B7_30-15 and (c) B7_100-15 concrete 64
Fig. 49: Examples of RCA with large porous areas 67
Fig. 50: Air void distribution of computed spheres for B7_0-0 68
Fig. 51: Air void distribution of computed spheres for B7_30-15 69
Fig. 52: Air void distribution of computed spheres for B7_100-15 69
Fig. 53: Comparison of air void distribution of B7_0-0 and B7_30-15 70
Fig. 54: Comparison of air void distribution of B7_0-0 and B7_100-15 71
Fig. 55: Comparison of air void distribution of B7_30-15 and B7_100-15 71

Die approbierte gedruckte Originalversion dieser Diplomarbeit ist an der TU Wien Bibliothek verfügbar
The approved original version of this thesis is available in print at TU Wien Bibliothek.
TU Bibliothek Your knowledge hub WIEN

List of Tables

Tab. 1: Components of the B7 concrete mixtures 10
Tab. 2: Grading requirements for NA 0-4 and NA 4-16 14
Tab. 3: Constituents of recycled aggregates RB LSB 0-4 and RB LSB 4-16 16
Tab. 4: Requirements for recycled aggregates for B7 concrete according to ÖNORM B 4710-1 [20] 17
Tab. 5: Concrete recipe to produce 1 m³ of concrete 23
Tab. 6: Mixing stages and durations for the $TSMA_{Ad}$ 24
Tab. 7: Specimens required for the experimental campaign 25
Tab. 8: Paste-to-solids ratio based on the concrete recipes 41
Tab. 9: Fresh concrete temperatures 42
Tab. 10: Theoretical and measured density of the fresh concrete 45
Tab. 11: Air content measured with the pressure gauge method 45
Tab. 12: Hardened density of the concrete specimens 47
Tab. 13: Compressive strength test results 48
Tab. 14: Acid-soluble chloride content per layer determined through potentiometric titration 51
Tab. 15: results of the regression analysis of chloride profile 51
Tab. 16: Cumulative mass of scaled material after 56 cycles 53
Tab. 17: Carbonation depth after 7, 28 and 70 days 56
Tab. 18: Properties of the images edited and processed in *ImageJ* 65
Tab. 19: Air void properties of the images analysed in *MATLAB* 67

Die approbierte gedruckte Originalversion dieser Diplomarbeit ist an der TU Wien Bibliothek verfügbar
The approved original version of this thesis is available in print at TU Wien Bibliothek.
TU Bibliothek Your knowledge hub WIEN

Appendix A – MATLAB Code

This appendix contains the MATLAB scripts and functions used to process and analyse the air-void system in the concrete samples examined in this thesis based on the method proposed by Fonseca and Scherer [58]. The code was developed and applied to perform digital image analysis, including segmentation of air voids, extraction of geometrical parameters, and reconstruction of the three-dimensional air-void size distribution using the Saltykov method.

All scripts are provided in their final working form to ensure transparency, reproducibility, and traceability of the analytical procedures.

All functions were written and executed using MATLAB R2024b.

A1. Image Import

File: `readimage_binary.m`

```
function readimage_binary(varargin)
% Adapted function to read an image and determine whether it's binary or gray-
scale.
% Stores either 'grayimage' or 'bw2' in the base workspace depending on the image
type.

% Check if a filename was passed
if nargin == 0
    error('A filename is a required input')
end

% Construct the file path
if nargin == 1
    fpath = varargin{1};
elseif nargin > 1
    fpath = fullfile(varargin{2}, varargin{1});
end

% Prompt the user to manually input the scale (pixels per millimeter)
ppmm = input('Enter the scale in pixels per millimeter (e.g., 100 pixels/mm): ');
assignin('base','ppmm',ppmm);

% Calculate and assign pixel size in microns
psize = 1 / (1000 * ppmm);  % microns per pixel
assignin('base', 'psize', psize);

% Display resolution information
disp(['The resolution of the image is ', num2str(ppmm), ' pixels/mm.']);
disp(['The size of each pixel is ', num2str(psize), ' microns.']);
disp(' ')

% Read the image
img = imread(fpath);

% Check if the image is binary (only 0 and 1 values)
```

Die approbierte gedruckte Originalversion dieser Diplomarbeit ist an der TU Wien Bibliothek verfügbar
The approved original version of this thesis is available in print at TU Wien Bibliothek.
TU Bibliothek Your knowledge hub WIEN

```
if islogical(img) || isequal(unique(img), [0; 255]) || isequal(unique(img), [0;
1])
    % Image is binary
    if ~islogical(img)
        img = imbinarize(img);        % Ensure it's logical
    end
    assignin('base', 'bw2', img);
    figure;
    imshow(img);
    title('Binary Image (bw2)');
    disp('Image is binary. Saved as "bw2" in base workspace.');
else
    % Image is grayscale
    grayimage = img;
    assignin('base', 'grayimage', grayimage);
    figure;
    imshow(grayimage);
    title('Grayscale Image');
    disp('Image is grayscale. Saved as "grayimage" in base workspace.');
end

end
```

Die approbierte gedruckte Originalversion dieser Diplomarbeit ist an der TU Wien Bibliothek verfügbar
The approved original version of this thesis is available in print at TU Wien Bibliothek.

A2. Image Import and Binary Detection

File: `basicanalysis_binary.m`

```
function basicanalysis_binary(varargin)

% Get "ppmm" from the base workspace
ppmm = evalin('base','ppmm');  % pixels per millimeter

% The user must pass the paste/solids ratio
if nargin < 1
    error('basicanalysis requires a paste:solids ratio as input.')
end

paste_solids = varargin{1};

% Optional threshold input
if nargin > 1
    thresh = varargin{2};
end

% Try to load bw2 (binary image) if available
bw_exists = evalin('base', 'exist(''bw2'', ''var'')');
gray_exists = evalin('base', 'exist(''grayimage'', ''var'')');

if bw_exists
    % Use existing binary image
    bw2 = evalin('base','bw2');
    disp('Using binary image (bw2) from workspace.');

    % Estimate crop dimensions from size of bw2
    cropdim = size(bw2) / ppmm;
else
    if ~gray_exists
        error('No image found. Make sure grayimage or bw2 exists in the base work-
space.');
    end

    % Use grayscale image and convert it to binary
    grayimage = evalin('base','grayimage');
    cropdim = size(grayimage) / ppmm;

    % If no threshold is provided, use Otsu's method
    if nargin < 2
        thresh = graythresh(grayimage) * 255;
    end
    assignin('base','threshold',thresh)

    % Convert to binary using threshold
    bw = im2bw(grayimage, thresh / 255);

    % Remove tiny objects (default: 1 pixel)
    tinyobjects = 1;
    neigh = 4;
    bw2 = bwareaopen(bw, tinyobjects + 1, neigh);

    assignin('base','bw2',bw2)

    % Show binary image
    figure;
    imshow(bw2);
```

Die approbierte gedruckte Originalversion dieser Diplomarbeit ist an der TU Wien Bibliothek verfügbar
The approved original version of this thesis is available in print at TU Wien Bibliothek.
TU Bibliothek Your knowledge hub WIEN

```
    title('Binary Image After Thresholding');

    disp(['Threshold used: ', num2str(thresh)]);
end

assignin('base','cropdim',cropdim);

% Find connected components
conn = 4;
cc = bwconncomp(bw2, conn);
assignin('base','cc',cc)

% Measure component properties
stats = regionprops(cc, 'Area', 'Perimeter');
assignin('base','stats',stats)

% Calculate measurements
areapix = [stats.Area];
areamm2 = areapix / (ppmm^2);
diameterpix = 2 * sqrt(areapix / pi);
diametermic = 2 * sqrt(areamm2 / pi) * 1000;
radiimic = diameterpix / 2;
assignin('base','radiimic',radiimic)

% Air content (%)
[m, n] = size(bw2);
aircontent = sum(areapix) / (m * n) * 100;
disp(['Air content: ', num2str(aircontent), ' %']);

% Specific surface
Ptot = sum([stats.Perimeter]);
Atot = sum(areapix);
specsurfpix = Ptot / Atot * (4 / pi);
specsurf = specsurfpix * ppmm;
disp(['Specific surface: ', num2str(specsurf), ' mm^-1']);

% Paste/air ratio
p_A = paste_solids * (100 - aircontent) / aircontent;
disp(['Paste/air ratio: ', num2str(p_A)]);

% Powers spacing factor
if p_A < 4.342
    Pspacef = p_A / specsurf;
else
    Pspacef = (3 / specsurf) * (1.4 * (1 + p_A)^(1/3) - 1);
end
disp(['Powers spacing factor: ', num2str(Pspacef), ' mm']);

end
```

Die approbierte gedruckte Originalversion dieser Diplomarbeit ist an der TU Wien Bibliothek verfügbar
The approved original version of this thesis is available in print at TU Wien Bibliothek.
TU Bibliothek Your knowledge hub WIEN

A3. Reconstruction of the 3D Air-Void Size Distribution

File: `reconstructspheres.m`

```
function reconstructspheres(varargin)

% If a binwidth is passed
if nargin > 0
    binwidth = varargin{1};
end

% If a maximum x-limit is passed
if nargin > 1
    XL2 = varargin{2};
end

% Get image size
if evalin('base', 'exist(''grayimage'', ''var'')')
    grayimage = evalin('base','grayimage');
    imgsize = size(grayimage);
elseif evalin('base', 'exist(''bw2'', ''var'')')
    bw2 = evalin('base','bw2');
    imgsize = size(bw2);
else
    error('Neither grayimage nor bw2 found in the base workspace.');
end

stats = evalin('base','stats');
ppmm = evalin('base','ppmm');

close all

areapix = [stats.Area];
areamm2 = areapix/(ppmm*ppmm);
diametermic = 2*sqrt(areamm2/pi)*1000;
radiimic = 0.5 * diametermic;

averageradmic = mean(radiimic);

% Estimate binwidth if not provided
if nargin == 0
    IQRradii = iqr(radiimic);
```

Die approbierte gedruckte Originalversion dieser Diplomarbeit ist an der TU Wien Bibliothek verfügbar
The approved original version of this thesis is available in print at TU Wien Bibliothek.

```
    binwidth = 2*IQRradii*length(radiimic)^(-1/3);
end

% Initial histogram
r = 0:binwidth:max(radiimic);
[N,X] = hist(radiimic,r);
freqN = N/sum(N);

% Number density on section plane
cropdim = 1/ppmm * imgsize;
NA = length(radiimic)/(cropdim(1)*cropdim(2));

figure;
NAr = NA/binwidth .* freqN;
bar(X,NAr);
ylabel('Number density per mm^2');
xlabel('Observed profile radii [\mum]');
XL = xlim; XL(1)=0;
if nargin>1, XL(2)=XL2; end
xlim(XL); ylim([0 inf]);

% Saltykov reconstruction
rmod = [0 r];
r = rmod;
NAr = [0 NAr]';
Dr = binwidth;

rm = max(r);
NVR = zeros(length(r),1);

for k=1:length(NAr)-1
    NVm = NAr(end-k+1)/(2*sqrt(2*(length(NAr)-k)-1)*Dr);
    NVR(end-k+1) = NVm;
    NArm = zeros(length(r),1);
    for i=1:length(r)-k+1
        NArm(i) = NVm*2*(sqrt(rm^2-(r(i)-Dr)^2)-sqrt(rm^2-r(i)^2));
    end
    rm = rm-Dr;
    NAr = NAr - NArm;
end
```

Die approbierte gedruckte Originalversion dieser Diplomarbeit ist an der TU Wien Bibliothek verfügbar
The approved original version of this thesis is available in print at TU Wien Bibliothek.
TU Bibliothek Your knowledge hub WIEN

```
NVR(NVR<0)=0;


figure;
bar(r,NVR);
ylabel('Number density per mm^3');
xlabel('Computed sphere radii [\mum]');
XL = xlim; XL(1)=0;
if nargin>1, XL(2)=XL2; end
xlim(XL); ylim([0 inf]);


disp(['The mean observed profile radius is ', num2str(averageradmic), ' microns.']);
disp(['The mean computed sphere radius is ', num2str(sum(NVR.*r)/sum(NVR)), ' microns.']);
disp(['The binwidth is ', num2str(binwidth), ' microns.']);


% Save reconstructed radii
[filename, filepath] = uiputfile('*.mat', 'Save radii data as');
if ischar(filename)
    save(fullfile(filepath, filename), 'radiimic');
    disp(['Saved radii data to ' fullfile(filepath, filename)]);
end


end
```

Die approbierte gedruckte Originalversion dieser Diplomarbeit ist an der TU Wien Bibliothek verfügbar
The approved original version of this thesis is available in print at TU Wien Bibliothek.

A4. Histogram Combination

File: `combine_histograms.m`

```
function combined_histogram = combine_histograms(folder_path, binwidth, xmax)

matFiles = dir(fullfile(folder_path, '*.mat'));
all_radiimic_values = [];

for i = 1:length(matFiles)
    fileName = fullfile(folder_path, matFiles(i).name);
    data = load(fileName);
    if isfield(data, 'radiimic')
        all_radiimic_values = [all_radiimic_values, data.radiimic];
        disp(['Loaded: ', matFiles(i).name]);
    end
end

radii_all = all_radiimic_values;
volumes_all = (4/3)*pi*(radii_all.^3);
total_volume_all = sum(volumes_all);

mask_small = radii_all <= 150;
total_volume_small = sum((4/3)*pi*(radii_all(mask_small).^3));
vol_percentage_300 = total_volume_small / total_volume_all * 100;

disp(['Volumetric % of voids with diameter ≤300 µm: ',
num2str(vol_percentage_300), '%']);

if nargin < 2
    IQRradii = iqr(radii_all);
    binwidth = 2*IQRradii*length(radii_all)^(-1/3);
end
if nargin < 3
    xmax = max(radii_all);
end

r = 0:binwidth:xmax;
[N, X] = hist(radii_all(radii_all <= xmax), r);
freqN = N/sum(N);

combined_histogram.X = X;
combined_histogram.N = freqN;

figure;
bar(X,freqN);
xlim([0 xmax]);
xlabel('Computed sphere radii [\mum]');
ylabel('Normalized Frequency');
title('Distribution of reconstructed air voids');
grid on;

end
```

Die approbierte gedruckte Originalversion dieser Diplomarbeit ist an der TU Wien Bibliothek verfügbar
The approved original version of this thesis is available in print at TU Wien Bibliothek.

A5. Comparison of Two Specimens

File: `compare_histograms.m`

```
function compare_histograms(folder1, folder2, binwidth, xmax)

histo1 = combine_histograms(folder1, binwidth, xmax);
histo2 = combine_histograms(folder2, binwidth, xmax);

figure;
hold on;
bar(histo1.X, histo1.N, 'FaceAlpha', 0.5, 'FaceColor', [0 0.4470 0.7410], 'EdgeColor', 'none');
bar(histo2.X, histo2.N, 'FaceAlpha', 0.4, 'FaceColor', 'r', 'EdgeColor', 'none');
hold off;

xlim([0 xmax]);
xlabel('Computed sphere radii [\mum]');
ylabel('Normalized Frequency');
title('Comparison of Air Void Size Distributions');
legend('Specimen 1', 'Specimen 2');
grid on;

end
```

Die approbierte gedruckte Originalversion dieser Diplomarbeit ist an der TU Wien Bibliothek verfügbar
The approved original version of this thesis is available in print at TU Wien Bibliothek.